Role of IGF-1R/IR signaling in epidermal and vascular barrier function

Inaugural-Dissertation
zur
Erlangung des Doktorgrades
Der Mathematisch-Naturwissenschaftlichen Fakultät
Der Universität zu Köln

vorgelegt von

Saeed Yadranji Aghdam
aus Tabriz

Köln, 2010

Berichterstatter:

Prof. Dr. med. Jens C. Brüning

Prof. Dr. rer. nat. Carien M. Niessen

Tag der mündlichen Prüfung: 10.01.2011

Abstract

The formation and maintenance of physical and functional barriers allows organisms to compartmentalize tissues, restrict the movement of cells, ions and small solutes as well as allows for terrestrial living. The main aim of this thesis was to examine if cell autonomous insulin/IGF-1 signaling regulates barrier formation/function in mammals, specifically the epidermal skin barrier as well as the vascular barrier. Mammalian epidermis is a multilayered stratified epithelium serving as a protective barrier against external insults and dehydration. Two compartments contribute to epidermal barrier function: (i) the outermost *stratum corneum* consisting of corneocytes embedded in a crosslinked matrix of mostly lipids and (ii) intercellular tight junctions present in the uppermost viable *Stratum granulosum*. Vascular barrier property on the other hand is largely dependent on functional intercellular junctions such as tight and adherens junctions that seal of the paracellular space between endothelial cells.

Using Cre-loxP technology, the cell autonomous role of insulin receptors (IR)/IGF-1 receptors (IGF-1R) in the formation of epidermal barrier and maintenance of vascular barrier were analysed in mice with epidermal- and adult vascular endothelial-specific inactivation of both receptors ($dko^{epi-/-}$ and $dko^{veinduc-/-}$). $Dko^{epi-/-}$ mice showed transepidermal water loss and lethality within two days after birth, implying compromised epidermal barrier formation. Analysis of outside-in barrier formation using dye exclusion assays showed a strongly delayed acquisition of embryonic epidermal barrier in $dko^{epi-/-}$ mice compared to control mice, suggesting impaired formation of the *stratum corneum*. This was accompanied by altered corneocyte morphology and a reduction in the level of free ceramides in combination with an accumulation of precursor ceramides (GlcCers) in the *stratum corneum* of $dko^{epi-/-}$ mice as well as a small reduction in monomeric filaggrin. Analysis of the insight-out barrier did not reveal any consistent differences yet, despite small differences in tight junctional protein expression. Thus, epidermal Insulin/IGF-1 signaling is essential for epidermal barrier formation by regulation proper formation of the *stratum corneum*.

Temporal inactivation of IR and IGF-1R in adult vascular endothelial cells did not result in any obvious morphological alterations in the vasculature in a range of tissues. Injection of tracer molecules with different molecular size followed by whole mount analysis of the retina or skin sections did not reveal any obvious vascular leakage or abnormal vascular patterning. Thus, vascular endothelial IR/IGF-1R signaling does not seem to regulate vascular integrity under steady state conditions. An important caveat in these experiments was the observation that the inactivation of the IGF-1R was variable and that loss of over 90% of IGF-1R is insufficient to disturb vascular integrity.

Zusammenfassung

Die Ausbildung und Aufrechterhaltung von physikalischen und funktionellen Barrieren erlaubt Organismen Gewebe in Kompartimente zu unterteilen, die Bewegungsfähigkeit von Zellen, Ionen und kleine gelöste Substanzen einzuschränken und sichert so die Überlebensfähigkeit im terrestrischen Leben. Das Hauptziel dieser Arbeit war herauszufinden, ob Zell autonome Insulin/IGF- Signalisierung Barriereausbildung und Funktion in Säugetieren, insbesondere die epidermale Hautbarriere und vaskuläre Barriere, reguliert.

Die Epidermis von Säugetieren repräsentiert ein geschichtetes Epithel, welches als schützende Barriere gegen äußere Einflüsse und Dehydrierung wirkt. Zwei Kompartimente tragen zur epidermalen Barrierefunktion bei: (i) das äußerste *stratum corneum* besteht aus Korneozyten, welche in eine vernetzte Matrix aus Lipiden eingebettet sind und (ii) intrazelluläre Verschlusskontakte (*zonula occludens, tight junction*), welche sich in dem obersten *Stratum granulosum* befinden. Vaskuläre Barriereeigenschaften sind größtenteils abhängig von funktionellen intrazellulären Kontaktstellen wie *tight* und *adheres junctions,* welche den parazellulären Raum zweichen Endothelzellen versiegeln.

Durch Nutzung der Cre-loxP Technology wurde die Rolle des Insulinrezeptors (IR) sowie des IGF-1 Rezeptors (IGF-1R) in der Ausbildung der epidermalen Barriere und Aufrechterhaltung von vaskulären Barrieren in Mäusen mittels epidermal-spezifischer sowie vaskulärer endothelial-spezifischer Inaktivierung von beiden Rezeptoren ($dko^{epi-/-}$ und $dko^{veinduc-/-}$) analysiert. $Dko^{epi-/-}$ Mäuse wiesen einen transepidermalen Wasserverlust auf und starben zwei Tage nach der Geburt, was auf eine beeinträchtigte epidermale Barrierefunktion hindeutet.

Analyse von Einwärtsbarriereausbildung durch Gebrauch von Farbstoff-Penetrations Versuchen wiesen eine verspätete Ausbildung der epidermalen Barriere in $dko^{epi-/-}$ im Vergleich zu Kontrollmäusen auf, welches auf eine beeinträchtigte Formation des *stratum corneums* hindeutet. Diese Beobachtung wurde unterstützt durch veränderte Korneozyten Morphologie und einer Reduktion bezüglich des Gehalts von freien Ceramiden in Kombination mit einer Akkumulierung von Vorläufer Cermaiden (GlcCers) im *Stratum Corneum* von $dko^{epi-/-}$ Mäusen sowie einer Reduktion monomerischen Filaggrins. Analyse der Auswärtsbarriere zeigten keine konsistenten Unterschiede zwischen Kontroll Mäusen und Mutanten, bis auf geringe Unterschiede bezüglich der Expression des *tight juncion* Strukturproteins Claudin 1. Insgesamt wurde gezeigt, dass epidermale Insulin/ IGF-1 Signalisierung essentiell für die Ausbildung der epidermalen Barriere durch die Regulation der Bildung des *Stratum Corneums* ist.

Temporelle Inaktivierung des IR und IGF-1R in adulten vaskulären Endothelzellen resultierte in keiner offensichtlichen morphologischen Veränderung in den Blutgefäßen im Bereich von Geweben. Injektion von Tracer Molekülen von unterschiedlicher Molekulargröße gefolgt von Retina Analysen konnten keine vaskuläre Durchlässigkeit oder abnormale vaskuläre Ordnung bestätigen.

Folglich scheint vaskulär endotheliales IR/ IGF-1R Signalisierung keine Rolle in der Regulierung der vaskulären Intaktheit unter Gleichgewichtsbedingungen zu besitzen.

Table of content:

1 Introduction

1 *In vivo* barriers……1

1.1 *In vivo* barriers and their functional importance……..1

1.2 Endothelial barriers…….....1

1.2.1 Adherens junctions, tight junctions and desmosomes……..1

1.2.2 Retina and Blood-Retinal-Barrier……..1

1.3 Epidermal skin barrier ……...3

1.3.1 Adherens junctions, tight junctions and desmosomes……..4

1.3.2*Stratumcorneum*…….4

1.3.3 Acquisition of outside-in epidermal barrier in mouse……..4

1.4 Molecular components of barriers ……..4

1.4.1 TJs, AJs and desmosomes ……5

1.4.1.1Claudin proteins……..5

1.4.1.2 Occludin…….6

1.4.1.3 Junctional adhesion molecules (JAMs)……..7

1.4.1.4 Zonula occludens (ZO) proteins ……7

1.4.1.5 Cadherin/catenin adhesion complex……..8

1.4.2 Regulation of TJs/AJs by the polarity complex aPKC/Par3/Par6…….8

1.4.2.1 Genomic structure and protein isoforms of mouse Par-3……...9

1.4.2.2 Protein domains and interaction partners of mouse Par-3…….9

1.4.3 The *stratum corneum*: protein and lipid barrier……...11

1.4.3.1 Protein components of the cornified envelope …….12

1.4.3.2 Filaggrin gene and protein structure in humans and mouse……..12

1.4.3.3 Filaggrin expression, function and processing…….…..13

1.4.4 Lipid components of the cornified envelope……..……13

1.5 The insulin-like growth factor (IGF) system…….…….14

1.5.1.1 IGF-1R and IGF-2R receptors and IGF binding proteins (IGFBPs)…….….14

1.5.1.2 Insulin..…….…...15

1.5.1.3 Structural homology of insulin receptor and IGF-1 receptor……..16

1.5.1.4 Hybrid insulin receptor/IGF-1 receptor……...16

1.5.1.5 Activation of receptors and signaling pathways…….17

1.5.2 Insulin signaling in diabetes and gene knockout models for IR/IGF-1R……...18

1.6 Regulation of endothelial function by Insulin/IGF-1 signaling and in Diabetes……19

1.6.1 Role of IR and IGF-1R signaling in endothelial cells……19

1.6.2 Blood-retinal-barrier breakdown in diabetes……19
1.7 Role of insulin/IGF-1 signaling in the skin……21
Aims of this study……22
2 Results
2.1.1 Increased levels of epidermal water loss in dko$^{epi-/-}$ mice……..23
2.1.2 Insulin/IGF-1 signaling might be essential for competent inside-out epidermal barrier formation……23
2.1.3 Insulin and IGF-1 signaling regulate outside-in epidermal barrier formation……..24
2.1.4 Abnormality in corneocyte morphology and size in dko$^{epi-/-}$ mice……25
2.1.5 Aberrant profilaggrin to filaggrin processing in dko$^{epi-/-}$ mice ……28
2.1.6 Reduced epidermal ceramides in dko$^{epi-/-}$ mice……..33
2.1.7 Impairment of tight junctions in cultured IGF-1R$^{-/-}$ keratinocytes ……....34
2.1.8 Normal recruitment of β-catenin and ZO-1 to cell-cell junctions in IGF-1R$^{-/-}$ keratinocytes……35
2.1.9 Impaired cldn-1 expression in differentiated IGF-1R$^{-/-}$ keratinocytes……36
2.2.1 Preparation of dko$^{veinduc-/-}$ mice to study vascular barrier property……..36
2.2.2 Variation in IGF-1R gene deletion after feeding with tamoxifen……..39
2.2.3 Viability and survival not affected in dko$^{veinduc-/-}$ mice……..39
2.2.4 Intact retinal vascular barrier integrity in the absence of IR/IGF-1R signaling…….39
2.2.5 Isolation of primary lung endothelial cells……41
2.2.6 Generation of double knockout IR$^{-/-}$ / IGF-1R$^{-/-}$ primary endothelial cells ……42
2.3 Generating a conditional knockout mouse for PAR-3 gene……..43
2.3.1 Detection of PAR-3 transcripts in primary mouse keratinocytes by RT-PCR……...43
2.3.2 Generation of a targeting plasmid for mouse Par-3 gene……...46
2.3.3 Production of PAR-3$^{exon4\ flox/+}$ embryonic stem cells……..46
2.3.4 Production of PAR-3$^{exon4\ +/-}$embryonic stem cells……47
2.3.5 Generation of chimeric mPAR-3$^{exon4\ flox/+}$ males……48
3 Discussion……49
3.1 Insulin/IGF-1 signaling in epidermal barrier morphogenesis……..50
3.2 Insulin/IGF1 signaling in vascular barrier function……55
3.3 Setbacks and prospects of the Par3$^{exon4flox/+}$ mouse project……55
4 Material and methods
4.1 Mice……57
4.1.1 Insulin receptor and IGF-1 receptor floxed mice……..57
4.1.2 Generation of PAR-3$^{exon4\ flox/+}$ mouse……57
4.1.3 Feeding with Tamoxifen diet……57

4.2 Molecular DNA techniques……..57
4.2.1 DNA Ligation……57
4.2.2 DNA Digestion and de-phosphorylation of DNA fragments……58
4.2.3 Recombinant DNA techniques……..58
4.2.4 Polymerase Chain Reaction (PCR)……....58
4.2.5 Southern Blot……58
4.2.6 Bacterial Transformation……...……59
4.3 Molecular RNA techniques……...……59
4.3.1 RNA isolation from cells……..59
4.3.2 cDNA synthesis……59
4.3.3 Semi-quantitative RT-PCR. ……59
4.4 Barrier function assays for epidermis and keratinocytes……...59
4.4.1 Measurement of transepidermal water loss…….…..59
4.4.2 Lufier yellow assay……59
4.4.3 Toluidine blue assay……59
4.4.4 Inside-out barrier assay with sulfo-NHS-Biotin……60
4.4.5 Transepithelial resistance measurement (TER) ……60
4.5 Retinal vascular barrier assay……60
4.5.1 Perfusion with 2000 kDa FITC-dextran……60
4.5.2 Systemic infusion with sulfo-NHS-Biotin……60
4.5.3 Preparation of retinal wholemounts……...60
4.6 Sample preparation and immunoblots analysis……60
4.6.1 Separation of the epidermis from dermis……...60
4.6.2 Immunoblot analysis of primary keratinocytes and epidermis……..61
4.6.3 Quantification of Immunoblot bands with ImageJ……61
4.7 Immunofluorescence techniques……..61
4.7.1 Paraffin embedding of experimental tissues……61
4.7.2 Immunofluorescence analysis of keratinocytes and tissue sections……..62
4.7.3 Immunofluorescent labelling of biotin in retinal wholemounts……62
4.8 Primary keratinocyte and endothelial cell culture……62
4.8.1 Isolation and culture of primary keratinocytes…….……62
4.8.2 Splitting……63
4.8.3 Differentiation and induction by Ca^{2+} switch……63
4.8.4 Mouse Lung Endothelial Cells (MLECs) isolation……..63
4.8.5 HTNC treatment of primary endothelial cells……..64
4.8.6 Tamoxifen treatment of primary endothelial cells……64

4.9 Corneocyte and lipid analysis……..64
4.9.1 Cornified envelope preparations……...64
4.9.2 Analysis of corneocytes by ImageJ……..64
4.9.3 Lipid extraction and analysis……64
4.9.4 Ceramide nomenclature legend……65
Table-2: List of primers and their respective PCR products……65
Table-3: Primary antibodies……..66
Table-4: Secondary antibodies……..67
5 Abbreviations……..…..67
6 References ……71
7 Acknowledgements……...84
8 Erklarung ……..85
9 CurriculumVitae……..……..86

1 Introduction

1.1 *In vivo* barriers and their functional importance

In multicellular organisms, certain tissues must be separated from each other and protected against the outside environment. Continuous epithelial and endothelial sheets accomplish this by providing cellular borders that cover the external and internal surfaces of the body. Ultrastructural visualization reveals the complexes between adjoining cells in these sheets as gap junctions, desmosomes, adherence junctions (AJs) and tight junctions (TJs). These intercellular complexes act in concert to selectively control the influx and efflux of molecules and particles through their protective shield. The epidermis which separates the body from the outside milieu acts as a barrier constructed *via* piled up stacks of differentiated keratinocytes. The intercellular junctional complexes between the flattened keratinocytes and the components of the cornified layer of the epidermis shape the barrier function of skin. Therefore, skin is a semipermeable epithelium with multiple functions including, protection against entry of infectious or toxic substances, barrier against dangerous solar UV irradiation and most importantly it prevents the escape of body moisture and heat (Reviewed by Candi *et al.,* 2005). The vascular barrier function on the other hand depends on a single sheet of endothelial cells lined next to each other and joint together by specific intercellular adhesion complexes (Fig.1). The vascular barrier is almost a one way barrier which controls the efflux of solutes and molecules out of the blood into underlying tissues (Turksen and Troy, 2004).

1.2 Endothelial barriers

1.2.1 Adherens junctions, tight junctions and desmosomes

An essential property of vascular endothelial cells is their assembly into a physical and ion- and size-selective barrier. According to ultrastructural observations it has been shown that endothelial cells have specialized junctional regions that are comparable to AJs/TJs in epithelial cells; however, whereas in most epithelia TJs are concentrated at the more apical side of the intercellular cleft, in the endothelium TJs are frequently intermingled with AJs all the way along the cleft. Furthermore, in contrast to epithelial cells, endothelial cells lack desmosomes (Fig.1) (Reviewed by Dejana, 2004).

Another difference of the vascular barrier system compared to epithelial barriers is the presence of vascular fenestrations in different tissues such as skin and choroids which provides a differential permeability preference based on the size parameter of the diffused molecules (Takada and Hattori 1972, Maxwell and Pease, 1956). In contrast to fenestrated endothelial cells in the choroid and skin vasculature, the TJs in the blood brain barrier tightly regulate the transpass of ions and molecules to the extravascular brain tissue (Nitta *et al*., 2003).

1.2.2 Retina and Blood-Retinal-Barrier

Retina is a transparent neural tissue positioned between the vitreous body and the retinal pigmented epithelium and consists of multiple layers; the nerve fiber layer, ganglion cell layer, inner plexiform layer, inner nuclear layer, outer plexiform layer, outer nuclear layer, and the outer segments of rods and cones. Central retinal artery and the choroidal blood vessels provide

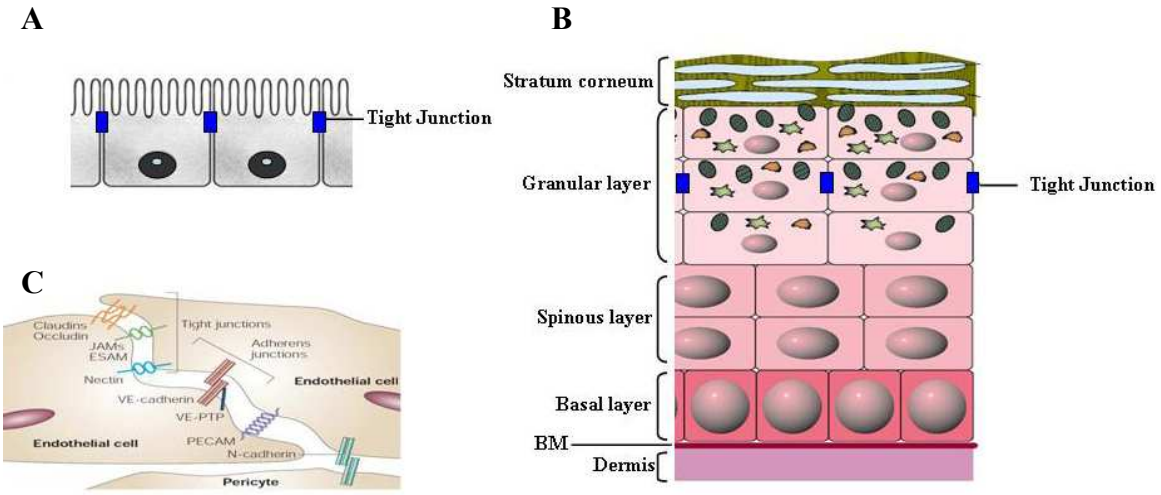

Figure 1: The organization of TJs in simple epithelium, stratified epithelia and endothelial cells. (A) Tissues with simple epithelia have TJs in the most apical pole of the cells. (B)TJs in the stratified epithelium of the skin are positioned in the mid-granular layer of the skin. (C) Endothelial TJs are located apically but they tend to be intermingled with AJs.

85% and 15% of retinal blood supply. In the human retina, four main branches arise from the central retinal artery to supply three capillary plexuses: the radial peripapillary in nerve fibre layer, the inner capillary in ganglion cell layer, and the outer capillary networks in junction of inner nuclear and outer plexiform layers. The mouse counterparts of retinal vessels are primary plexus, inner or superficial and outer deeper plexus (Fig.2A) (Reviewed by Erickson et al., 2007). TJs in retinal pigment epithelium (RPE) and the blood vessels of the retina form the outer and inner barriers of the blood-retinal-barrier (BRB) respectively. The BRB is similar to the blood brain barrier in that it serves as a size and charge selective barrier that regulates the local environment of the neural retina. As with TJs elsewhere, RPE cells express tight junctional proteins, occludin-1, cldns, and ZO-1 (Williams and Rizzolo, 1997; Tserentsoodol et al., 1998) and control the flow of solutes and fluid from the surrounding fenestrated capillaries of the choriocapillaris into the outer retina (outer retinal barrier) and the retinal vessels directly restrict diffusion from the vessel lumen into the retinal parenchyma (inner retinal barrier) (Fig.2B) (Shakib and Cunha-Vaz, 1966).

Although permeability of BBB or BRB is controlled by the biochemical and biophysical properties of microvascular endothelial cells, the vascular barrier function in CNS is generally the outcome of interactions of endothelial cells with the basement membrane and bordering glial

cells, such as microglia and astrocytes, which together with neurons and perivascular pericytes constitute the neurovascular unit (NVU) (Fig.2C) which is an essential assembly in the vascular barrier function of CNS. Among other cell types in NVU, pericytes are believed to closely contribute to the integrity of neural vascular barrier as they share the same basement membrane with the endothelial cells and cover 22 to 32% of the capillary surface. Pericyte positioning on the microvessel and the coverage amount varies between different microvessel types which seems to correlate with the degree of tightness of the endothelial junctions (Reviewed by Cardoso *et al*., 2010).

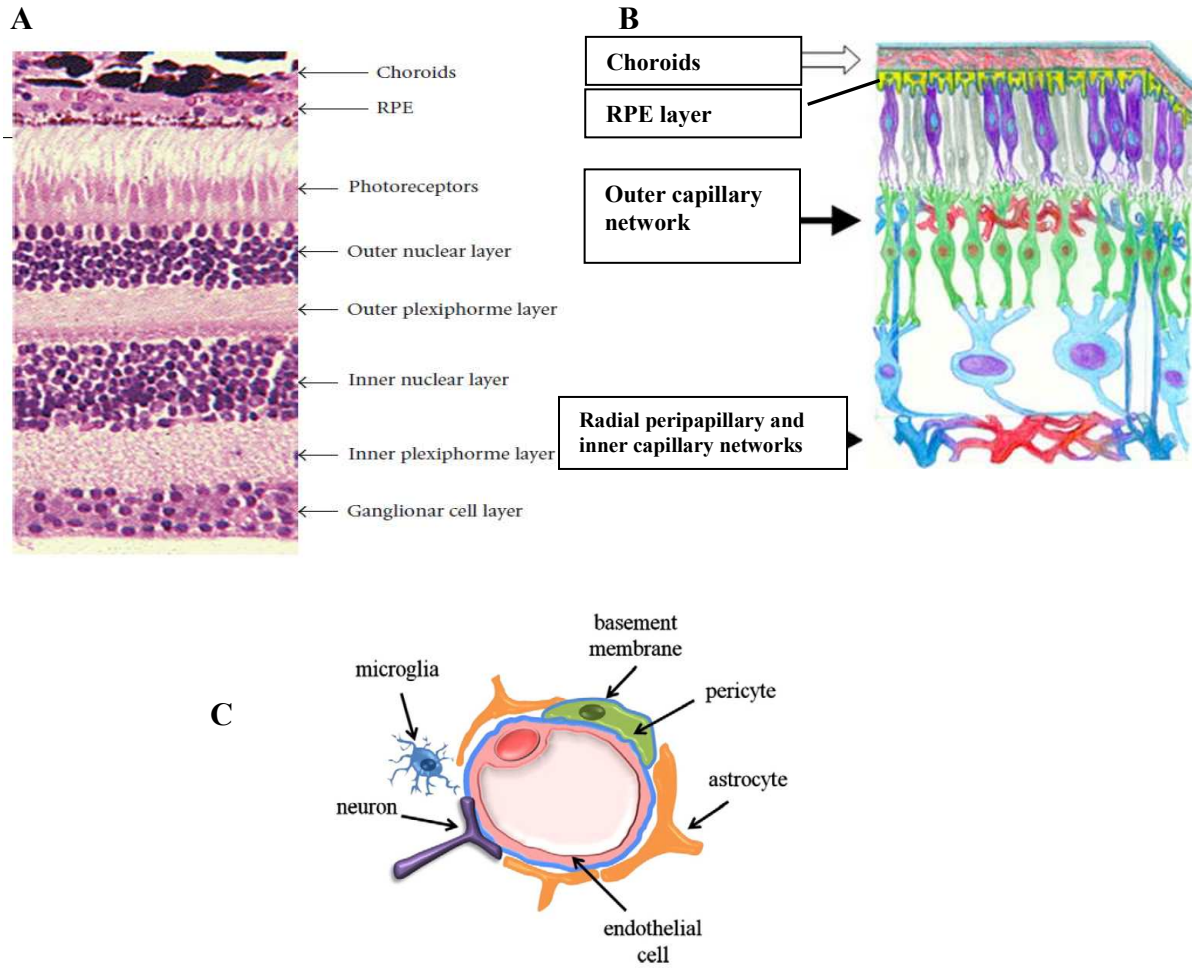

Figure 2: (A) H&E showing different cell types in retinal section. **(B) Scheme showing the neural and vascular network in normal retinal cross section.** Arrowhead: radial peripapillary and underlying inner capillary networks, arrow: outer capillary network. These networks build the inner BRB. Open arrow: The choroids supply nutrients to the outer retina. Diffusion into the retina is controlled by the retinal pigmented epithelium (RPE). RPE layer forms the outer BRB **(C) Scheme of neurovascular unit assembly**. Endothelial cells are covered by a basement membrane (shown in blue) and surrounded by different cell types; pericytes, astrocytic endfoot, neurons and microglial. Part B and part C are adapted from Erickson et al., 2007 and Cardoso et al., 2010 respectively.

1.3 Epidermal skin barrier

1.3.1 Adherens junctions, tight junctions and desmosomes

The competency of epidermal barrier depends at least on proper function of three major components: the cornified envelope and lipid lamellar sheets in the cornified layer and intercellular AJ/TJ complexes in the upper granular layer. Based on dye penetration assays on mouse skin using lucifer yellow and toluidine blue, cornified layer forms the outside-in barrier (Hardman et al., 1998; Jennemann et al., 2007; Epp et al., 2007). The AJ formation in the epidermis leads to proper TJ assembly in the epidermis and TJs are engaged in the formation of inside-out barrier, as TJs in granular layer restrict the diffusion of subcutaneously injected biotin to the cornified layer (Furuse *et al.*, 2002; Tunggal *et al.*, 2005). In the epidermis hemidesmosomes are restricted to the basal layer, whereas desmosomes are found in all layers of the epidermis (Getsios et al., 2004).

1.3.2 *Stratum corneum*

Cornified envelope replaces the plasma membrane of cells in the cornified layer and comprises a series of crosslinked protein components which ultimately result in the formation of a highly resilient corneocytes. The corneocytes are therefore very resistant to boiling in solutions containing detergent and reducing reagents. Interconnected corneocytes by corneodesmosomal components and intercorneocyte lipid stcks together form the *stratum corneum* (Rice *et al.,* 2003).

1.3.3 Acquisition of outside-in epidermal barrier in mouse

Analysis of embryonic mouse skin using dye penetration assay with toluidine blue has determined that the development of such a barrier happens late in gestational period. Indeed Harman *et al.,* (1998) identified the start points of barrier acquisition as sites which blocked dye penetration in late embryonic E16 skin at distinct initiation sites. The barrier acquisition in mouse follows a highly patterned order during development with the emergence of initial barrier-competent start sites in the back skin and then on cranial site and nostrils which gradually spreads in the form of moving fronts to the front skin over 1-2 days of development depending on the mouse strain.

Skin barrier development happens concurrently with the component deposition, maturation and thickening of the cornified layer. Mature (26 kDa) FLG would not account for barrier acquisition as despite the presence of the profilaggrin and 2X-FLG intermediates, monomeric FLG was detected only in post-barrier (17 day) epidermis. Since loricrin as one of the last components to be incorporated into the cornified envelope, has constant expression during the last stages of barrier acquisition and due to its overlapping redistribution to the cornified cell membranes during barrier development, it is possible that cornified envelope maturation correlates with acquisition of barrier function (Harman *et al.,* 1998).

1.4 Molecular components of barriers

1.4.1 TJs, AJs and desmosomes

In simple epithelia which consist of a single layer of polarized cells, TJs are the most apical structure of the apical complex demarcating the border between apical and basolateral membrane domains. However in stratifying epithelia of the mammalian epidermis functional TJs occur only in the upper viable part of the granular layer. The intercellular membrane space of TJs is almost completely obliterated, hence their alternative name zonulae occludens. AJs are positioned immediately below TJs and characterized by two apposing membranes, which are separated by ~20 nM, that run parallel over a distance of 0.2-0.5 mm (Reviewd by Niessen, 2007, Michels *et al*., 2009a).

A combination of transmembrane and cytoplasmic proteins constitutes both the AJs, TJs and desmosomes. These components can be categorized into three general categories: (i) structural proteins necessary for initiation of the junctions, (ii) plaque proteins associated with the cytoskeleton, and (iii) signaling/polarity proteins. The nectin-afadin and cadherin-catenin complexes are building components of AJs where nectin and cadherin are transmembrane proteins and afadin and catenin are cytoplasmic proteins, the latter two proteins can interact with actin cytoskeleton thereby linking the AJs to cytoskeleton (reviewed by Niessen, 2007). Desmosomes are formed by adhesion receptors belonging to the cadherin super family *i.e.* desmogleins and desmocollins. Desmosomes link intermediate filament cytoskeleton to the plasma membrane (Nathke *et al.*, 1994).

Single-pass membrane proteins such as junctional adhesion molecules (JAM), and four-pass transmembrane domains such as cldns and occludin together with cytoplasmic proteins of ZO family and cingulin are involved in the connection of TJs to the actin cytoskeleton. These scaffolding proteins recruit several signaling proteins and transcription factors to the TJ sites (Fig.3). More than 40 proteins, including transmembrane, scaffolding and signaling proteins, have been found to be associated with TJs and form multimeric protein complexes to receive and send regulatory signals (González-Mariscal *et al*., 2003).

1.4.1.1Claudin proteins

Cldns are Transmembrane proteins, with MW of 20–27 kDa that appear to constitute the ultrastructural TJ strands. Transfection of cldn-1 and -2 into cultured fibroblasts resulted in the formation of a network of typical tight junctional strands as evidenced by freeze-fracture analysis (Furuse *et al*., 1998b). Subsequent research has expanded the member number of this multigene family in mouse and human to 24 genes. Differential expression has been described for cldns, suggesting their tissue specific function. For instance cldn-1 deficient mice die rapidly due to accelerated epidermal water loss and show poorly developed TJs in their epidermis, indicating

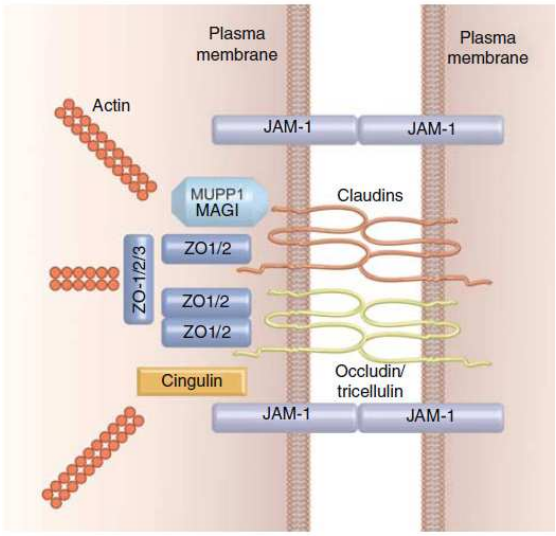

Figure3: Schematic representation of the basic structural transmembrane and cytoplasmic components of tight junctions. Cldns and occludin are 4-pass proteins while JAM-1 is single-pass. Each cytoplasmic protein, ZO-1 or ZO-2 is important for clustering of cldns and occludin, resulting in the formation of tight junctional strands. The role of the other scaffolding proteins (ZO-3/MAGI/MUP1) is less clear. The ZOs and cingulin can provide a direct link to the actin cytoskeleton (adapted from Niessen, 2007).

that cldn-1 is the crucial barrier type cldn in the epidermis and is required for the maintenance of the inside-out barrier in mammalian epidermis. In addition to cldn-1 other cldn proteins including cldns-4 -5 -6 -7 -11 and -12 are also found to be expressed in the epidermis, although the role of each cldn in the maintenance of epidermal barrier property is not clear (Furuse *et al*., 2002).

On the other hand, cldn-1 and -5 are associated with maintenance of normal BBB function (Vorbrodt and Dobrogowska, 2003) and appear to be important in angiogenesis and in disease processes with disturbed vascular permeability. Indeed cldn-5 knockout mice are characterized by a size-selective loosening of TJs in BBB against small molecules (<800 Daltons) but not larger molecules showing that cldn-5 regulates size selectivity of the BBB (Nitta *et al*., 2003).

1.4.1.2 Occludin

Occludin as the first TJ transmembrane molecule discovered is a protein with MW of approximately 65 kDa (Furuse *et al*., 1993). Occludin deficiency in mice did not exhibit an evident alteration in epidermal barrier function although the vascular barrier function in these mice was not determined, nevertheless, the mice exhibited several different phenotypes, such as growth retardation, male sterility, gastritis and mineral deposits in the brain, suggesting vascular barrier impairment in CNS (Saitou *et al*., 2000). Occludin shows a highly consistent expression in cerebral endothelium and reveals staining in distinct continuous pattern along the cell margins in CNS endothelium, while it is almost sparsely distributed in non-neural endothelium

(Hawkins and Davis, 2005). Tricellulin is another TJ protein identified with structural similarity to occludin. Unlike other TJ proteins, tricellulin is enriched only at tricellular TJs, where it enforces the barrier function of epithelial cell sheets (Ikenouchi *et al*., 2005).

1.4.1.3 Junctional adhesion molecules (JAMs).

The 40-kDa, IgG-like JAM family proteins are the third group of transmembrane receptors found at tight junctions. The JAM family comprises JAM-1, JAM-2, and JAM-3, also designated as JAM-A, JAM-B and JAM-C, respectively. In the form of single-pass proteins, JAMs have a large extracellular domain that mediates homophilic and probably also heterophilic interactions in the tight junctional region but do not induce the formation of TJ strands when expressed in fibroblasts. Cell type specificity seems to govern cellular tendency in expressing different JAM members. For example, JAM-1 is predominantly expressed in epithelial cells while epithelia do not express other related JAMs (-2 and -3) and lymphatic cells express only JAM-1 and -2. On the other hand all JAM family proteins (-1, -2 and -3) are present in various endothelial cells, where they appear to differentially regulate paracellular permeability. Brain endothelial cells express only JAM-1 but not JAM-2 which together with JAM-1 expression in epithelia implies a putative function in TJ formation or function (Aurrand-Lions *et al*., 2001).

However, expression of JAMs is not exclusively restricted to cells with TJs but also other cells such as circulating monocytes, neutrophils, lymphocytes, and platelets, as well as dendritic cells also express JAMs thereby contributing to their transendothelial migration (reviewed by Ebnet *et al*., 2004)

1.4.1.4 Zonula occludens (ZO) proteins

Scaffolding zonula occludens or ZO proteins are cytoplasmic phosphoproteins that associate with the cytoplasmic side of TJs and provide a link between TJs and the actin cytoskeleton. Importantly as so far no direct interactions have been identified between occludins, cldns and JAMs, cytoplasmic binding partners must fulfil this scaffolding function. ZO proteins (ZO-1, ZO-2, and ZO-3) belong to the membrane-associated guanylate kinase-like homologs family and are characterized by three N-terminal PDZ domains, an SH3 domain followed by the GUK domain. The multiple binding domains in ZO-1 have scaffolding function, with the PDZ-1 region binding to the cldn, the PDZ-2 domain binding to ZO-2, and the SH3-GuK region binding to both the occludin and the adherens junction proteins afadin and cadherin via α-catenin. The C-terminus of ZO molecules can associate with actin which provides a direct link with the cytoskeleton (reviewed by Niessen, 2007). ZO-1, a phosphoprotein with MW 220-kDa and broad expression in most endothelial and epithelial cells is localized to tight junctions via its actin-binding domain and despite its expression in cell types without TJ formation, no TJ exists without ZO-1 therefore immunostaining for ZO-1 reflects maturation status of TJs. In addition,

ZO-1can also directly interact with JAMs and form homodimers or heterodimers with either ZO-2 or ZO-3. Very much like ZO-1, ZO-2 associates with transmembranous proteins of the TJ and transcription factors, and it is localized in the nucleus during stress and proliferation. It is not only considered as an extremely important structural protein, but also a nuclear factor affecting gene expression and blocking cell cycle progression (Niessen, 2007).

1.4.1.5 Cadherin/catenin adhesion complex

Classical cadherins were the first family of adhesion molecules found in the adherens junction and include type I, single-pass transmembrane glycoproteins that mediate Ca^{2+}-dependent intercellular adhesion. Specific adhesion function is conferred by the cadherin ectodomain, which engages an identical molecule on the surface of an opposing cell, thereby called "homophilic" interaction; whereas the cadherin cytoplasmic domain mediates key structural and signaling activities required for adhesion through its association with three distinct cytoplasmic proteins known as catenins. β-catenin (or the highly homologous γ-catenin/plakoglobin) are arm-repeat proteins (Michels *et al*., 2009a-b).

Calcium is key factor to allow homophilic interaction between E-cadherin molecules and crystal structures of ectodomain regions containing multiple EC domains show that the connections between successive domains are rigidified by Ca^{2+} coordination (Reviewed by Shapiro and Weis, 2009). In cultured keratinocytes, increased extracellular calcium levels stimulate formation of adherens junctions, causing both cytoskeletal reorganization and complexing of junctional proteins such as E-cadherin and α-catenin. Actin polymerization and formation of filopodia are among the earliest responses to raised extracellular Ca^{2+} leading to keratinocytes differentiation (Vasioukhin *et al*., 2000).

Three major cytoplasmic partners of E-cadherin are α-catenin, β-catenin, and plakoglobin (also known as γ-catenin). The cytoplasmic region of E-, N-, and P-cadherins bind to β-catenin or plakoglobin, which in turn binds to α-catenin. The high level of sequence identity in the cadherin cytoplasmic region suggests that all classical cadherins interact with the catenins in this fashion. α-Catenin has a number of binding partners, including actin. In addition, p120 catenin, which belongs to a subfamily of armadillo proteins, interacts with juxtamembrane fragment of the cadherin cytoplasmic domain (Reviewed by Shapiro and Weis, 2009; Niessen and Gottardi, 2008).

1.4.2 Regulation of TJs/AJs by the polarity complex aPKC/Par3/Par6

Several proteins regulating epithelial cell polarity have been characterized at TJs and AJs. One such complex is ternary aPKC/Par3/Par6 complex which was initially identified in a genetic screen searching for mutations that disrupted polarization of the *Caenorhabditis elegans* zygote (Tanentzapf and Tepass, 2003). Functional interference with any of these proteins affects

paracellular permeability, indicating their importance in the assembly of functional TJs (Anderson *et al*., 2004; Shin *et al*., 2006; Chen and Macara, 2005).

The Par complex is potentially capable of regulating AJ formation in endothelial cells. This relies on direct interaction of Par-3 and Par-6 with VE-cadherin. Among other types of cadherin molecules, this binding in only possible for VE-cadherin as P- N- and E-cadherin lack the PDZ domain required for interaction with Par proteins. This association might account for the distinct type of cell polarity pattern which is seen in endothelial cells. This interaction is suggestive of a uniquely localized aPKC-free Par-3, Par-6 protein complex at AJs via direct binding of both Par proteins with VE-cadherin which does not appear to cause polarization (Iden *et al*., 2006).

1.4.2.1 Genomic structure and protein isoforms of mouse Par-3

According to the available online genomic data, the mammalian homologue of *C. elegans* Par-3 gene, ASIP (atypical PKC isotype-specific interacting protein) which was initially characterized by Izumi and colleagues (1998), is mapped to the distal end of the mouse chromosome 8 in chromatid region E2. The full-length mouse Par-3 transcript comprises 25 known coding exons (Fig.4A) and yields a 180 kDa protein of 1337 amino acids which consists of three domains, CR1 in the NH2-terminal domain, CR2 in the middle and a CR3 domain in the COOH-terminal (variant3, Pubmed ID, NM_033620.1). There are also other splice variants present in mouse tissues and cells which have the molecular weight of 150 and 100 kDa and result from termination of transcription in exons 19 and putative 15b of the full length gene respectively. The 180 kDa isoform appears to be the most abundant variant during embryonic development and in mouse brain whereas in heart and kidney the usual isoform is the 150 kDa variant (Fig.4B) (Izumi, *et al*., 1998; Lin *et al*., 2000). However Duncan and colleagues (2005) have reported the presence of additional transcripts for Par-3 in mouse oocyte and fertilized eggs which had not been characterized earlier and are supposedly originated via utilizing an alternative start codon which maps to exon 4 of the full length gene. The novel isoforms consist of 13 and 21 exons resulting in proteins with corresponding molecular weights of 73/76 kDa, (variant 2, Pubmed ID NM_001013580.2) and 133/135 kDa (variant1, Pubmed ID, NM_001013581.2) respectively. (Duncan *et al.,* 2005).

1.4.2.2 Protein domains and interaction partners of mouse Par-3

Par-3 CR1 domain in the N-terminal region, is an oligomerization domain required for Par3 self-oligomerization as in yeast two-hybrid system the full length Drosophila homolog of the Par3, Bazooka, was able to bind to the mammalian CR1 domain. This interaction is direct and has been further validated using *in vitro* translation system (Benton and St.Johnston, 2003). The CR2 domain comprises 3 PDZ domains, PDZ-1, PDZ-2 and PZD-3. The PDZ1 domain is interacting partner for another polarity protein, Par-6 (Johansson *et al*., 2000; Ebnet *et a.l*, 2001) as well as for integral Ig-like cell-cell adhesion molecules, JAM-1, -2 and -3, nectin-1 and

nectin-3 (Ebnet *et al*., 2003; Takekuni *et al*., 2003). Par3 is expressed by endothelial cells in most tissues such as the tongue and the heart endothelium where its association with JAMs is proposed to anchor the PAR-3/aPKC/PAR-6 complex to TJs (Ebnet *et al.,* 2003). Besides mediating role in cell polarity and TJ formation, it is shown recently that the N-terminal dimerization and PDZ1 domains of Par-3 bind to dynein light intermediate chain 2 that results in the proper centrosome orientation during cell migration via local regulation of MT dynamic (Schmoranzer *et al*., 2009).

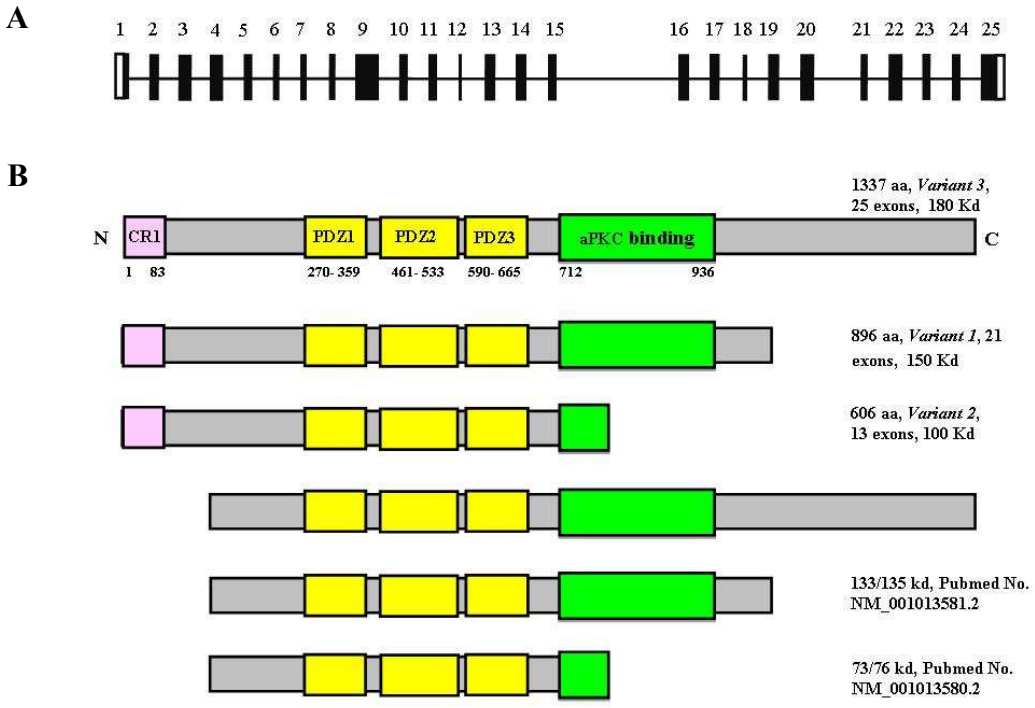

Figure 4: (A) Genomic structure of PAR-3. Exons, represented as boxes, are numbered and drawn to scale. White fraction of box in exons 1 and 25 shows 5´and 3´UTR regions. **(B) Diagrams of different possible Par-3 proteins isoforms.** All possible protein isoforms are drawn under their respective coding exon in the genome. Two Par-3 start codons and three stop codons exist. The first start codon is situated in exon 1 and second one in exon 4. In total six isoforms are possible. The N-terminal region with CR-1 domain, three PDZ domains and the aPKC binding site is shown. The PDZ domains but not CR-1 and aPKC domains are present in all isoforms.

The PDZ2 domain of Par-3 shows high affinity to phosphoinositides (PIPs) and this binding is critical for the its localization to cell membrane in MDCK cells, interestingly the same study revealed direct binding of the PIP Phosphatase, PTEN, to the juxtaposing PDZ3 domain of Par-3 which could facilitate quick hydrolysis of PIP3 by nearby PTEN (Wu *et al*., 2007). Later it was demonstrated that localization of the PTEN to cell-cell junctions is essential for the polarization of mammalian epithelial cells *in vitro*. As polarized distribution of PIP-2 and PIP-3 lipids is important determinant of cell polarity, Par-3 appears to function as a gate

keeper to maintain the phosphoinositide concentration gradient in polarized cells and therefore guide the polarity cues (Feng *et al*., 2008).

The CR3 domain contains aPKC binding site, inside which there is a region with two highly conserved serine residues (827 and 829). Par-3/aPKC association leads to Par-3 Ser827 phosphorylation by aPKC resulting in its detachment from aPKC that is observed during the initial phase of tight junction formation and is believed to be a critical step in epithelial polarization in mammalian cells (Izumi *et al*., 1998; Hirose *et al*., 2002; . Nagai-Tamai *et al*., 2002). The carboxy-terminal region of Par-3 contains a direct binding site for the Rac exchange factor Tiam1. Par-3 binding with Tiam-1 is speculated to either inhibit Tiam1 activity or sequester Tiam1 to a region of the cell where it is not accessible to Rac. Nevertheless, this binding is essential for tight junction assembly in simple epithelial cells via inhibition of Rac by Tiam1 in TJ sites (chen and Macara, 2005). Overall, Par-3 appears to nucleate the recruitment of the Par complex proteins to TJs via binding to JAM molecules and is required for assembly and function of TJs.

1.4.3 The *stratum corneum*: protein and lipid barrier

Constant regeneration of the skin requires stem cells with almost unlimited mitotic potential in the basal layer which are subject to a complex series of differentiation scenarios during their upward journey towards the skin surface. Final differentiation outcome for keratinocytes in the suprabasal layer is the formation of the cornified envelope (CE). The CE formation is dependent on the expression of certain type of keratins in the suprabasal layer of the epidermis. This happens concomitant with extensive protein-protein and lipid-protein crosslinking activities mediated by transglutaminase enzymes that catalyze the formation of protein-protein epsilon-(gamma-glutamyl) lysine cross-links in ascending, differentiating keratinocytes. Crosslinking activity will culminate in the formation of a firm insoluble CE structure in epidermal surface. CE is composed of flattened cage like lipid coated structures containing keratin intermediate filaments, called corneocyte envelopes. Concerted with synthesis, deposition and crosslinking of CE proteins, the granular layer keratinocytes produce a diverse spectrum of specialized lipids that accumulate in vesicles entitled lamellar bodies. The lamellar bodies will finally fuse with the apical membrane of the topmost keratinocytes in the granular layer and exocytose their lipid content into the interface between the granular and cornified layers. The excreted lipids are crosslinked to the exterior face of the CE and also form the extracellular lipid sheets that surround the dead corneocytes. The corneocyte interconnection to each other and to the granulocytes *via* corneodesmosomal proteins in combination with extracellular lipid lamellae forms the functional barrier of the cornified envelope. The dead corneocytes will be peeled off in a process called desquamation or

shedding of the cornified cells in the most exterior zone of the skin (Reviewed by Candi *et al.,* 2005; Kalinin and Kajava, 2002; Sandhoff, 2010).

1.4.3.1 Protein components of the cornified envelope

There are a growing number of proteins which are being identified as components of the CE. The key proteins incorporated into CEs are Loricrin, Involucrin, Periplakin, Envoplakin, Small Proline-Rich proteins (SPRs), trichohyalin and late cornified envelope proteins (LCE). CE proteins have several shared features such as having highly basic isoelectric charge but each one show a distinctly unusual amino acid composition compared to the others. On the other hand, filaggrin-bound keratin intermediate filaments composed of keratin-1 and -10, and corneodesmosomal proteins such as desmoplakin are minor CE components (Steinert and Marekov, 1999). The majority of the CE structural proteins are encoded by a gene cluster region called the Epidermal Differentiation Complex (EDC) on human chromosome 1q21 (Marenholz *et al.,* 2001) and mouse chromosome 3 (Moseley and Seldin, 1989). Most of the genes within this region show similarity in their genomic structure and amino acid sequence. For instance loricrin, involucrin and SPRs show peptide sequence homology in their N- and C-terminal domains with enrichment of conserved Gln AND Lys residues. Additionally the exonal structure of involucrin, loricrin, most of SPR genes and LCE genes is similar. These genes comprise two exons with a single intron and the entire open reading frame is located in exon 2. The mentioned similarities have resulted in hypothesis that the genes within EDC region have diverged from a single ancestral gene by gene duplication. Subsequently the genes have evolved their unique characteristics through further gene duplications and DNA base change events (Backendorf and Hohl, 1992; Gibbs *et al.,* 1993).

1.4.3.2 Filaggrin gene and protein structure in humans and mouse

Filaggrin or 'filament-aggregating protein' was first coined in 1981 to represent a class of structural protein isolated from the *stratum corneum* (Steinert *et al*., 1981). Human profilaggrin is encoded by the FLG gene within the EDC region on chromosome 1q21. The FLG gene comprises three exons and two introns (Presland *et al*., 1992; Markova *et al*., 1993). Exon 1 is noncoding and protein translation starts within exon 2, while the bulk of profilaggrin protein is encoded by the large third exon (~12.5 kb). Human profilaggrin is a histidine-rich protein with MW of ~400 kDa which comprises between 10 and 12 tandemly oriented filaggrin repeats, which are flanked on both sides by two partial filaggrin repeats and by N- and C-terminal domains. Human filaggrin repeats are identical in size having 324 amino acids and contain a short linker domain that is cleaved during conversion of the profilaggrin into active monomeric filaggrin (Gan *et al*., 1990; McKinley-Grant *et al*., 1989; Presland *et al*., 1992).

Mouse *flg* gene is located on chromosome 3 within EDC region and comprises two types of repeating units, type A and type B which are dispersed within gene sequence. In total 20 FLG repeats have been reported including 9 type A repeats and 11 type B repeats. Type A repeats (765 bps) encode 255 amino acids, whereas type B repeats (750 bps) encode peptides containing 250 amino acids (Rothnagel *et al*., 1994; Rothnagel and Steinert, 1990). Mouse profilaggrin is a short-lived large protein with MW >300 kDa consisting of multiple tandem repeats separated by a short 7-10 amino acid linker peptide (Dale *et al*., 1994).

1.4.3.3 Filaggrin expression, function and processing

Profilaggrin is initially synthesized as a highly phosphorylated insoluble proprotein and is accumulated in keratohyalin granules in granular layer of epidermis. The early phosphorylation appears to prevent its premature binding to keratin filaments. The insoluble nature of the proprotein might facilitate its packing into keratohyalin granules. During cornification it is proteolytically cleaved in linker sites and dephosphorylated to release individual filaggrin monomers. Mouse monomeric FLG is ~26 kDa in size and is responsible for binding to intermediate keratin fibrils and aggregating them to keratin bundles in the cornified layer. The aggregation function of FLG would provide a model causing shape change of cornified keratinocytes from ellipsoid to flattened morphology. Altogether CE proteins, keratins and filaggrin contribute approximately 80-90% to dry mass of the epidermis. Furthermore, highly histidine-rich composition of FLG plays a key role in hydration of the skin, as processing of FLG into a mixture of hygroscopic compounds and their derivatives, such as pyrrolidone carboxylic acid (PCA), results in providing the natural moisturising factor (NMF) for the skin (Review by Candi *et al*., 2005). A novel role for FLG is protection against UV light; which comes from a study showing that mice deficient in a Caspase-14, a protease involved in proteolytic degradation of FLG resulted in increased sensitivity to UV damage (Denecker *et al.*, 2007).

Processing of profilaggrin to FLG occurs in several steps. It initiates with excision of the N-terminus happening concurrently with processing of the poly-filaggrin sequence, first into 2-4 filaggrin repeat intermediates and finally into mature (monomeric) FLG. Several endoproteases are known to engage profilaggrin processing, including calpain I (μ-calpain), a chymotrypsinlike enzyme, PEP1, furin or a related proprotein convertase (with specific involvement in cleavage of the N-terminus from profilaggrin), matriptase (MT-SP1), and the serine protease prostatin (CAP1/Prss8). Caspase-14 can cleave profilaggrin within the N-terminal portion as well inside each filaggrin domain. Caspase-14 is specially important during final step in filaggrin degradation to free amino acids within the *stratum corneum* (Reviewed by Presland, 2009).

1.4.4 Lipid components of the cornified envelope

Barrier function of the cornified layer is conferred by conducive function of previously described proteins as well as lipid components including cholesterol, free fatty acids and ceramides. Major class of lipids in CE formation are ceramides, accounting for over 50% of the CE lipids. CE ceramides exist either as free unbound lipids in the extracellular lipid lamellae or lipids covalently crosslinked to proteins on the exterior face of the cornified envelope specially involucrin. Ceramides belong to the class of sphingolipids and display the greatest molecular heterogeneity in terms of sphingoid base and fatty acid composition. They are composed of a sphingoid base, sphingosine, phytosphingosine or 6-hydroxysphingosine which is N-acylated by a long-chain fatty acid. The lipids components of the extracellular matrix are synthesized by keratinocytes in the *strata spinosum and granulosum* and packed into disk-like, lipid membrane structures within specialized vesicles, called lamellar bodies. Lamellar bodies exocytose their content to the cell surface shortly before the keratinocytes transform into dead corneocytes.

Esterification of the ω-hydroxy group of ceramides with very long chain allows their covalent crosslinking to other lipids or CE proteins; as a result, they are either bound to long chain fatty acids, especially linoleic acid, or to glutamate residues of cornified envelope proteins (Sandhoff, 2010).

As precursor for epidermal ω-hydroxy ceramides and other lipids, epidermis also contains lower concentrations of corresponding ω-hydroxy glucosylceramides (GlcCers) which are also referred to as probarrier lipids. As a major step in the production of epidermal ceramides and in a process of extracellular lipid modification, free and protein bound ω-hydroxy GlcCers are degraded to ω-hydroxy ceramides. This conversion is mediated by β-glucocerebrosidase (β-GlcCerase) and inactivation of either β-GlcCerase or its activator protein Prosaposin (pSAP) in the epidermis results in disturbed epidermal permeability barrier formation and reduced epidermal ceramide content (Doering *et al*., 1999-a, 1999-b).

1.5 The insulin-like growth factor (IGF) system

1.5.1.1 IGF-1R and IGF-2R receptors and IGF binding proteins (IGFBPs)

The evolutionarily conserved IGF system is involved in regulation of growth, proliferation and survival. The system operates through polypeptides; 1) IGF-1, IGF-2 and insulin, 2) the IGF binding proteins; 1-6, 3) the receptors; IGF-1R, IR, hybrid IR/IGF-1R, IGF-2R; and 4) IGFBP-proteases: IGF-1, IGF-2 and insulin polypeptides are highly homologous showing derivation from a common ancestral precursor hormone (Daughaday and Rotwein, 1989), (Reviewed by Denley *et al*., 2005; Rajpathak *et al.*, 2009). IGF-I is predominantly synthesised in the liver and delivered to target tissues via systemic circulation (endocrine secretion), but based on its local production in most tissues, paracrine/autocrine signaling manner is also

possible (Abbas *et al*., 2008). IGF-I has also been suggested to have a role in glucose and lipid metabolism by promoting peripheral uptake of glucose and protecting against insulin resistance (reviewed by Rajpathak *et al*., 2009).

IGF-2 is a close relative of IGF-1 and according to both murine models and humans plays important roles during prenatal life by regulating the normal foetal growth and development (Chao and Amore, 2008). Systemically circulating IGF-2 is maintained in humans throughout life and is actually the predominant IGF in adult humans, the levels being 5-10-fold higher than IGF-1 (Frystyk, 2004). IGF-2 signal transmission occurs through binding to IGF-IR, with as high affinity as to its own receptor IGF-2R, and also through the IR isoform A to which it binds with equal affinity as insulin (Denley *et al*., 2004). For long time the assumed role for IGF-2R was modulation of IGF-2 bioavailability by internalizing and targeting IGF-2 for lysosomal degradation (Ellis *et al.,* 1996); however, studies on endothelial progenitor cells from umbilical cord blood showed endothelial progenitor cells to have a high expression of IGF-2R, where IGF-2 and IGF-2R contributed in vasculogenesis at ischemic or tumour sites (Maeng *et al*., 2009).

The level of free IGFs in the circulation is regulated by IGF-binding proteins (IGFBP) 1-6, mainly IGFBP-3, acting as IGF depot in the blood. IGFBPs control IGF bioavailability by forming complexes with IGFs, thereby extend their metabolic half-life and modulate the direct binding of IGFs to their receptors. IGFBP-3 as the most common IGFBP forms a ternary complex of 150 kDa together with each of IGF and the acid-labile subunit (ALS). *In vivo* the majority of IGF-1 and IGF-2 polypeptide pool is bound to IGFBPs and only less than 1% is free and bioactive (Frystyk, 2004). The IGF-1-IGFBP-3 complex extends the IGF-1 half-life in serum from 10 minutes to 12-15 hours by preventing IGF-I proteolysis (Rajpathak *et al*., 2009).

1.5.1.2 Insulin

Insulin is a key regulator of glucose metabolism by regulating glucose uptake and production and is also involved in other metabolic reactions such as lipolysis and protein synthesis. Insulin secretion from β-cells in the pancreas is stimulated by high blood glucose and amino acids. The central given function of activated insulin receptor is promoting glucose uptake in adipose tissue and skeletal muscles via translocation of the insulin responsive glucose transporter (GLUT4) to the cell surface (Saltiel and Kahn, 2001). In the circulation insulin is free, i.e. not bound to binding proteins which enables it to act quickly. Unlike IGFs, blood insulin level is prone to changes induced by glucose uptake, with high postprandial peaks in response to meals and low levels between meals and during the night (Frystyk, 2004).

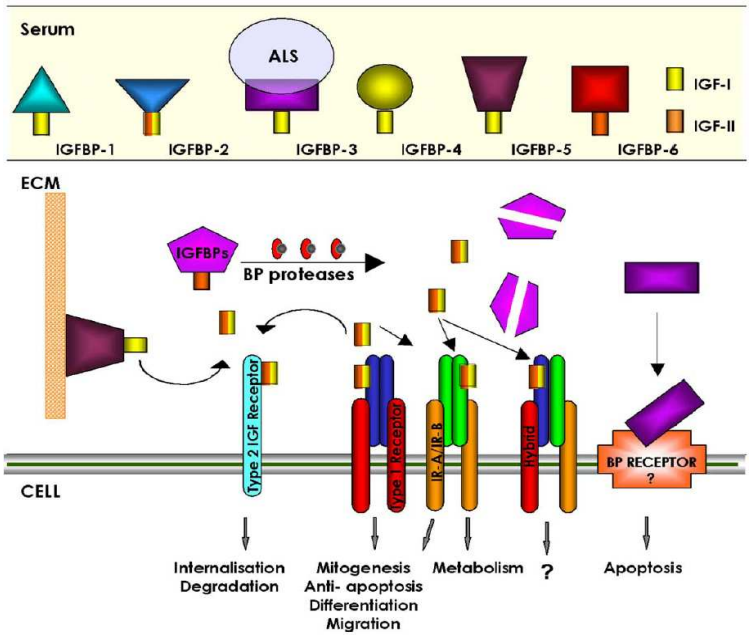

Figure 5: Schematic representation of the IGF system. The IGF system consists of the receptors (IGF-1R, two IR isoforms, IGF-1R:IR hybrids and IGF-2R), the peptides (IGF-I, IGF-II and insulin) and six high affinity IGFBPs. IGFs circulate mainly in an IGF:IGFBP-3:ALS complex. Release of IGFs from IGFBPs occurs upon IGFBP proteolysis or extracellular matrix (ECM) binding. IGFBPs can also act independently of IGF entering the cell via as yet undefined receptors. IGF-2R modulates the bioavailability of IGF-II (adapted from Denley et al., 2005).

1.5.1.3 Structural homology of insulin receptor and IGF-1 receptor

The heterotetrameric membrane glycoproteins, insulin receptor (IR) and IGF-1 receptor (IGF-1R) belong to the tyrosine kinase family and show 84% homology in the β-subunit of tyrosine kinase domains. Unlike other receptor tyrosine kinases, which are activated by ligand dimerization, IR and IGF-1R are already dimerized at the cell surface as a tetramer composed of two disulphide-linked αβ-dimers, where each αβ-dimer consists of an extracellular α-subunit and a transmembrane β-subunit (Ullrich *et al*., 1986). The extracellular α-subunits of the IR and IGF-IR contain six structural domains, of which ligand-binding determinants have been localized to the L1, cysteine-rich and L2 domains and to the C-terminal peptide sequence. β-subunits as intracellular domains of the receptor are the parts which are tyrosine phosphorylated and subsequently transduce the signal (Benyoucef *et al*., 2007).

1.5.1.4 Hybrid insulin receptor/IGF-1 receptor

Given the close homology between IR and IGF-1R, in tissues with normal expression of each single receptor, hybrid IR/IGF-1R receptors (HR) are known to form by random assembly of receptor hemidimers consisting of one IR αβ-dimer and one IGF-1R αβ-dimer (Moxham *et al*., 1989; Soos and Siddle, 1989). Hybrid receptors have been demonstrated in many tissues

including skeletal muscle, adipose tissue, placenta, breast cancer cells and osteoblasts. (Reviewed by Arnqvist, 2008; Frasca *et al*., 2008). Studies carried out with purified hybrid receptors suggest that these receptors mostly bind IGF-1, while they bind insulin with a much lower affinity (Soos *et al*., 1993; Pandini *et al*., 1999) although their roles in cellular responses remain unclear and present a challenge to IGF/insulin researchers (Fig.6).

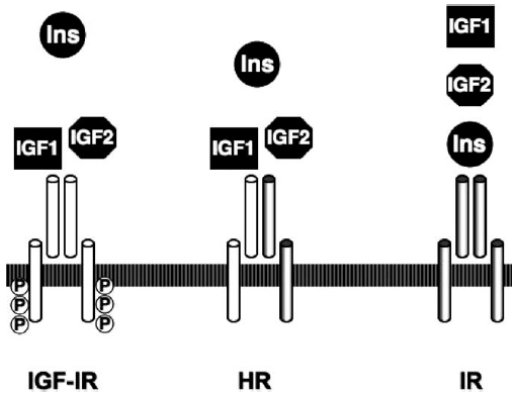

Figure 6: Schematic representation of hybrid receptors. In cells and tissues expressing both IR and IGF-1R, IR hemireceptors may heterodimerize with IGF-1R hemi-receptors, leading to the formation of hybrid IR/IGF-1Rs (HRs), which bind IGF-1 and IGF-2 with high affinity and insulin with a much lower affinity (adapted from Frasca et al., 2008).

1.5.1.5 Activation of receptors and signaling pathways

First step in the initiation of biological effects of insulin, IGF-1 and IGF-2, is binding to their receptors, IGF-1R, IR or hybrid IR/IGF-1R. The putative ligand binding pockets are located in the cysteine rich portion of the extracellular α subunits whereas the β subunit contains tyrosine kinase domain, ATP and substrate binding pockets and autophosphorylation sites (De Meyts and Whittaker, 2002).

Insulin/IGF-1 ligand binding will cause a conformational change in the receptor structure which will bring the receptor domains close together and initiate autophosphorylation of several tyrosine residues on the β-subunits. IGF-1R and IR demonstrate overlap in directing downstream signaling events, the critical nodes being IRS proteins 1-4, phosphatidylinositol 3-kinase (PI3K) and Akt in the PI3K-pathway which is generally considered to be responsible for most of the metabolic effects, and Erk 1/2 in the Ras mitogen-activated protein kinase (MAPK) pathway which in cooperation with the PI3K-pathway control mitogenic and differentiation responses (Taniguchi *et al*., 2006).

The downstream Akt pathway is activated by mTOR to ensure both a reasonable level of nutrients and a positive signal for cell growth and division. The binding of IGF-1 to its tyrosine kinase receptor (IGF-1R) results in the recruitment of the PI3 kinase (PI3K) to the plasma membrane and its activation. PI3K, in turn, phosphorylates the phosphoinositides, increasing the concentration of PIP3 at the plasma membrane. Increased PIP3 activates PDK1

and mTORC2 (PDK2). The resultant phosphorylation of Akt on Thr_{308} by PDK1, and on Ser_{473} by mTORC2, respectively, leads to the full activation of Akt. Akt then phosphorylates several cellular proteins, including FOXO transcription factors, BAD, MDM2, and GSK3α/β to facilitate cell survival and cell cycle entry. The IGF-1/ Akt pathway regulates mTORC1 through Akt phosphorylation of TSC2 on multiple sites; this inhibits the TSC2 GTPase activity, resulting in the activation of Rheb and mTORC1. This coordination of IGF1/ Akt and mTOR pathways enables the activation of mTOR that in turn promotes cell growth in response to the stimulation of growth factors, including insulin and IGF-1 (Reviewed by Feng and Levine, 2010). Therefore IR/IGF-1R signaling will result in the regulation of cell metabolism, proliferation, and survival (Baserga and Hongo, 1997; Pollak, 2008), depending on cell type (Fig.7).

1.5.2 Insulin signaling in diabetes and gene knockout models for IR/IGF-1R

In pathological condition of diabetes mellitus type 2, insulin insensitivity occurs which is due to decreased insulin receptor signaling and leads to abrogated glucose take up in insulin target tissues resulting in increased circulating glucose or hyperglycemia (Clauser, 1994).

Mice lacking insulin receptors are born with normal visible parameters but develop early postnatal diabetes and die of ketoacidosis (Accili *et al*., 1996). On the other hand inherited mutations nullifying the human IR gene, result in severe intra-uterine growth retardation, failure to thrive, and hypoglycemia which indicates that insulin receptor also promotes embryonic growth (Reviewed by Kitamura *et al*., 2003).

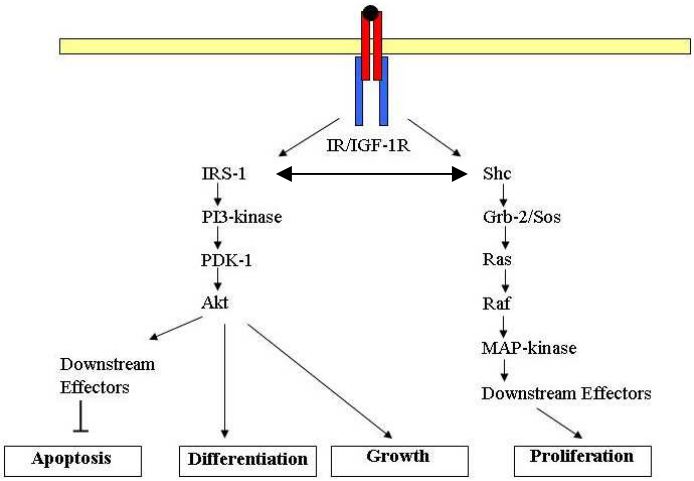

Figure 7: scheme showing IR/IGF-1R signaling pathway. Insulin/IGF-1 ligand binding to the IR/IGF-1R leads to autophosphorylation on different tyrosines in the kinase domain, followed by recruitment of IRS-1 and PI3K activation. This interaction leads to recruitment and activation of phosphoinositide dependent kinase-1 (PDK1) and AKT/protein kinase B via phosphatidylinositol 3, 4, 5-triphosphate (PIP3) production. Another pathway activated through IRS-1 signaling is the MAPK pathway. Downstream molecules in IR/IGF-1R axis have diverse roles in promoting growth, proliferation, differentiation and protection against apoptosis.

The knowledge about mammalian IGF-1R in development was obtained from analysing the IGF-1R null mice. IGF-1R knockout mice have 45% of the size of their wild type siblings at birth and die shortly after birth due to severe organ hypoplasia (Liu *et al*., 1993). Cultured IGF-1R$^{-/-}$ fibroblasts showed slower growth compared to wild-type fibroblasts and were not able to proliferate under anchorage-independent conditions (Sell *et al*., 1993). Together with IR, skeletal muscle also shows abundant expression of IGF-IR that can enhance muscle glucose uptake *via* mobilisation of GLUT-4. Inactivation of IGF-IR in skeletal muscle in mice causes severe insulin resistance and type 2 diabetes at an early age, implicating an important function for IGF-I in glucose homeostasis (Fernandez *et al*., 2001).

1.6 Regulation of endothelial function by Insulin/IGF-1 signaling and in Diabetes

1.6.1 Role of IR and IGF-1R signaling in endothelial cells

Endothelial insulin and IGF-1 signaling pathways alone do not appear to play an essential role in the normal development of retinal vasculature and vascular barrier function under steady state homeostasis conditions. *In vivo* inactivation of mouse IR or IGF-1R genes had no major consequences on vascular development or glucose homeostasis under basal conditions (Vicent *et al*., 2003). However, early postnatal hypoxia stimulation to induce artificial retinal neovascularization in mice with either endothelial specific inactivation of IR or IGF-1R resulted in 57% and 34% reduction of neovascularization areas respectively (Kondo *et al*., 2003). This is suggestive of the central role of insulin and IGF-1 signaling under challenging hypoxia conditions. In contrast to the stimulatory effect of IGF-1 signaling in the development of retinopathy in mice (Kondo *et al*., 2003), human preterm infants born with low levels of IGF-1 in their serum show a higher risk of developing retinopathy of prematurity (ROP), a hypoxia induced pathological neovascularization in retina (Heidary *et al*., 2009). Intraocular overexpression of IGF-1 ligand in transgenic mouse models contributed to accumulation of VEGF and BRB breakdown, marked by increased vessel paracellular permeability to mannitol (182 Da) and HRP (44 kDa) (Haurigot *et al*., 2009). IGFBP-3 as key regulator of IGF-1 activity is seen to be significantly increased in neovascular tufts of the OIR retina, suggesting the local regulatory functions of IGFBP-3 in the retina (Lofqvist *et al*., 2009).

Angiogenesis response in healing skin wounds that leads to the formation of new blood vessels in the wound bed is driven by hypoxia (Wattel *et al*., 1990). Wound healing procedure is significantly impaired in diabetic wounds resulting in decreased time of closure. Following the role described for IGF-1 signaling in retinal neovascularization and vascular leakage, it is an open question if disturbed insulin/IGF-1 signaling in endothelial cells can underlie the defective wound healing response seen in diabetic patients.

1.6.2 Blood-retinal-barrier breakdown in diabetes

Increased vascular permeability associated with angiogenesis underlies the pathology of diabetic retinopathy (DR) in type 1 diabetic patients. DR is a late onset complication of diabetes and is the major cause of vision loss in the working age population in developed countries. On the other hand excessive edema due to the breakdown of the BRB is the main event involved in the pathogenesis of diabetic macular edema (DME) seen in type 2 diabetic patients (Reviewed by Simó *et al*., 2010). Despite reported increase of intraocular IGF-I levels in diabetic patients, the induction switch for such IGF-1 elevation and the source of IGF-I production is not clear (Haurigot *et al*., 2009). Nevertheless, studies with systemically infused small molecular weight tracers have shown leaky interendothelial cell tight junctions in retinal vessels of diabeteic rats and dogs (Wallow and Engerman, 1977; Ishibashi *et al*., 1980) indicating uncontrolled fluid diffusion through disrupted endothelial TJs in diabetic retinopathy.

The development of DR is hypothesized to be at least in part driven *via* elevated intraocular VEGF expression. VEGF induced vascular permeability is accompanied with rapid phosphorylation of the intracellular tail of VE-cadherin leading to its endocytosis and disruption of the endothelial barrier function (Gavard and Gutkind, 2006).

Elevated MMP-mediated proteolytic degradation of endothelial type VE-cadherin and reduction in its transcript levels is seen in retinal vessels of streptozotocin-induced diabetic rats which was coincident with increase in retinal vascular leakiness (Navaratna *et al*., 2007). Similar to interrupted VE-cadherin expression and processing, reduction in cadherin-5 is presumably another landmark of leaky endothelial junctions in DR (Davidson *et al*., 2000).

Occludin as an integral TJ protein is reportedly target for deregulation in retinal vessels from DR. For instance, rats with STZ-induced chronic diabetes represented decreased occludin content and immunostaining at cell junctions parallel with increased BRB permeability (Harhaj *et al*., 2006). Similar change in occludin content was also recapitulated *in vitro* by VEGF treatment of bovine retinal endothelial cells. VEGF mediated reduction in occludin level depends on urokinase plasminogen activator suggestive of increased extracellular proteolytic activity contributing to occludin degradation and probably vascular barrier breakdown (Harhaj *et al*., 2006). Affirmatively *in vivo* immunohistochemical analysis has shown inverse relationship between occludin immunoreactivity signal and the degree of vascular permeability in the retina of STZ-induced diabetic rats or in non-diabetic rats with intravitreal VEGF-injection (Barber and Antonetti, 2003). However the authors reported no change in immunoreactivity signal for cldn-5 which is the main cldn type present in endothelial intercellular junctions. Therefore changes in occludin content, phosphorylation and localization accompanied by alterations in barrier properties seen in DR substantiates the key role of occludin in the maintenance of BRB.

In addition to impaired cell-cell junctions, abnormal transendothelial vesicular transport (Hofman *et al*., 1999) and endothelial cell apoptosis (Mizutani *et al*. 1996; Joussen *et al*., 2001) have also been shown to underlie increased retinal vascular permeability in DR. It is possible that endothelial cell death would be the key disturbance accounting for major retinal vascular leakage in diabetes as suppression of endothelial apoptosis is presented as a potent approach to prevent BRB breakdown in STZ-induced diabetic rats (Joussen *et al*., 2003).

1.7 Role of insulin/IGF-1 signaling in the skin

Keratinocytes of human skin express both insulin and IGF-1 receptors, but they do not synthesize IGF-1 or insulin ligands (Barreca *et al*., 1992; Tavakkol *et al*., 1992). Dermal fibroblasts could support the proliferation of keratinocytes in the epidermis by secreting IGF-1 and insulin (Barreca *et al*., 1992; Tavakkol *et al*., 1992). Epidermal inactivation of mouse IR showed a very subtle reduction in skin thickness while IGF-1R gene deletion resulted in an obviously thinner epidermis. Both type of these knockout mice were viable while deletion of both epidermal IR and IGF-1R genes resulted in translucent and shiny skin culminating in early prenatal lethality within few hours after birth (Stachelscheid *et al*., 2008). However the underlying reason leading to lethality in these mice awaited clarification.

Consistently, inactivation of IGF-1R signaling components such as IGF-1R, IGF-1 and/or IGF-2 (Liu et al. 1993), Insulin receptor substrate 1 (IRS1) (Sadagurski *et al*., 2007) or both of the downstream kinases AKT1 and AKT2 (Peng *et al*., 2003) in mice each resulted in a disturbed epidermal stratification, generating hypomorphic epidermis although the exact downstream regulators in the pathway are yet unclear.

As an expected role for a growth factor, transgenic mice with overexpression of either IGF-1 or IGF-2 in the basal layer of epidermis, represented epidermal hyperplasia, hyperkeratosis and squamous papillomas (Bol *et al*., 1997; DiGiovanni *et al*., 2000; Bennett *et al*., 2003). This observation could link IGF-1R signaling in skin to carcinogenesis.

Aims of this study

The overall goal of this thesis was to analyze the role of cell autonomous insulin/IGF-1 signaling in the regulation of *in vivo* barriers with a focus on vascular endothelial and epidermal skin barrier function.

Specifically, the following specific aims were addressed:

1. To determine the cause underlying early prenatal lethality of $dko^{epi-/-}$ mice
2. Does the loss of epidermal IGF-1R and IR affect epidermal outside-in and inside-out barrier formation?
3. Which molecular components of the outside-in and inside-out barriers are perturbed in the absence of epidermal insulin and IGF-1 signaling?
4. Does IR/IGF-1R signaling regulate vascular barrier function in the adult retinal vasculature?
5. Generate a tissue specific inactivation mouse model for the polarity protein Par3, a downstream component of IR/IGF-1R, which regulates tight junctional barrier formation *in vitro*.

To this end we generated either epidermal specific knockouts for IR and IGF-1R, using K14-Cre mice, as well as inducible vascular endothelial specific knockouts for IR and IGF-1R, using $Tie2Cre^{ERT2}$ and analysed barrier function.

2.1.1 Increased levels of epidermal water loss in epidermal deficient IR/IGF-1R mice

Inactivation of both the insulin receptor (IR) and IGF-1R receptor (IGF-1R) in the epidermis of mice (dko$^{epi-/-}$) using Cre-loxp technology with Cre driven by the K14-promotor resulted in perinatal lethality within the first day after birth. These mice were born with a thin and translucent skin that is slightly shiny compared to control mice (Stachelscheid *et al*., 2008). This suggested that the skin barrier might be compromised in the absence of epidermal IR/IGF-1R signaling. To directly test if newborn dko$^{epi-/-}$ mice showed increased loss of water compared to their control siblings, transepidermal water loss (TEWL) measurements were performed. An approximately two-fold increase in water loss was observed in dko$^{epi-/-}$ in comparison with control mice (Fig.8), which suggests that dehydration is the primary cause of lethality in dko$^{epi-/-}$ mice.

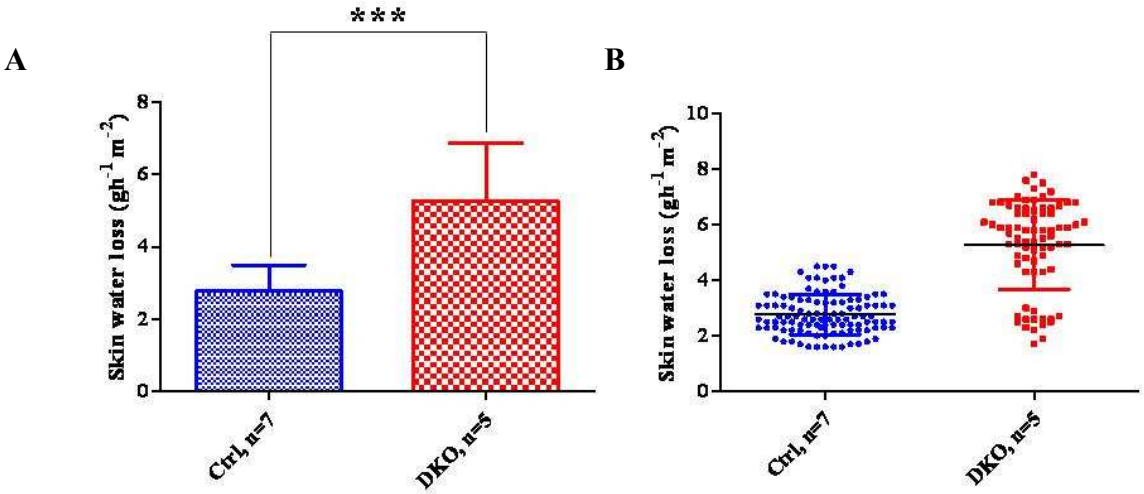

Figure 8: Increased transepidermal water loss in dko$^{epid-/-}$ mice. (A) Average TEWL measurements ± S.D. of Ctrl (n=7) and dko (n=5). For each mouse, 15 highest steadfast values were measured and then all mouse values were pooled. (B) Total distribution of the 15 highest TEWL values ± S.D. per mouse of either control (Ctrl) or dko$^{ep-/-}$ mice. (*) indicates P value summary of F test to compare variances.

2.1.2 Insulin/IGF-1 signaling might be essential for competent inside-out epidermal barrier formation

To examine if increased inside-out permeability of the skin also contributed to the observed water loss in dko$^{epi-/-}$ mice, newborn mice were dermally injected with amine reactive biotin and its diffusion across different layers of the epidermis was assessed. Biotin diffusion is normally only observed only up till the *stratum granulosum*, the layer that contains the functional tight junctions and thereby restrict diffusion into the *stratum corneum* (Furuse *et al*., 2002; Tunggal *et al*., 2005). As expected, in many areas in our control mice biotin staining was observed only in the viable layers of the epidermis with a sharp demarcation where the tight junctions were, visualized by ZO1 (Fig.9A, arrows). However, in a few positions biotin staining was observed above the tight

junctions (Fig.9A, arrow head). This suggested that the skin barrier of control mice was slightly compromised in these sections, perhaps due to scratching of mice. In sections examined of dko$^{epi-/-}$ mice very little staining was visible in the epidermis, suggesting that within these sections little biotin had diffused into the epidermis as compared to those of control where biotin staining revealed an intercellular distribution in the viable layers of the epidermis (Fig.9A). Although some faint biotin staining was positive above the tight junctions in the granular layer, it was unclear if this was specific or not. Overall, the result made the experiment hard to interpret and will require a repetition of the experiment and further functional analysis if the inside-out barrier was perturbed upon loss of IR/IGF-1R.

To examine if loss of IR/IGF-1R in the epidermis alters the localization of claudin-1, a tight junctional membrane component that contributes to tight junctional strand formation and is crucial for skin barrier function (Furuse et al., 2002), immunofluorescence analysis was conducted. All suprabasal layers showed staining at sites of cell-cell contacts with no obvious difference between control and dko$^{epi-/-}$ mice (Fig.9B). In addition, WB analysis of epidermal lysates did not reveal any difference in cldn-1 protein expression (Fig.9C).

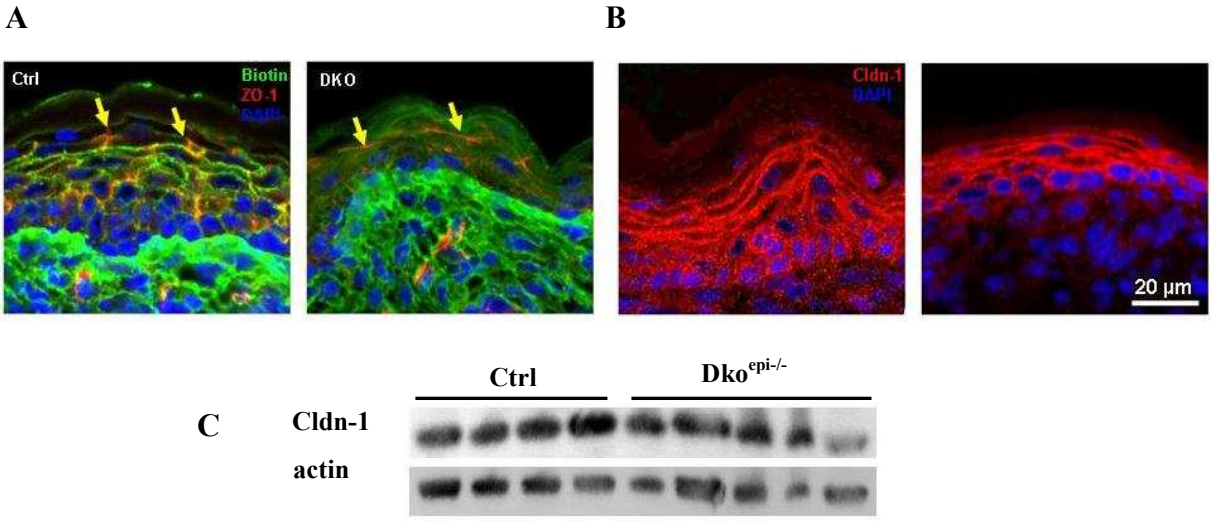

Figure 9: Assessment of the inside-out barrier function in ctrl and dko$^{epi-/-}$ mice (A) **Biotin diffusion assays.** (A) Biotin was injected subcutaneously under back skin. Biotin in cryo sections was detected with Alexa-488 conjugated Streptavidin. Marked by yellow arrows, ZO-1 immunostaining demarks the site of tight junctions in the granular layer. (B) Cldn-1 immunostaining in the epidermis of Ctrl and dko mice. C. Western blot shows the levels of Cldn-1 in Ctrl and EDKO mice. Bar= 20 µm.

2.1.3 Insulin and IGF-1 signaling regulate outside-in epidermal barrier formation

In order to investigate the integrity of the outside-in barrier in dko$^{epi-/-}$ mice, toluidine blue dye penetration assay were done on E16.5-18.5 embryos and P0 mice (Hardman et al., 1998). Control E16.5 mice showed penetration of toluidine blue at the ventral side whereas only patched staining was observed at the dorsal or back skin, indicating partial acquisition of barrier (Fig.10A). One day later, E17.5, the back skin was completely impermeable to toluidine blue indicating a functional outside-in barrier, whereas the ventral side now showed a partial penetration. At E18.5 almost all of the skin of control mice was impermeable to toluidine blue except for some ventral patches. Newborn control mice showed no staining for toluidine blue indicating a fully developed outside-in barrier. Such a gradual developmental acquisition of the outside-in barrier has been reported previously (hardman *et al*., 1998: Tunggal *et al*., 2005). In contrast, no functional outside-in barrier could be observed at E16.5 dko$^{epi-/-}$ embryos, as shown by complete penetration of toluidine blue (Fig.10A). In E17.5 dko$^{epi-/-}$ embryos were almost completely penetrated by toluidine blue with the exception of very small patches at the back skin, suggesting an impaired and strongly delayed formation of the epidermal barrier. This was further confirmed in E18.5 dko embryos in which the complete ventral and a significant part of the back skin were still stained by toluidine blue. However, newborn dko$^{epi-/-}$ mice were impermeable to the dye with exception for small spots near the whisker follicles and randomly distributed over the body (Fig.10A). To confirm proper outside-in epidermal barrier formation in P0, as shown by complete toluidine blue exclusion in dko$^{epi-/-}$ mice, lucifer yellow (LY) penetration was tested through the back skin of the viable mice which differs from toluidine blue procedure where the skin is not fixed in LY protocol. In both control and dko$^{epi-/-}$ mice, lucifer yellow was arrested in the superficial layers of *stratum corneum* and did not show penetration to deeper epidermal layers (Fig.10B). Overall these experiments indicates a strongly delayed formation of the functional outside-in barrier, suggesting either a developmental delay in the formation of a fully functional *stratum corneum* or an impaired formation of the *stratum corneum* that later is partially restored by compensatory mechanisms.

2.1.4 Abnormality in corneocyte morphology and size in dko$^{epi-/-}$ mice

Delayed outside-in barrier formation in dko$^{epi-/-}$ mice indicated disturbance in *stratum corneum* function. Therefore, corneocytes, as major constituents of SC, were isolated from the E18.5 embryos, newborns and adult IGF-1R$^{epi-/-}$ mice for microscopic analyses in order to reveal any abnormality in shape and size. Based on microscopic morphology, corneocytes from age matched ctrl and dko groups in E18.5 and P0 were similar in size and roundness (Fig.11A). Due to the fact that dko$^{epi-/-}$ mice showed early prenatal lethality, it was not possible to analyse the adult corneocytes; therefore, based on the previous description by Stachelscheid and coworkers (2008), IGF-1R$^{epi-/-}$ mice demonstrated thinner epidermis compared to IR$^{epi-/-}$ mice, which indicated that IGF-1 signaling played a more critical role in epidermal morphogenesis. Therefore, adult IGF-

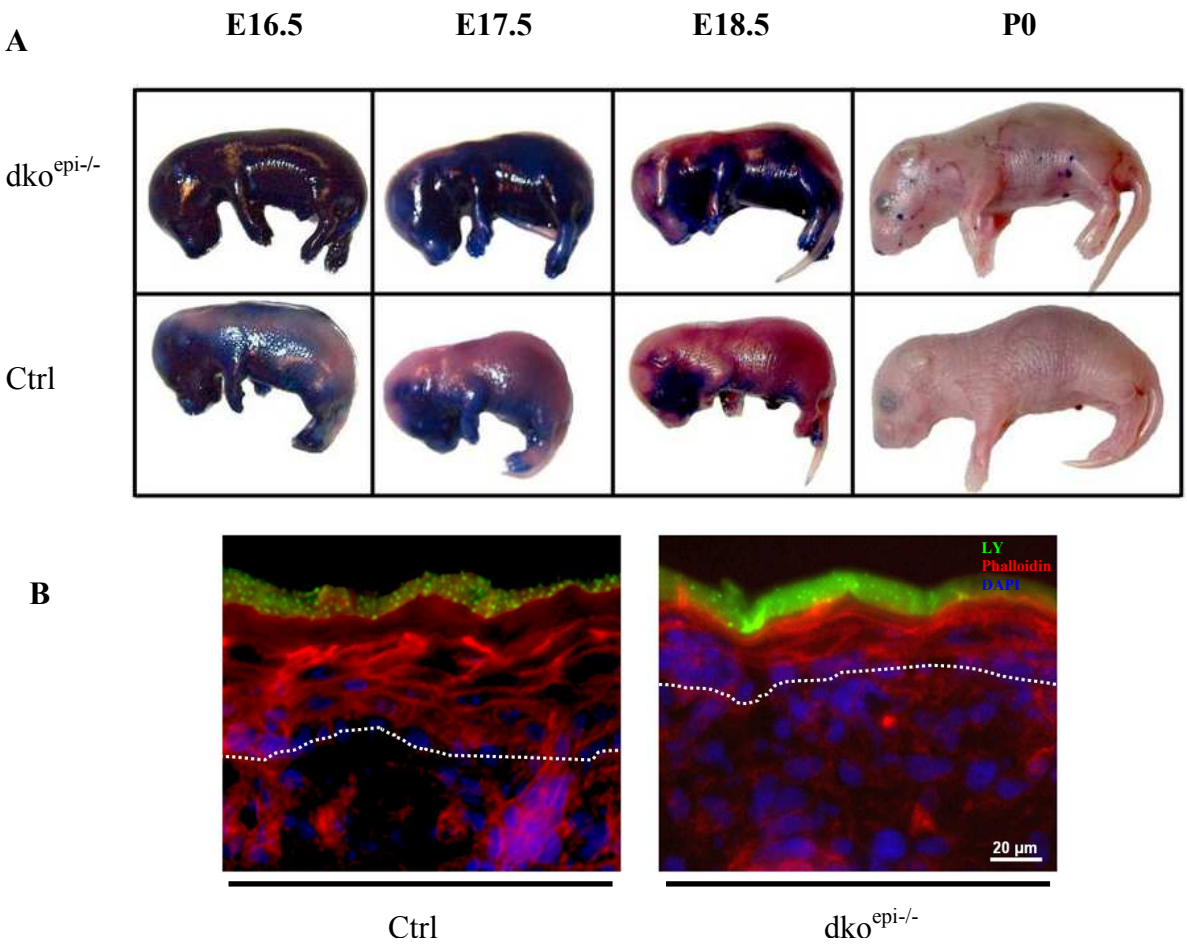

Figure 10: Delayed outside-in epidermal barrier formation in dko$^{epi-/-}$ mice. (A) Embryos in gestational ages E16.5, 17.5 and 18.5 and in newborn mice (P0) were fixed with methanol and stained with toluidine blue. (B) The penetration of LY dye in the epidermis of P0 mice is shown for control and DKO mice on cryo sections. Samples were counterstained with Phalloidin to visualize actin cytoskeleton. Bar=20 µm.

1R$^{epi-/-}$ corneocytes were analysed. Interestingly isolated IGF-1R$^{epi-/-}$ corneocytes were more heterogenous in shape compared to that of control ones (Fig.11B), showing the importance of IGF-1 signaling in corneocyte production in adult skin. In order to quantify any variation in corneocyte appearance between ctrl and dko mice, two important features of corneocytes, i.e., size and circularity indices were investigated. Objects with circularity index closer to 1 are more circular and hence reflecting the extent of the compactness of an object. Embryonic dko$^{epi-/-}$ E18.5 corneocytes were smaller (Fig.12A) and less circular (Fig.12B) compared to those of their control littermate corneocytes.

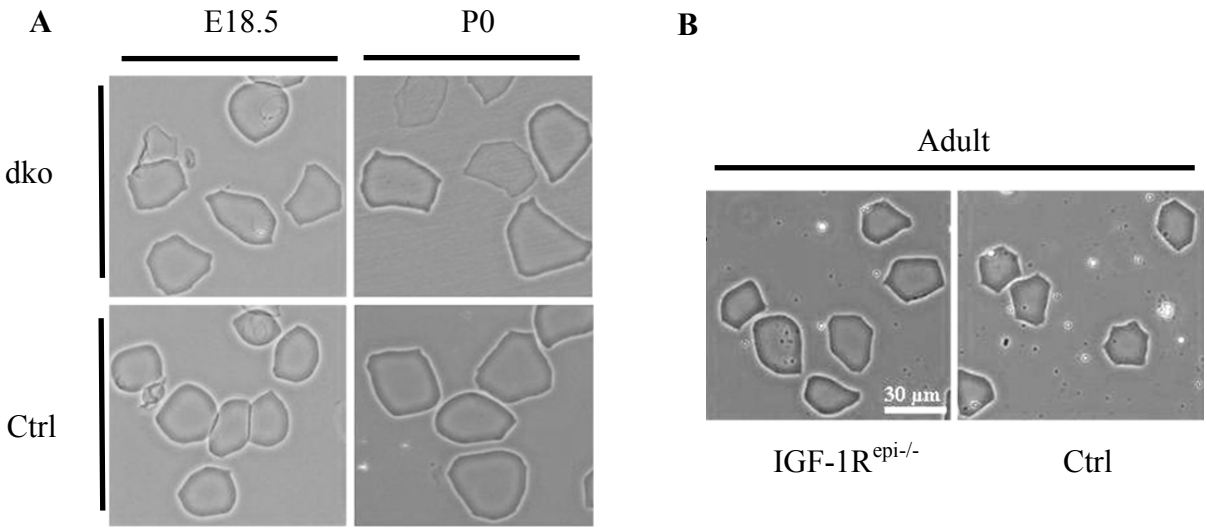

Figure 11: Microscopic view of the corneocytes isolated from E18.5 embryos, P0 and adult wild type and IGF1R$^{epi-/-}$knockout mice. Corneocytes were isolated from the ears following SDS-DTT boiling protocol and resuspending in Tris/EDTA buffer for imaging by light microscope. Bar= 30 µm.

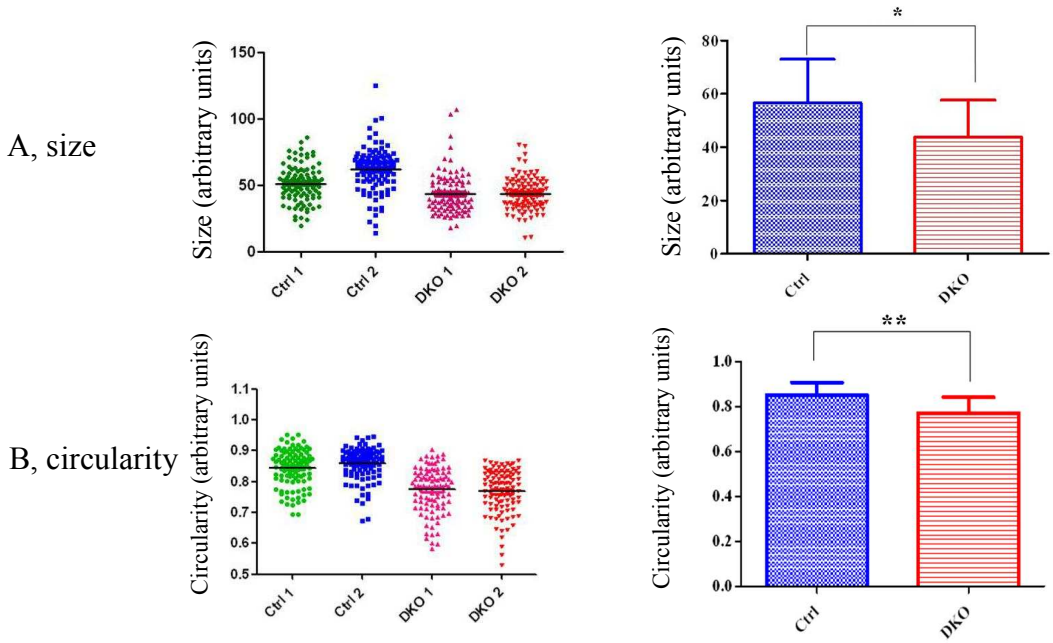

Figure 12: Corneocyte area and circularity index in Ctrl and dko$^{epi-/-}$ E18.5 embryos. (A) Left, distribution of size index. For each mouse 100 corneocytes were analysed by area function of ImageJ software. Right, the measured values for two control and two dko$^{epi-/-}$ mice are pooled. Results are means ± S.D (B) Left, distribution of circularity index. For each mouse 100 corneocytes were analysed by circularity function of ImageJ software. Right, the measured values for two control and two dko$^{epi-/-}$ mice are pooled. Results are means ± S. (*) indicates P value summary of F test to compare variances.

In P0 corneocytes while there was not highly significant difference in circularity index between the experimental samples (Fig.13B), there was significant variation in the size of corneocytes as

dko$^{epi-/-}$ samples were bigger and showed a high level of heterogeneity in size distribution compared to controls (Fig.13A).

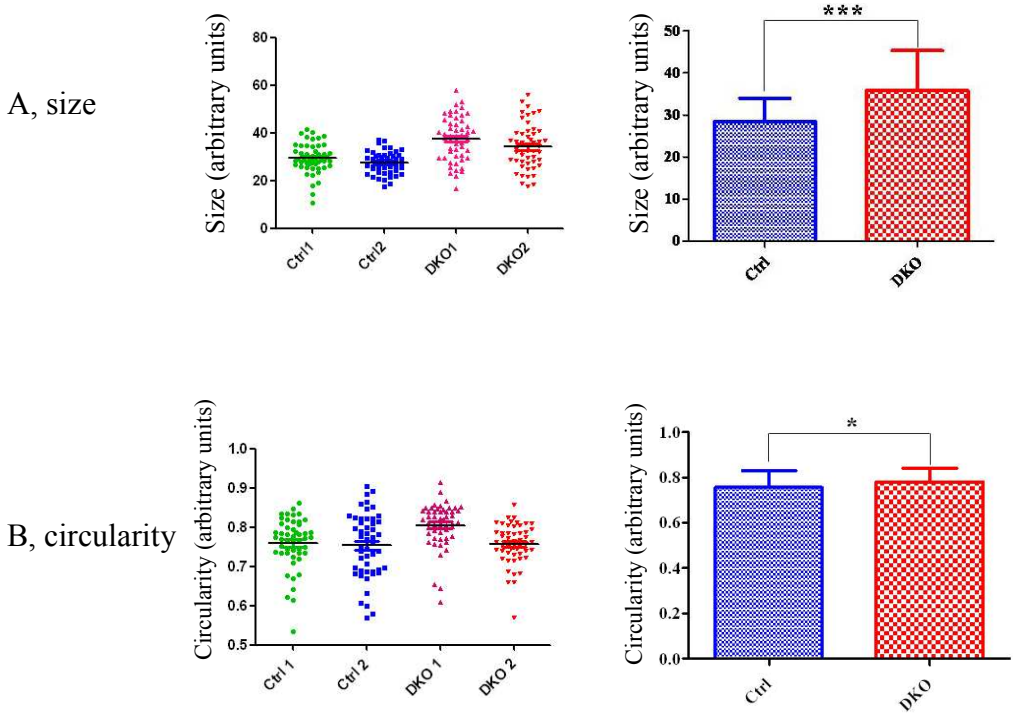

Figure 13: Corneocyte area and circularity index in Ctrl and dko$^{epi-/-}$ P0 embryos. (A) Left, distribution of size index. For each mouse 100 corneocytes were analysed by area function of ImageJ software. Right, the measured values for two control and two dko$^{epi-/-}$ mice are pooled. Results are means ± S.D (B) Left, distribution of circularity index. For each mouse 100 corneocytes were analysed by circularity function of ImageJ software. Right, the measured values for two control and two dko$^{epi-/-}$ mice are pooled. Results are means ± S. (*) indicates P value summary of F test to compare variances.

Corneocytes isolated from adult IGF-1R$^{epi-/-}$ mice showed no difference in circularity index compared to those of control samples (Fig.14B) but they were larger and provided a broad distribution in size distribution, hence considered to be heterogeneous in respect with size values (Fig.14A).

2.1.5 Aberrant profilaggrin to filaggrin processing in dko$^{epi-/-}$ mice

Following documentation of the disturbances in outside-in and corneocyte envelopes in knockout mice, it was decided to evaluate the expression of the late differentiation markers, filaggrin, loricrin and involucrine by WB analysis and immunolocalization.

There were no obvious differences in the expression levels of loricrin, involucrin (Fig.15A) and filaggrin (Fig.15B) in the epidermis of E18.5 control and dko$^{epi-/-}$ embryos (Stachelscheidt *et al.*, 2008). However, protein levels of the final processed form of monomeric 26 kDa filaggrin was dramatically reduced in dko$^{epi-/-}$ E18.5 and P0 epidermis (Fig.15B). The reduction of filaggrin was very striking as this monomeric form is essential for collapsing keratin bundles in the epidermis

(Lynley and Dale, 1983), suggesting that failure in epidermal filament aggregation could contribute to the major barrier defect observed in dko$^{epi-/-}$ mice.

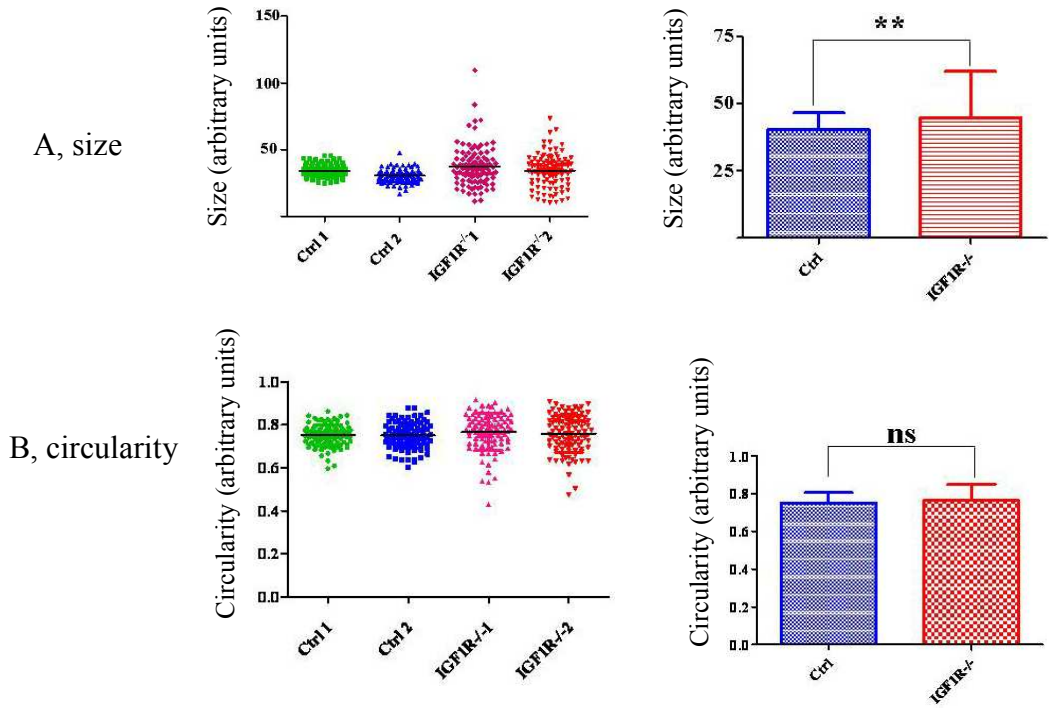

Figure14: Corneocyte area and circularity index in Ctrl and IGF-1R$^{epi-/-}$ adult mice. (A) Left, distribution of size index. For each mouse 100 corneocytes were analysed by area function of ImageJ software. Right, the measured values for two control and two IGF-1R$^{epi-/-}$ mice are pooled. Results are means ± S.D (B) Left, distribution of circularity index. For each mouse 100 corneocytes were analysed by circularity function of ImageJ software. Right, the measured values for two control and two IGF-1R$^{epi-/-}$ mice are pooled. Results are means ± S. ns: not significant. (*) indicates P value summary of F test to compare variances.

Caspase-14 has been identified as an important protease involved in filaggrin processing (Denecker *et al*., 2007). Due to the reduction of monomeric filaggrin in dko$^{epi-/-}$ mice, the question was raised to see if abnormal filaggrin processing in dko$^{epi-/-}$ mice was caused by altered Casp-14 expression or activation. No change was seen in the levels of the non-active (33 kDa form) and activated Casp-14 (p10/p20 isoforms) in E18.5 epidermal samples (Fig.15C). This data implies that IR/IGF-1R signaling does not regulate the expression of Casp-14 in mouse epidermis and aberrant filaggrin processing in dko$^{epi-/-}$ mice was not caused by impaired Casp-14 activation. Therefore other filaggrin-processing proteases may be responsible to adverse affect occurring in dko$^{epi-/-}$ epidermis.

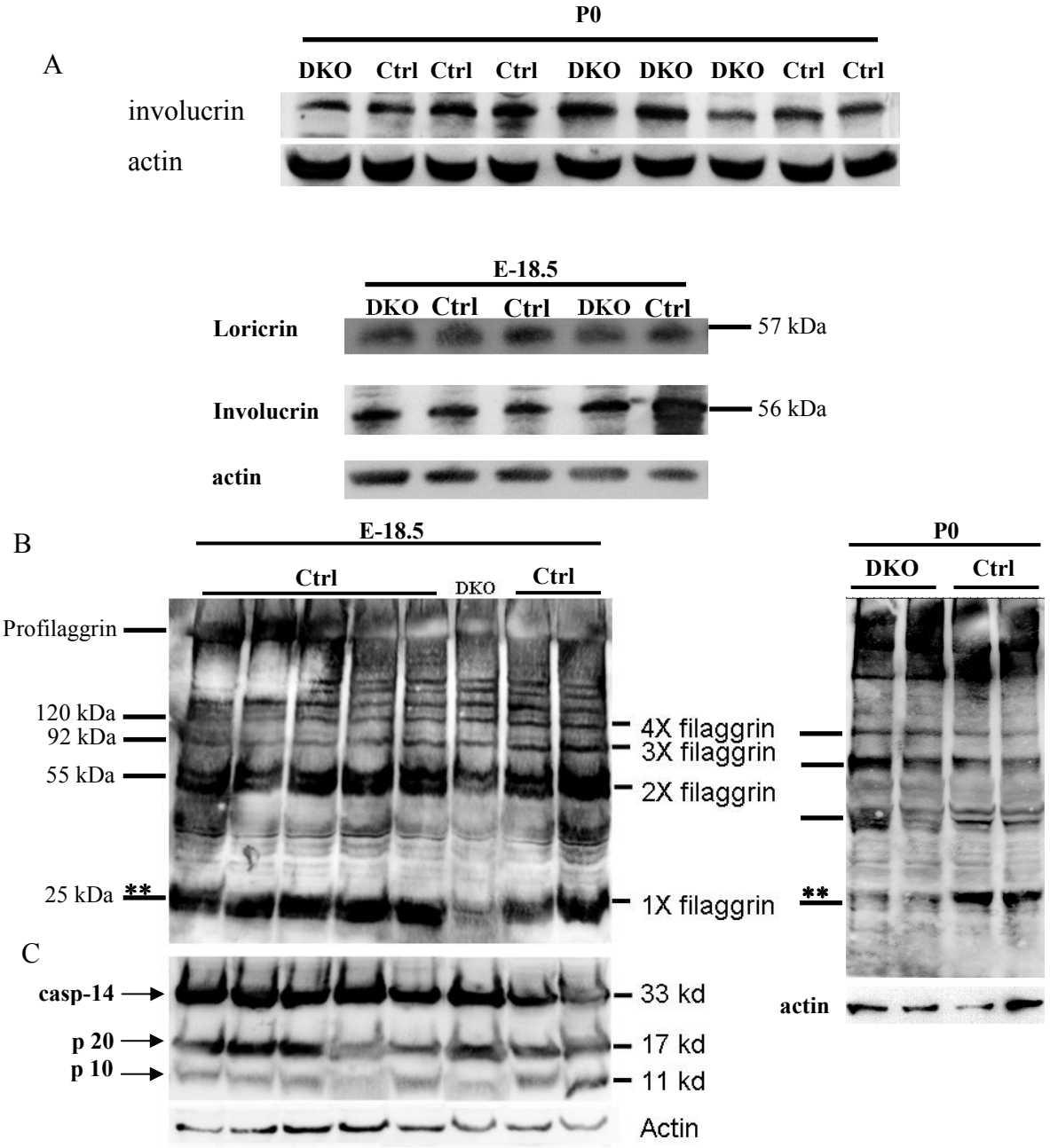

Figure 15: Expression levels of loricrin, involucrin, filaggrin and casp-14 in the epidermis of ctrl and dko$^{epi-/-}$ mice. (A) Expression of loricrin and involucrin in the epidermis of ctrl and dko$^{epi-/-}$ E18.5 and P0 mice. (B) Expression and processing of profilaggrin to filaggrin in E18.5 and P0 epidermis. Asterisks mark the final cleaved filaggrin monomer. (C) Expression of non-active (33 kDa) and active (11, 17 kDa) casp-14 in E18.5 epidermis. Actin is loading control.

To check whether deletion of IR/IGF-1R in the epidermis affected the localization of terminal differentiation markers filaggrin, loricrin, involucrin and casp-14, immunofluorescence was performed using corresponding antibodies.

Filaggrin signal was detected in the epidermis in E17.5 and there was no discernible difference in the punctuate labelling of the epidermal keratohyalin granules in the granular layer of the epidermis which harbour the precursor proprotein profilaggrin. The apparent reduction in the stained granular stacks is due to the thinner epidermal formation in the dko$^{epi-/-}$ mice. The increase in the intensity of the filaggrin signal from E17.5 to P0 is overlapping with the epidermal barrier function recovery which was shown with toluidine blue dye penetration assay (Fig.16).

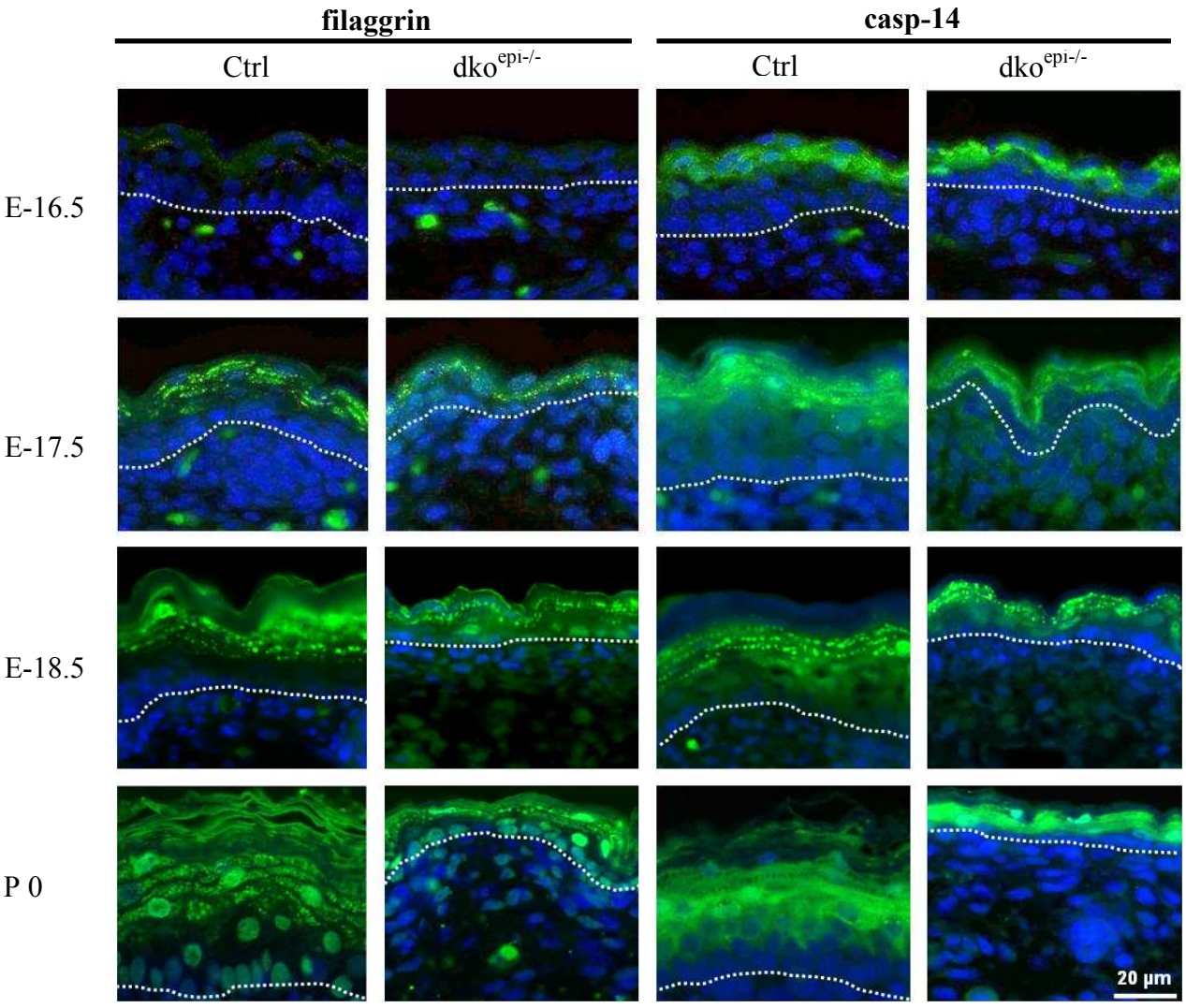

Figure 16: Immunolocalization of filaggrin and casp-14 in the epidermis of E16.5, 17.5, 18.5 and P0 control and dko$^{epi-/-}$ mice. Paraffin sections were counterstained with DAPI to distinguish the nuclei following immunolabelling with respective antibodies. Dashed line marks the basal layer. Bar= 20 µm.

For casp-14, a staining pattern similar to filaggrin was observed. Except in E16.5, positive cytoplasmic diffuse signal was seen in the epidermis of control and dko$^{epi-/-}$ mice. Similar to filaggrin staining in the corresponding embryonic age E18.5, casp-14 revealed punctuate cytoplasmic staining in the epidermis of both dko$^{epi-/-}$ and control samples. This data suggested

casp-14 localization in keratohyalin granules which was converted again to cytoplasmic labelling in newborn P0 mice and extended to lower spinous layer as well, while filaggrin staining was mainly restricted to keratohyalin granules in granular layer (Fig.16).

Both control and dko$^{epi-/-}$ mice provided a very similar immunofluorescence signal for loricrin, a major crosslinked epidermal protein which accounts for up to 60%-80% of total protein composition of the cornified envelop (Steinert and Marekov, 1995) in both ctrl and dko$^{epi-/-}$ mice for all the time points. Together with WB results shown for loricrin (Fig.15A), insulin/IGF-1 signaling is not likely to be required for loricrin expression in the epidermis (Fig.17). Involucrin staining was seen in the granular layer and showed a similar pattern during E17.5, E18.5 and newborn epidermis but was absent from dko$^{epi-/-}$ epidermis in E16.5 stage which might be linked to severe epidermal barrier abnormality in dko$^{epi-/-}$ mice (Fig.17).

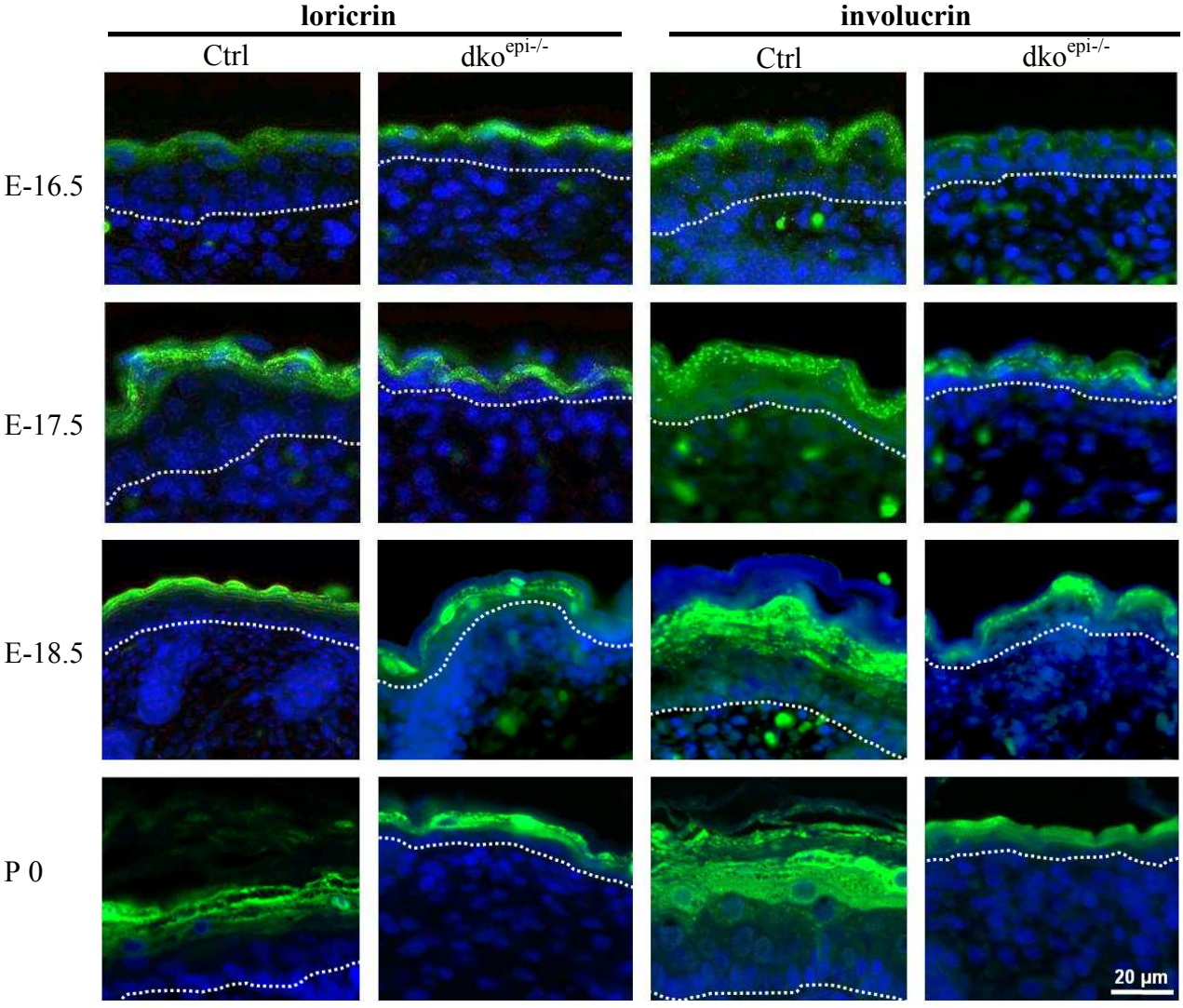

Figure 17: Immunolocalization of loricrin and involucrin in the epidermis of E16.5, 17.5, 18.5 and P0 control and dko$^{epi-/-}$ mice. Paraffin sections were counterstained with DAPI to distinguish the nuclei following immunolabelling with respective antibodies. Dashed line marks the basal layer. Bar= 20 µm.

2.1.6 Reduced epidermal ceramides in dko$^{epi-/-}$ mice

Owing to the observed clear delay in the outside-in barrier formation demonstrated with toluidine blue penetration in dko$^{epi-/-}$ mice and high amount of epidermal water loss observed in newborn dko$^{epi-/-}$ mice, question was raised if Insulin/IGF-1 signaling regulated lipid composition of the outer epidermis. Therefore, unbound free extractable lipids from *stratum corneum* of control, IR$^{epi-/-}$ and dko$^{epi-/-}$ mice were analysed by Thin Layer Chromatography (TLC).

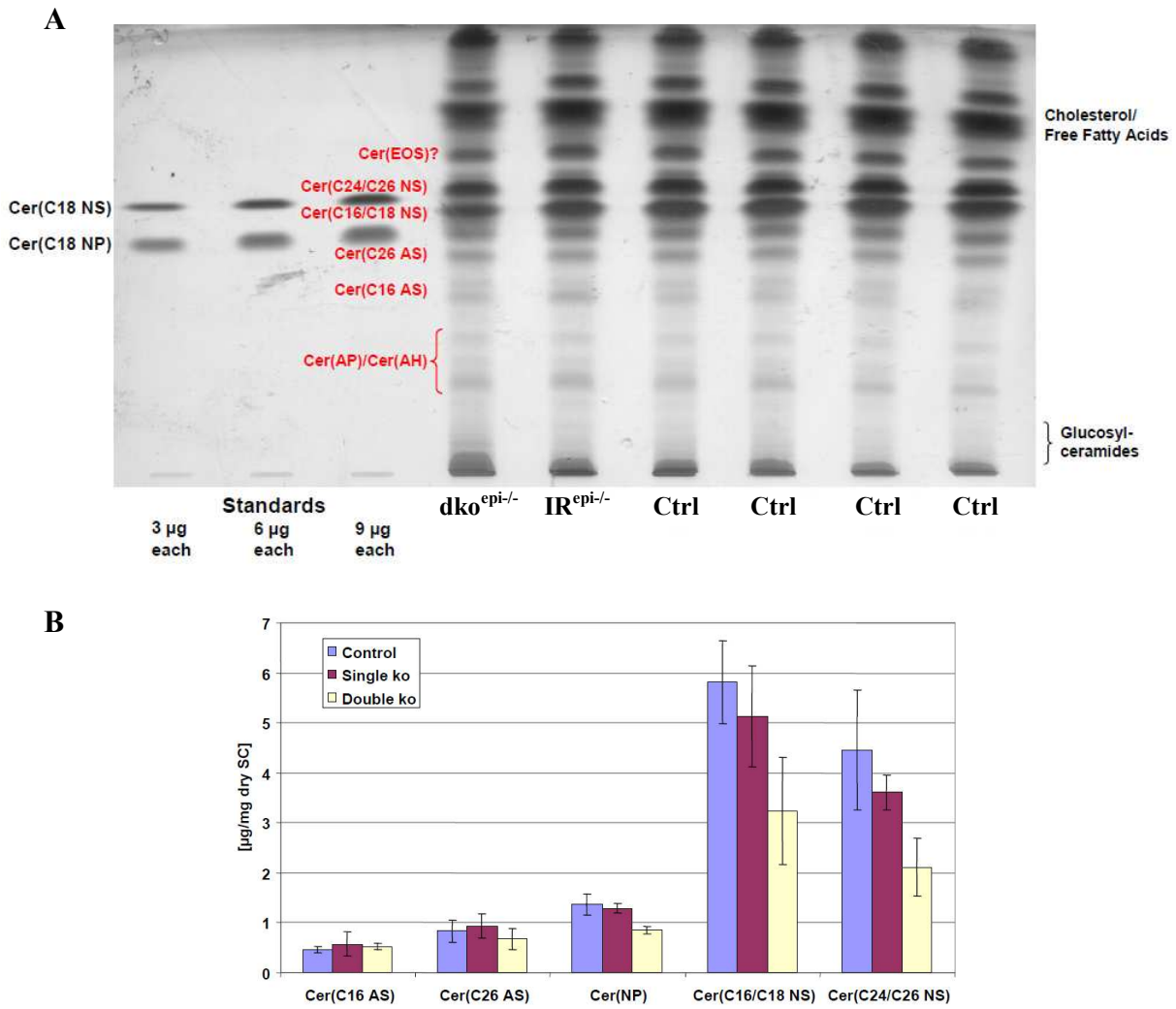

Figure 18: Analysis of free extractable epidermal lipids by TLC. (A) TLC of crude epidermal extracts. The levels of Cer (C24/C26 NS), Cer (C16/C18 NS) and Cer (NP) are significantly reduced in the dko$^{epi-/-}$ samples. For the control and IR$^{epi-/-}$ mice samples from every single mouse were loaded. Dko$^{epi-/-}$ samples represent pooled lipid extracts from 3 mice (B) The quantification of the various ceramides. Data are represented as means ± S.D. of 6 control, 4 IR$^{epi-/-}$, and 2 DKO replicates.

As dko$^{epi-/-}$ mice had a thinner epidermis compared to control mice, less lipid could be extracted from their epidermis, thus in order to obtain an equal loading amount of 2.6 mg, the *stratum corneum* extracts of three dko$^{epi-/-}$ mice were pooled together. There was an obvious reduction in

the intensity of the lipid bands for ceramides, Cer(C24/C26 NS), Cer(C16/C18 NS) and Cer(NP) in the strat*um corneum* of newborn dko$^{epi-/-}$ mice (Fig.18A) compared to those of IR$^{epi-/-}$ and control mice. IR$^{epi-/-}$ mice also exhibited a mild reduction in the amount of Cer (C24/C26 NS), Cer (C16/C18 NS) ceramides.

According to the statistical quantification of total extracted cornified layer ceramides there is almost 40% reduction in the amount of Cer(C16/C18 NS) and two fold reduction in the levels of Cer(C24/C26 NS) in dko$^{epi-/-}$ mice compared to those of control animals (Fig18B).

Levels of glucosylceramides (GlcCers), the so called pro-barrier lipids, which are considered to function as key component of the epidermal lipid barrier (Jennemann *et al*., 2007), were elevated in dko$^{epi-/-}$ mice compared to those of control mice. This data may reflect a defect in ceramide procressing in these mice as GlcCers are considered to be the major source for ceramide production in mouse epidermis (Doering *et al*., 2002).

Dko$^{epi-/-}$ mice provided critical reduction in the levels of epidermal ceramides. Corneocytes are surrounded by a cornified cell envelope made up of proteins, mainly loricrin and involucrin. Specially involucrin in the corneocytes is a known to covalently bind to the hydroxyceramide lipid molecules (Candi *et al*., 2005). As demonstrated previously by WB analysis, the reduced ceramide levels did not influence involucrin expression in the dko$^{epi-/-}$ epidermis in P0 (Fig.15A). This means that involucrin expression or stability is not dependent on proper ceramide deposition in the epidermis.

2.1.7 Impairment of tight junctions in cultured IGF-1R$^{-/-}$ keratinocytes

Abnormal diffusion of subcutaneously injected biotin above the granular layer to the cornified layer in dko$^{epi-/-}$ mice followed with exceedingly high amounts of epidermal water loss in these mice provided critical evidence about malfunction of epidermal tight junctions *in vivo*.

To further assess whether IGF-1R regulates tight junctional barrier formation, the *in vitro* Ca^{2+} switch model was used to analyse barrier formation in primary keratinocytes isolated from control and IGF-1R$^{-/-}$ epidermis. These cells are normally cultured under low Ca^{2+} conditions to prevent terminal differentiation. Increase of Ca^{2+} in the medium does not only trigger differentiation, but also induces intercellular junction formation and stratification by allowing the Ca^{2+} dependent engagement of cadherins (Michels *et al.*, 2009a-b).

The measurement of transepithelial electrical resistance (TER) allows following the proper tight junction-mediated sealing of the paracellular space over time, thus assessing TJ function.

Whereas control keratinocytes successfully elevated the levels of TER after Ca^{2+} switch, IGF-1R$^{-/-}$ keratinocytes showed an almost 50% reduction in TER, suggesting impairment of TJ function TJ (Fig.19B).

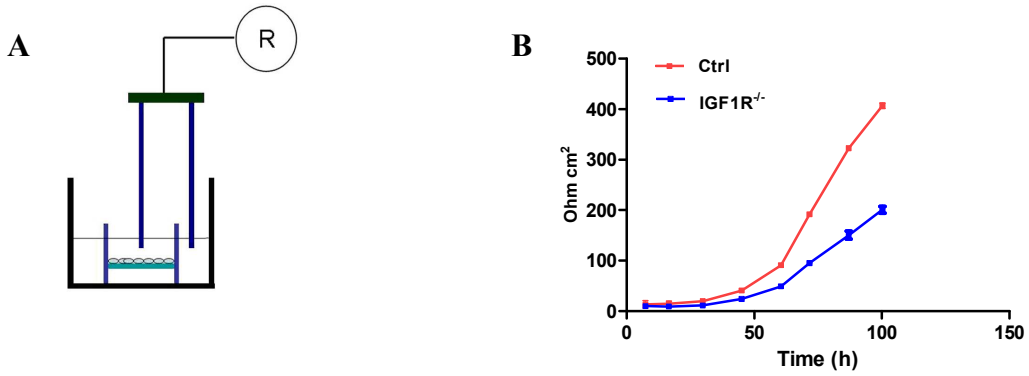

Figure 19: Impaired *in vitro* barrier formation in IGF-1R$^{-/-}$ keratinocytes. (A) Schematic drawing of experimental setup. Keratinocytes were plated on porous filter inserts and electrical resistance of trans epithelia was measured using an automated Ohm meter. (B) Trans-epithelial resistance (TER) measurement of control and IGF-1R$^{-/-}$ keratinocytes. Values represent ± S.D. of 2 controls and 2 knockout cell line replicates.

2.1.8 Normal recruitment of β-catenin and ZO-1 to cell-cell junctions in IGF-1R$^{-/-}$ keratinocytes

To test whether the observed reduction in TER was due to impairment of intercellular junction formation, immunolocalization of the adherens junction component β-catenin was analyzed. 48 h after Ca^{2+} switch both control and IGF-1R$^{-/-}$ keratinocytes recruited β-catenin to sites of intercellular contacts, suggesting normal formation of adherens junctions. In addition, ZO-1, a key component of TJs, was normally recruited to sites of intercellular contacts 48 h after Ca^{2+} switch, a time point that marks the onset of TER formation, indicating TJ formation. Thus, IGF-1R does not seem to affect TJ function by regulating ZO-1 localization (Fig.20).

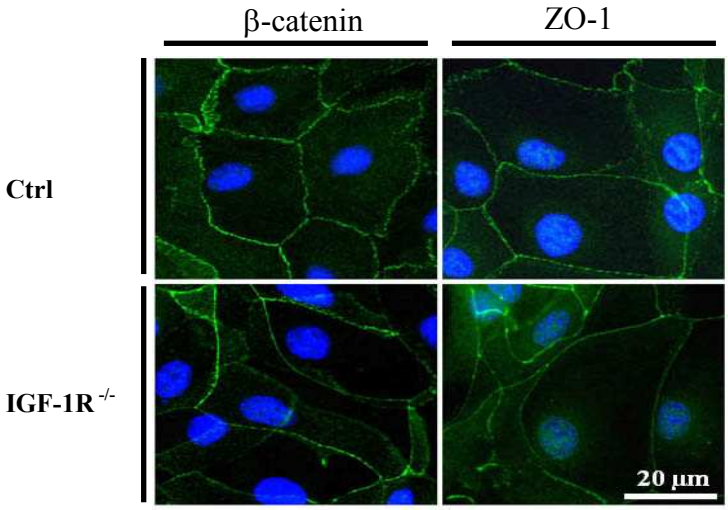

Figure 20: Adherens junction and tight junction formation in IGF-1R $^{-/-}$ keratinocytes (A) Immunofluorescence analysis of adherens junction (β-catenin) and tight junction (ZO-1) components. Keratinocytes were differentiated in high Ca^{2+} for the 48 h. Bar= 20 µm.

2.1.9 Impaired cldn-1 expression in differentiated IGF-1R$^{-/-}$ keratinocytes

Cldn-1 is a critical component of the epidermal barrier (Furuse *et al.*, 2002). To assess whether alterations in cldn-1 levels are responsible for the observed impairment of barrier formation, WB analysis was conducted. Ca^{2+}-induced differentiation caused increase in the levels of cldn-1 in control cells whilst in IGF-1R$^{-/-}$ cells there was no such increase to levels similar to control cells 24 h after calcium. Even prolonged differentiation of IGF-1R$^{-/-}$ keratinocytes for 72 h did not induce increase in cldn-1 levels similar to control cells (Fig.21A,B), while the levels of ZO-1 were apparently unchanged (Fig.21A), indicating that IGF-1 signaling is regulating cldn-1 expression in cultured murine keratinocytes.

To ask whether this regulation occurred on the level of transcription, RT-PCR analysis was performed to measure cldn-1 transcript levels. Semi-quantitative RT-PCR with cldn-1 specific primers was performed on 0 h and 48 h differentiated control and IGF-1R$^{-/-}$cells. According to the band intensity on the gels at 48 h time points, there was clear reduction in transcript levels for knockout cells compared to those of controls. This data corresponds closely with that of TER analysis and provides further evidence that IGF-1 signaling is required for regulation of cldn-1 expression (Fig.21D).

β-catenin levels did not differ within 24 h following differentiation in control and knockout keratinocytes which complied with immunofluorescence results (Fig.21C).

2.2.1 Preparation of dko$^{veinduc-/-}$ mice to study vascular barrier property

The observed deformities in epidermal barrier property for dko$^{epi-/-}$ mice supported the idea that insulin/IGF-1 signaling are potential regulators of both the outside-in and inside-out epidermal barrier functions. Also *in vitro,* IGF-1 signaling regulates TJs in stratifying epithelia at least *via* controlling the expression of cldn-1 in differentiating keratinocytes. Hence to examine if insulin/IGF-1 signaling could similarly regulate the vascular barrier function mediated by endothelial cells, double knockout mice, termed vascular endothelial double knockout (dko$^{veinduc-/-}$ for IR$^{ve-/-}$/ IGF-1R$^{ve-/-}$) having both vascular endothelial cell–specific deletion of the insulin receptor (VENIRKO) and IGF-1 receptor (VENIFARKO) were obtained using tamoxifen induced Cre-recombinase mediated deletion in adults, in which regulatory elements of Tie2 promoter drove Cre expression (Fig.22).

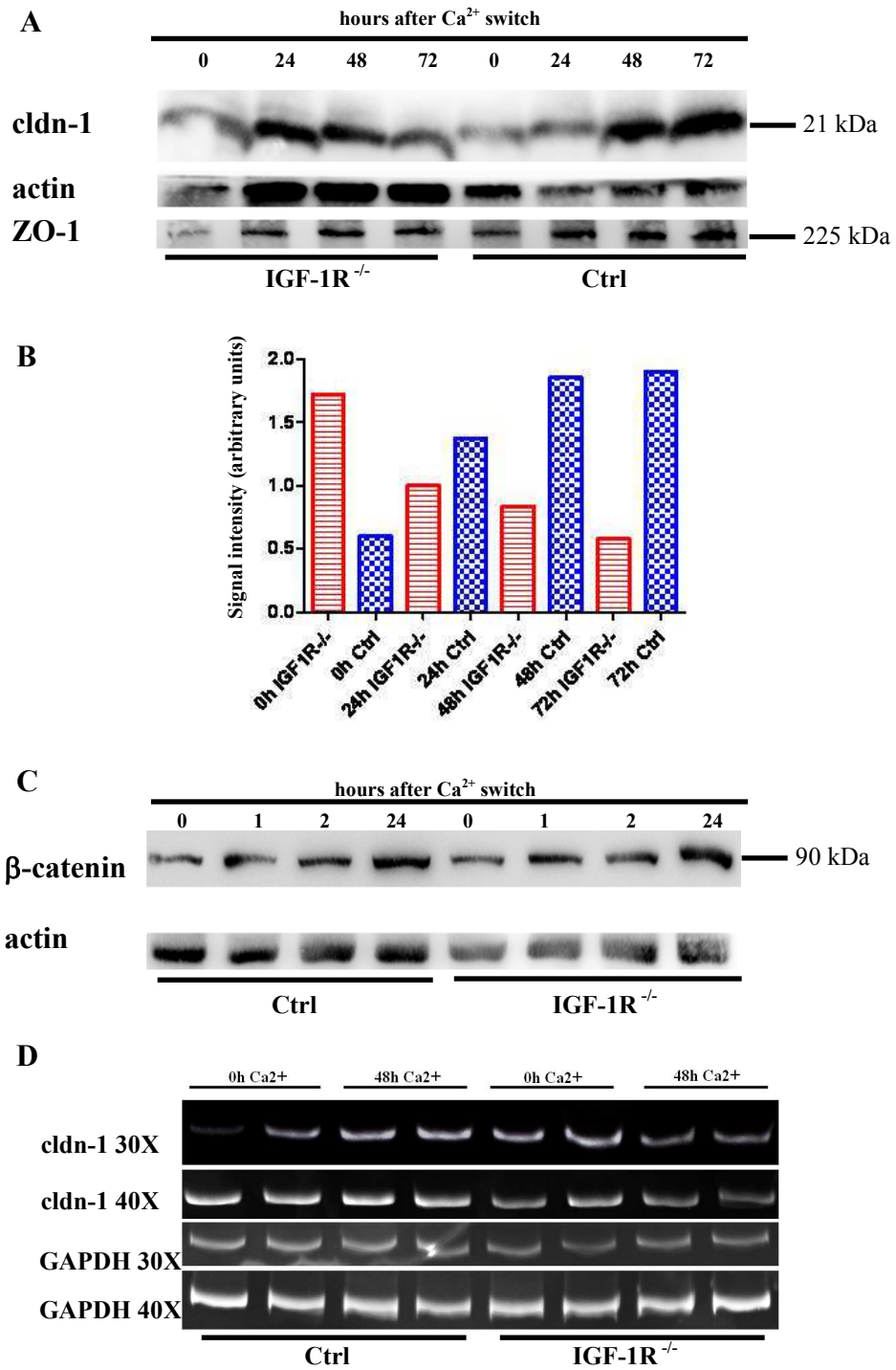

Figure 21: Impaired cldn-1 expression in differentiated IGF1R$^{-/-}$ keratinocytes. (A) Impairment in the cldn-1 but not ZO–1 levels in Ca^{2+} differentiated IGF1R$^{-/-}$ keratinocytes**.** Protein levels in 0, 24, 48 and 72 h differentiation time points are shown. (B) The quantification of the WB signal for cldn-1 shows the change in its expression within described time points. Signals for cldn-1 in each group were normalized to intensity of actin band signal. (C) No difference in β-catenin expression between control and IGF1R$^{-/-}$ keratinocytes during 24 h differentiation. (D) Lower cldn-1 transcript levels in 48 h differentiated IGF-1R$^{-/-}$ keratinocytes compared to control shown by RT-PCR in 30 and 40 amplification cycles. GAPDH is loading control.

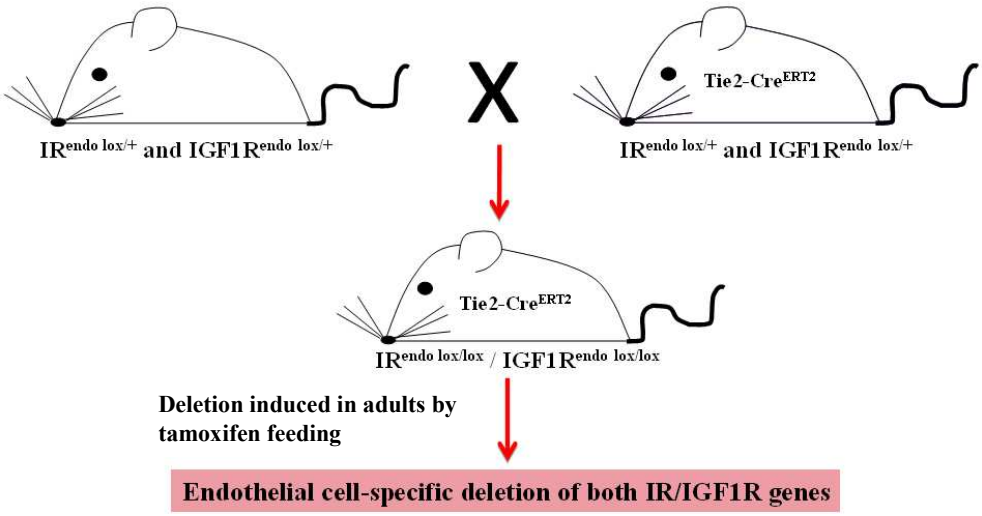

Figure 22: Schematic illustration of the crossing and feeding to obtain dko$^{veinduc-/-}$ mice. Deletion is achieved in adults *via* continuous feeding with tamoxifen for 5-6 weeks.

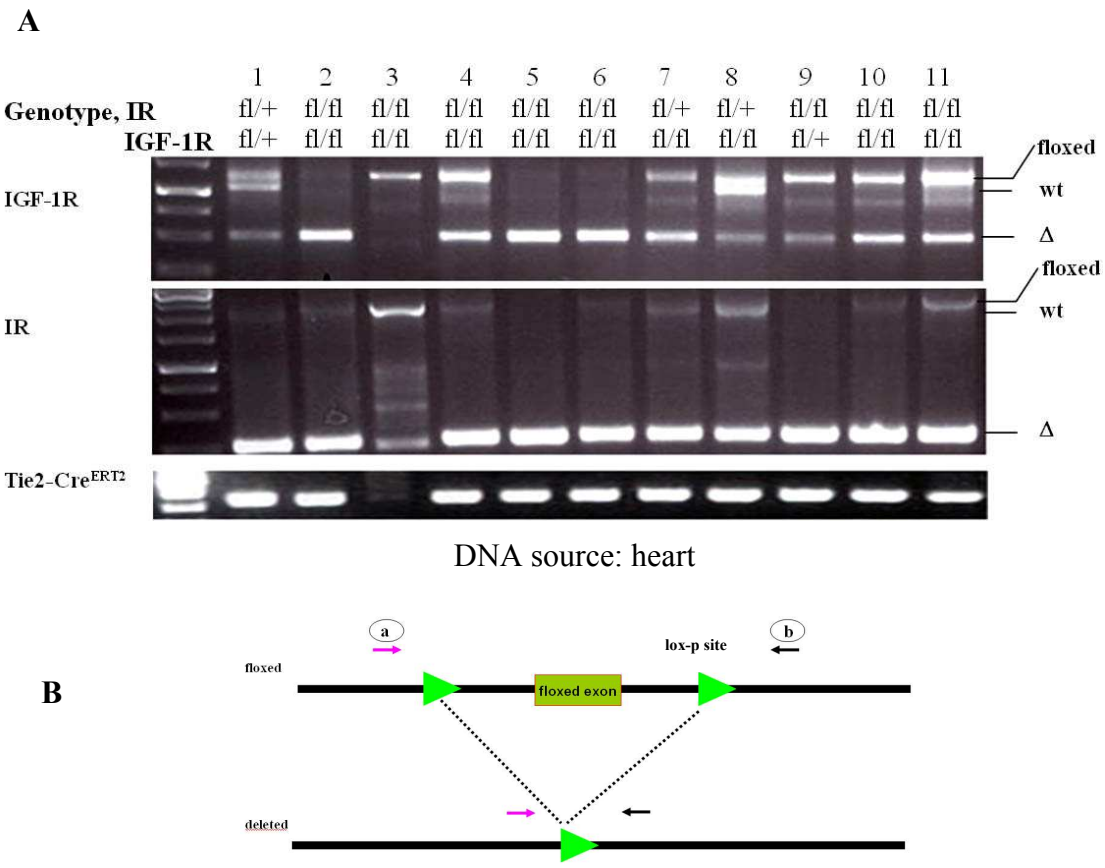

Figure 23: Deletion efficiency for IR/IGF-1R genes in dko$^{ve-/-}$ mice by PCR. (A) Mice no. 2, 5 and 6 show complete deletion of IGF-1R gene. Mice 4, 7, 10 and 11 show less effective deletion of IGF-1R gene. Consistently high level of IR deletion in all mice carrying the Tie2-Cre^{ERT2} is detected. Mouse no. 3 does not carry the transgene. (B) The position of primers for deletion screening by PCR is illustrated schematically.

2.2.2 Variation in IGF-1R gene deletion after feeding with tamoxifen

In order to obtain dko$^{veinduc-/-}$ mice with deleted IR/IGF-1R genes, adult 4 weeks old mice carrying the Tie2-Cre^{ERT2} transgene were fed with a tamoxifen diet for 5-6 weeks following recommended procedure (Forde *et al*., 2002) after which the deletion efficiency for both IR and IGF-1R genes was determined by PCR primers spanning the floxed genomic region (Fig.23B) for each gene, using DNA template obtained from the heart as it provided a better estimation of the deletion efficiency compared to other DNA resources from the same mouse.

Among dko$^{veinduc-/-}$ mice fed for equal time points with tamoxifen diet, there was variation in the extent of the deletion for IGF-1R allele; on the other hand deletion for IR allele was consistently complete for all the mice examined in the experiments (Fig.23A).

2.2.3 Viability and survival not affected in dko$^{veinduc-/-}$ mice

To investigate if deletion of both IR/IGF-1R genes in endothelial cells had any effect on the survival of dko$^{veinduc-/-}$ mice, the viability of the mice was followed for 4 months after termination of tamoxifen feeding. dko$^{veinduc-/-}$ mice survived into adulthood comparably similar to control littermates and did not show any lethality or abnormality in macroscopic parameters like weight and height (data not shown).

Histological analysis by of different tissues in VEDKO mice by Hematoxylin and Eosin (H&E) staining showed no abnormality compared to control mice (Fig.24).

2.2.4 Intact retinal vascular barrier integrity in the absence of IR/IGF-1R signaling

To check if endothelial-specific deletion of IR/IGF-1R genes had any effect on retinal vascular barrier property, the dko$^{veinduc-/-}$ mice were either perfused cardiacally or injected systemically with tracers of different molecular sizes i.e., 2000 kDa FITC-dextran or 443 Daltons amine reactive biotin (see 2-1-2) respectively.

Retina wholemount samples from all dextran and biotin infused mice were analysed to visualize the primary plexus, inner deeper plexus and outer deeper plexus in both dko$^{veinduc-/-}$ and control mice. According to the vascular segregation pattern visualized by FITC-dextran in different vascular levels of retina, there was no obvious difference in the branching and vascular morphology or density in all studied retinas for control and knockout groups (Fig.25B). High vascular competency to retain relatively bigger dextran tracer in control and knockout groups was indicative of apparently intact vascular barrier (Fig.25B). Biotin detection in retinal paraffin sections allowed visualizing the extensive leakage in choroidal blood vessels (Fig.25C) that are porous vessels with vascular fenestrations (Bernstein and Hollenberg, 1965). Vessels of the primary plexus showed certain amounts of leakiness in both control and dko$^{veinduc-/-}$ mice which should not be interpreted as abnormal and could be accounted for by the fact that the vasculature in these layer form extensive ramification and branching into deeper retina to form the inner plexuses which is erroneously reflected as leaky.

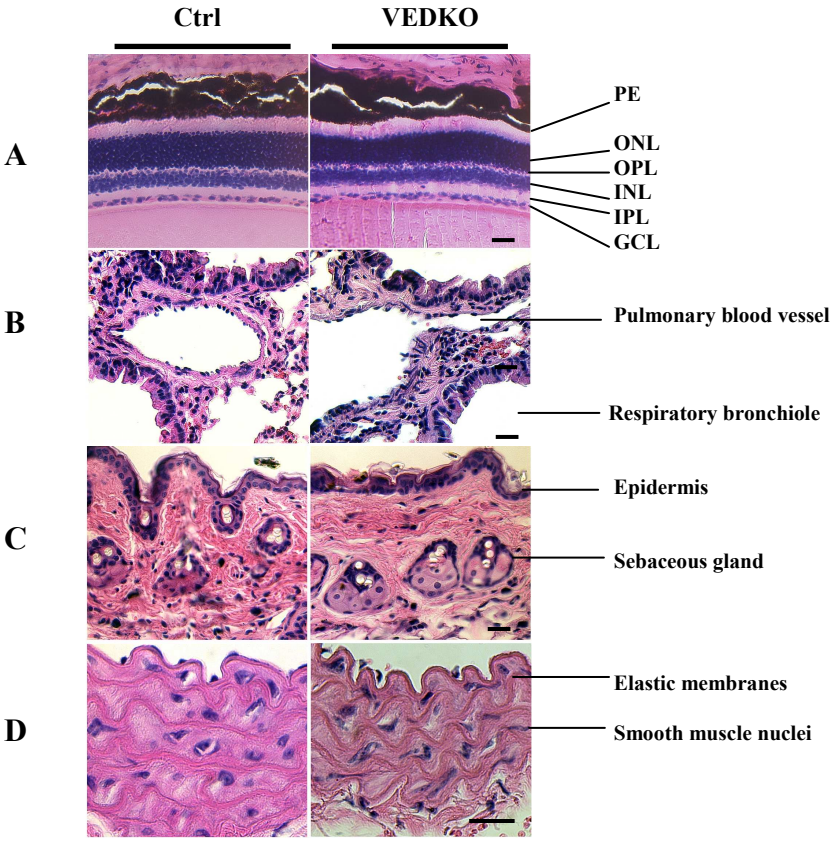

Figure 24: H&E staining of different tissues in dko$^{veinduc-/-}$ and control mice. (A) Retina; ganglion cell layer (GCL), inner nuclear layer (INL), outer nuclear layer (ONL) inner plexiform and outer plexiform layers (IPL and OPL). PE is pigmented epithelium. (B) lung, (C) skin, (D) aorta. Bar= 20 µm.

On the other hand according to normal histological staining (Fig.24A) and tracer perfusion results (Fig.25B, C) there was no indication of pathological oxygen-induced retinopathy (OIR) phenotype, a vasoproliferative condition characterized by the growth of tortuous and leaky vessels that form tuft-like structures towards the vitreous (Chen and Smith, 2007). The vascular retentiveness to the smaller 443 Daltons tracer in the retinal vasculature of the studied mice led to the conclusion that ablation of endothelial IR/IGF-1R genes does not cause any alteration in retinal vascular barrier function of adult mice (Fig.25C), although the full deletion of both genes in dko$^{veinduc-/-}$ could not be fully certified using other techniques such as RT-PCR, immunofluorescence or WB.

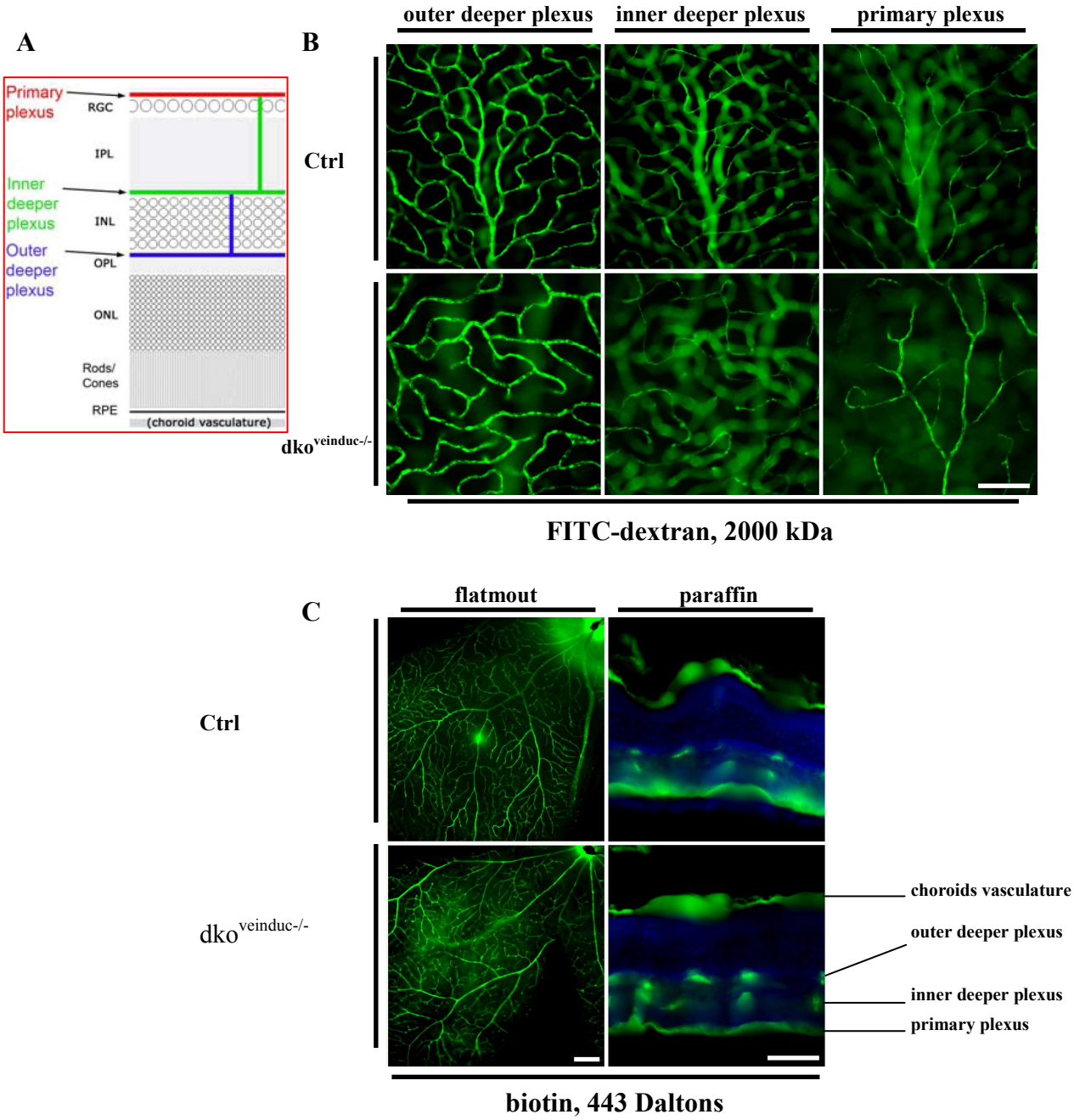

Figure 25: Normal retinal vascular barrier integrity in dko$^{veinduc-/-}$ **mice.** (A) Panel depicts various types of vessels in the longitudinal retinal section. (B) Normal retention of 2000 kDa FITC-dextran in three different retinal vessel types in dko$^{veinduc-/-}$ and control mice. (C) Normal retention of biotin shown in flatmounted retinal quarter and retinal paraffin sections. Different types of retinal vessels are marked. Bar=100 µm.

2.2.5 Isolation of primary lung endothelial cells

As vascular permeability in the CNS is controlled by the biochemical properties of the neurovascular unit (NVU) (Cardoso *et al*., 2010); therefore in dko$^{veinduc-/-}$ mice, any disturbance in permeability sealing function of endothelial cells could be disguised by compensatory functions of the cells in the NVU conformation.

Subsequently to understand the role of insulin/IGF-1 signaling in the endothelial barrier function *via* TER measurements as was described previously for the keratinocytes, primary endothelial cells were isolated from the lungs of 3 weeks old adult mice (Fig.26) using PECAM-1 antibody conjugated beads to obtain $IR^{endo\ fl/fl}$/ $IGF\text{-}1R^{endo\ fl/fl}$ endothelial cells in an effort to convert these cells to dko cells using a TAT-Cre recombinase (Peitz *et al*., 2002) *in vitro*.

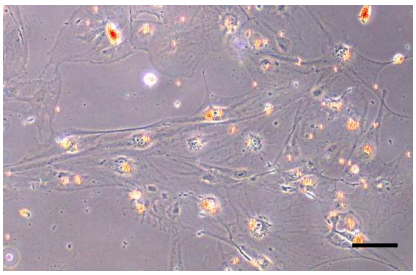

Figure 26: Monolayer growth of freshly isolated primary lung endothelial cells. Endothelial cells were isolated from lung tissue homogenates using PECAM-1 conjugated beads and grown on plastic dishes. Bar=10 µm.

2.2.6 Generation of double knockout $IR^{-/-}$ / $IGF\text{-}1R^{-/-}$ primary endothelial cells

In order to obtain dko endothelial cells, primary endothelial cells in passage 1 were treated with either 2µm 4-OHT or different concentrations of a purified cell permeable Cre-recombinase (HTNC) protein which can potently ablate floxed genes in cultured cells (Peitz et al., 2002).

In transgenic Tie2-Cre^{ERT2} cells, translocalization of Cre^{ERT2} protein from cytoplasm to nucleus requires binding of tamoxifen (TA) or its derivative 4-hydroxytamoxifen (4-OHT) to ERT2 domain which does not tend to bind to endogenous estrogens. This binding will carry the recombinase from cytoplasm into nucleus which finally drives gene deletion (Feil *et al*., 1996).

Based on PCR results, even prolonged 4-OHT treatment for 4 days did not cause any deletion of the target genes (Fig.27A); whereas, both IR and IGF-1R genes were effectively excised by overnight HTNC treatment. As a result while IR gene showed highly efficient deletion already at 625nM concentrations of HTNC, IGF-1R gene required 5µm concentration of the recombinase to show complete deletion (Fig.27A). These observations exhibited a nice overlap with deletion efficiency for both genes *in vivo*, where excision was induced by tamoxifen inducible Cre (Fig.23A) and IGF-1R gene showed variable levels of deletion in different mice while IR gene was effectively deleted in all mice.

The cellular toxicity induced by applying micromolar concentrations of HTNC necessitated intermission of one week and further passaging of cultured cells to achieve recovery and propagation. Unfortunately endothelial cells in passage 2 showed restoration of the floxed IGF-1R allele which obstructed further usage of the cells for the planed experiments indicating that not all HTNC treated cells were completely deleted for IGF-1R gene and growth advantage of such cells caused outnumbering effect over $IGF\text{-}1R^{-/-}$ cells (Fig.27B).

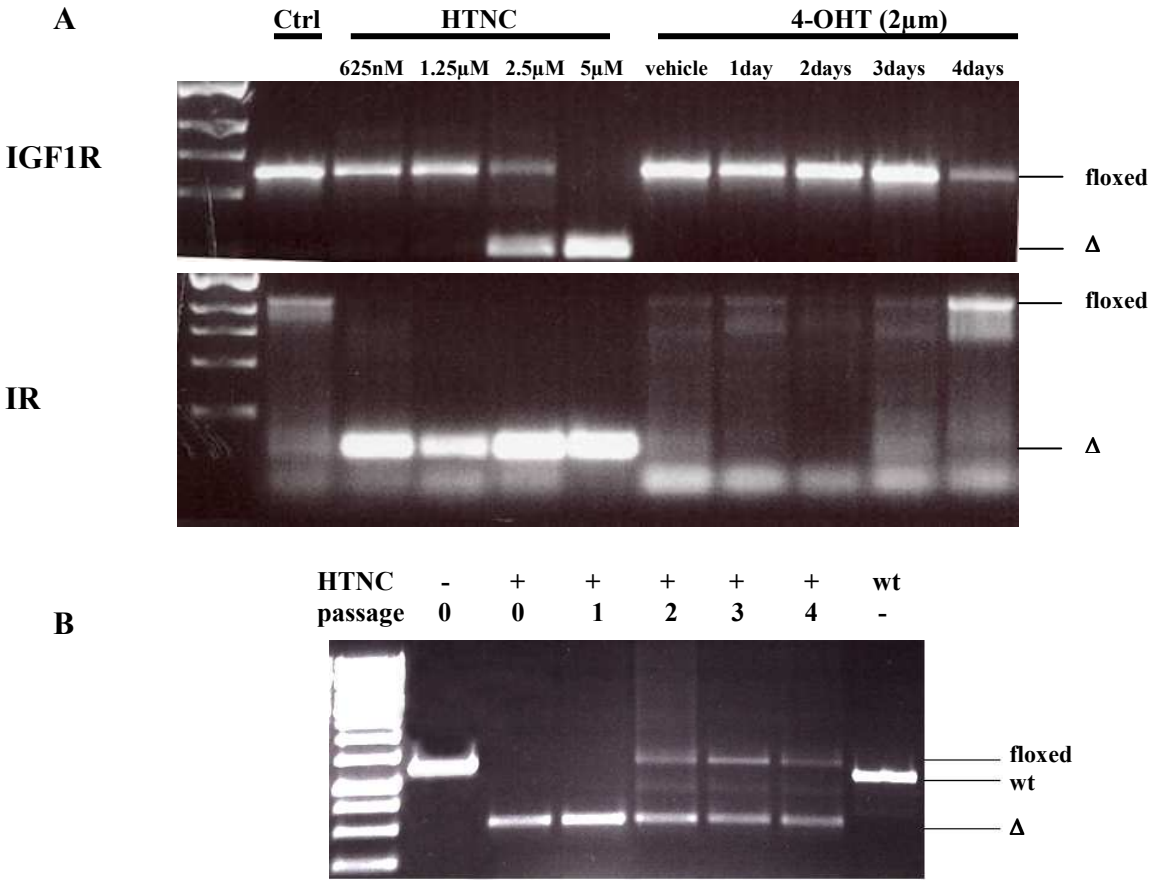

Figure 27: PCR showing deletion of IR and IGF-1R genes in cultured endothelial cells treated with HTNC and 4-OHT. (A) IGF-1R gene requires higher levels of HTNC for proper deletion compared to IR gene. Lack of gene deletion in cells treated for the indicated time points with 4-OHT. (B) Restoration of the floxed IGF-1R allele in HTNC treated dko endothelial cells in passage 2.

2.3 Generating a conditional knockout mouse for PAR-3 gene

Double epidermal IR/IGF-1R gene inactivation highly implicated alteration of tight junction function both *in vivo* and *in vitro*. Therefore, mouse PAR-3 gene was targeted as a downstream candidate for regulation *via* IGF-1 signaling in the mouse epidermis using homologous recombination to replace the PAR-3 genomic DNA sequence with a lox-p flanked fragment of the same region.

2.3.1 Detection of PAR-3 transcripts in primary mouse keratinocytes by RT-PCR

Multiple spliced variants of PAR-3 are found in mammalian cell lines and tissues (Gao *et al*., 2002). All of the known splice variants were shown to arise from a single start codon located in the CR1 domain of the protein (Fig.28B) and a knockout mouse model was generated based on the assumption of a unique start codon (Hirose *et al*., 2006), while later a novel start codon was identified by Duncan and colleagues (2005), as they showed the existence of transcripts in mouse oocyte arising from a second start codon located in exon number 4. Therefore, the expression of

all possible transcripts in mouse cultured keratinocytes was evaluated by RT-PCR initially using primers specific for the 5´UTR region of the transcript derived from exon 4, exon 1 and 3´UTR site specific primers to identify all possible transcripts (Fig.28).

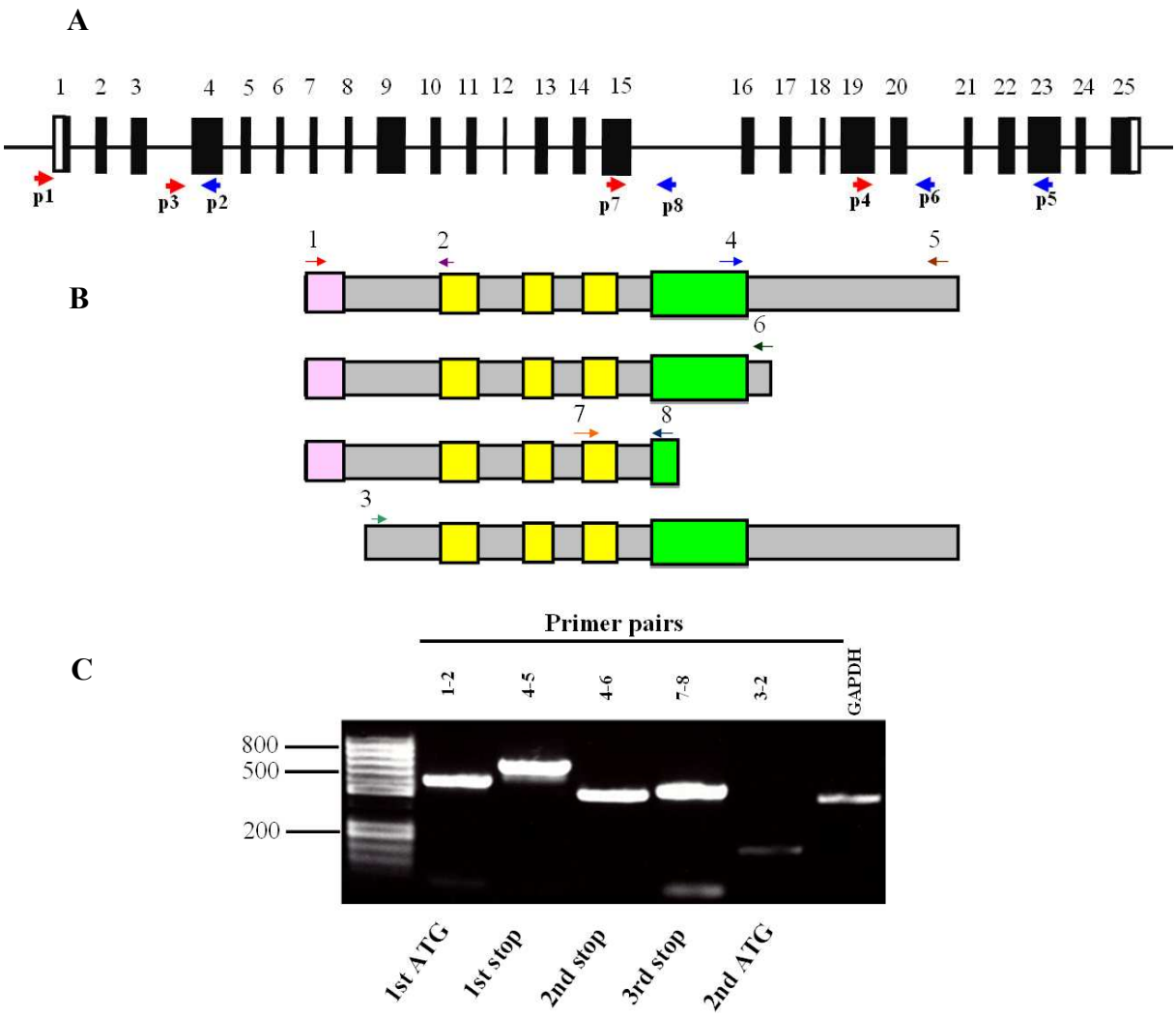

Figure 28: Detection of various start and stop codon sites for PAR-3 transcripts in cultured mouse keratinocytes by RT-PCR. (A) The relative position of primers on the genome used for RT-PCR analysis. The exons and introns are not drawn to scale. Exons are drawn as solid vertical bars. (B) Protein domain organization of various translated PAR-3 transcripts and the respective site of the primers for RT-PCR with their number is shown. (C) RT-PCR products of PAR-3 using assigned primers. All start and stop sites are amplified. Product size; 1-2: 590 bps, 4-5: 747 bps, 4-6: 495 bps, 7-8: 521 bps, 3-2: 198 bps.

Using different primer sets, all previously known start and stop codon sequences were amplified. A faint band with expected size of 198 bp was amplified using primers 9 and 10 suggesting the expression of the novel transcript with second ATG utilization in cultured keratinocytes (Fig 28C). According to RT-PCR data, the second start site provided lesser abundance compared to the first start site, implying limited use of this transcript by translational complex in keratinocytes.

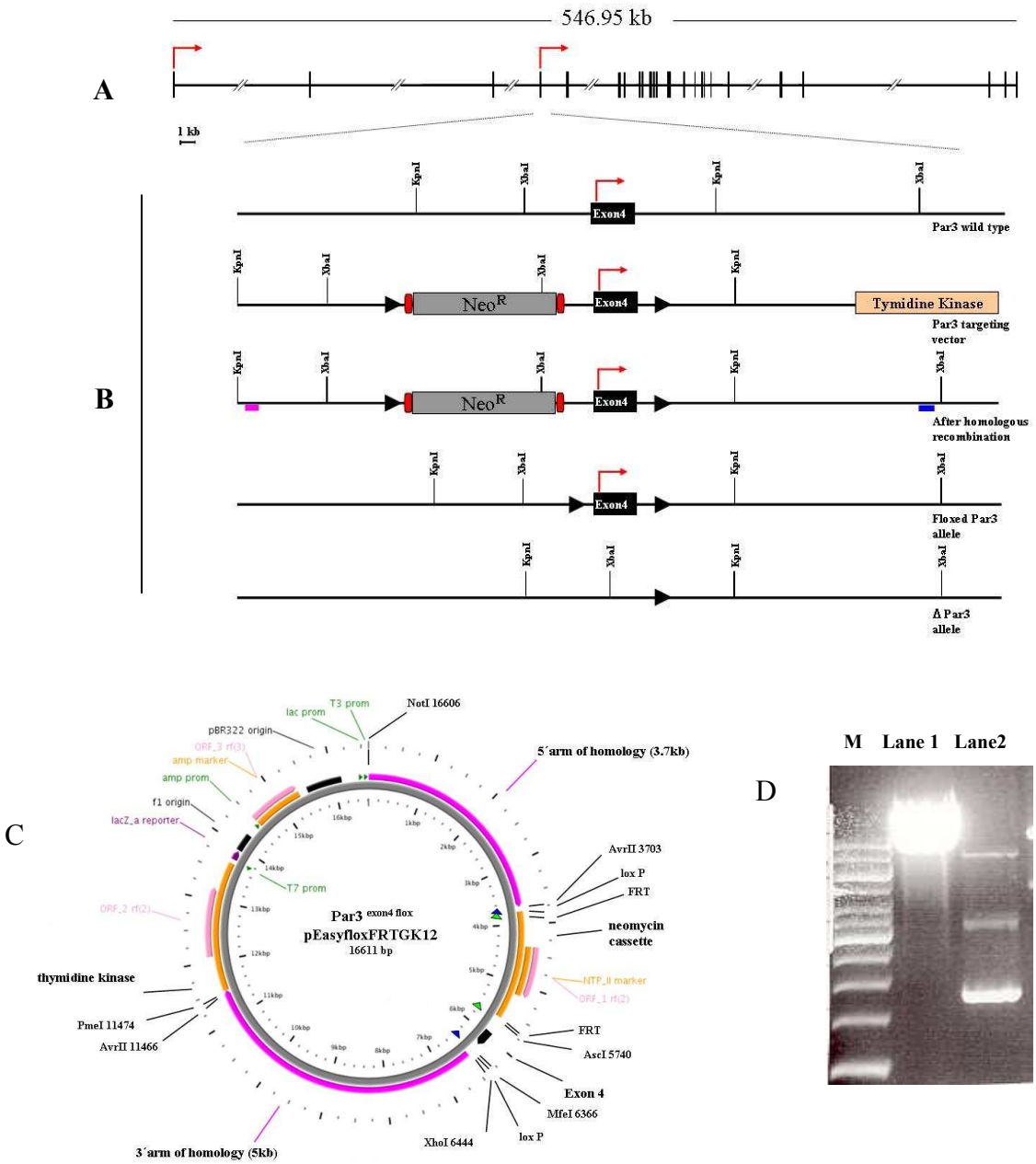

Figure 29: Diagram of PAR-3 genomic organization, targeting strategy and PAR-3$^{exon4\ flox}$ targeting construct. (A) Exons are shown as vertical bars with relatively close ratio to their corresponding genomic size. Two start sites are marked with red arrows. (B) Respective position of the restriction sites, selection cassettes, probes for southern blot screening (pink and blue bars) and lox-p sites (black triangles) are illustrated. (C) PAR-3^{exon4flox} plasmid used for homologous recombination in embryonic stem cells. Restriction sites, FRT and lox-P sites, homology arms and the vector backbone fragments are shown. (D) Agarose gel showing the linear PAR-3$^{exon4\ flox}$ vector (lane-1, 16611 bps) digested with NotI next to a non-digested supercoiled construct (lane-2).

2.3.2 Generation of a targeting plasmid for mouse PAR-3 gene

Mouse par3 gene consists of 25 known exons and as mentioned before two transcription start sites have been characterized for the gene, the first one in exon1 and second one in exon4 (Fig.29A). We planned to produce a conditional knockout mouse which will cause timed and/or tissue specific deletion of the exon4 which allows (i) production of a truncated protein via a premature stop codon due to frame shift in exon5 provided that the first start codon is used (ii) removal of the second start codon in exon4 leading to no production of PAR3 mRNA transcripts given the usage of the second start codon (Fig.29B). The resulting targeting construct was ~ 16.6 kb and was linearized on NotI site just before short homology arm. Linearized construct was used for electroporating the ES cells (Fig.29C and Fig.29D).

2.3.3 Production of PAR-3$^{exon4\ flox/+}$ embryonic stem cells

PCR and Southern blot analysis using site specific primers and probes were used to identify the correctly targeted ES cell clones for blastocyst injection. PCR using primers spanning the Neo^R cassette, 5´ FRT and lox-p sites and 5´upstream left arm of homology with product size of 4.3 kb and primers to amplify 3´ lox-p site and 3´downstream right homology arm with product size of 5.6 kb, showed two ES clones with correctly targeted Par3 allele. The clones H1 and H12 were identified as promising clones for generating chimeric males and were further validated for correct recombination *via* southern blotting (Fig.30).

Southern blot using the probes for left and right homology arms using KpnI and XbaI restriction enzymes validated PCR results for two selected clones, H12 and H1. A blot with probe for Neo^R site further supported the single integration event of the plasmid arms in homologous genomic site as both the mentioned clones were showing a single band with expected size of approximately 9 kb for KpnI digest (Fig.31).

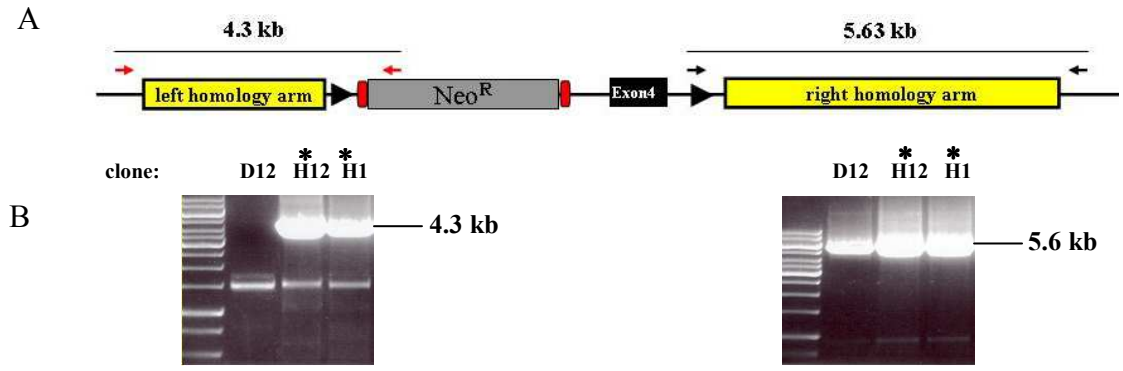

Figure 30: PCR to identify ES cell clones with correctly targeted PAR-3^{exon4}. (A) Picture showing the orientation of the primers used for each PCR and their respective product size. (B) Marked with asterisks, clones H12 and H1 show bands of expected sizes for both left and right PCRs. Clone D12 was not a correctly targeted clone according to left arm PCR.

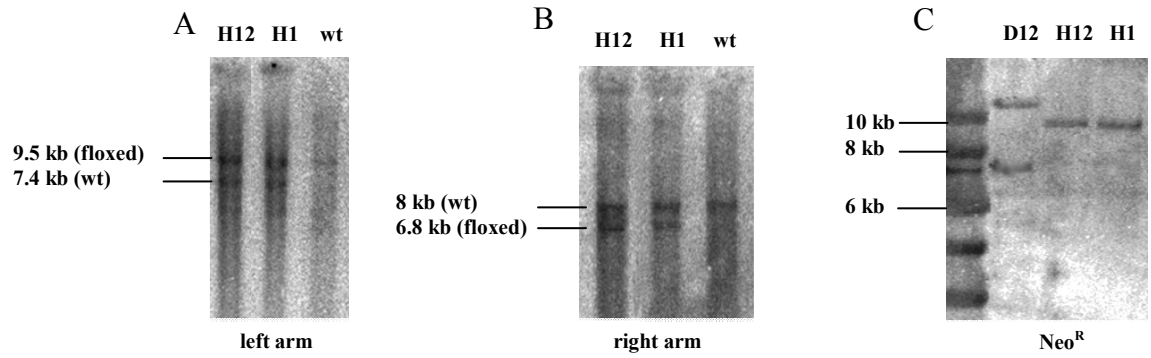

Figure 31: Southern blot confirmation of correct Par3^{exon4} targeting in ES cell clones. (A) Radiolabeled probe to distinguish wt (7.4 kb) and floxed (9.5 kb) alleles for the left arm of homology using KpnI digest. (B) Probe to distinguish wt (8 kb) and floxed (6.8 kb) alleles for the right arm of homology using XbaI digest. (C) Neo^R-specific probe to detect single integration of the targeting fragment using KpnI digest.

2.3.4 Production of PAR-3$^{exon4\ -/+}$ embryonic stem cells

In order to functionally scrutinize the ability of the lox-p sites in mediating the excision of the exon 4 in selected clones at the presence of the Cre recombinase, the cell permeable Cre recombinase (HTNC) was applied to test cultured ES cells. Subsequently, a deletion PCR was performed on genomic DNA following Cre treatment to distinguish between wt (1.9 kb), floxed (4 kb) and deleted (1.5 kb) alleles (Fig.32). Both selected clones provided a deletion band of the expected size below wild type band upon HTNC treatment but floxed allele was not amplified, may be due to preference of *Taq*-polymerase in amplifying shorter fragments while using the same primers.

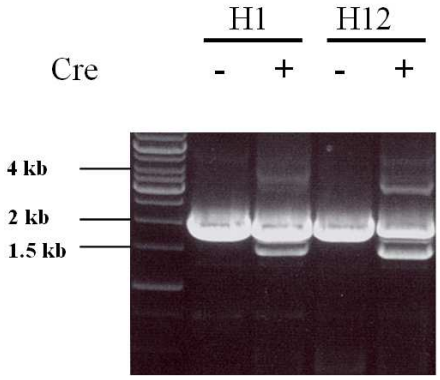

Figure 32: Deletion-competent lox-p sites in ES cell clones selected for generating knockout PAR-3 mouse. PCR using primers in 5´and 3´flanking regions of left and right lox-p sites shows deletion band in both selected clones only in the presence of HTNC.

2.3.5 Generation of chimeric mPAR-3$^{exon4\ flox/+}$ males

The selected clones were injected into 60 hosting CB-20 blastocysts and were implanted to psuedo-pregnant foster-mothers to obtain chimeric offspring. In total 11 males were born (Fig.33) of which 5 had chimeric skin patch ratio of above 50% and were used in crossing with C57/Black6 females to obtain transmitted floxed allele in the offspring which required to be checked by both PCR and Southern blot. In sum, 1000 pups were born and analyzed by PCR to detect transmission of the floxed allele to the progeny and even 2 mice with black coat color were born; all of which were wild type. A better alternative is to obtain new targeted clones using low passage ES cells for blastocyst injection to increase the chance of having highly chimeric males.

Figure 33: Chimeric PAR-3$^{exon4\ flox/+}$ males obtained from injecting the selected ES cells. Chimeric males are distinguished by typical patchy coat color and were crossed with wt C57/Black6 females for germline transmission.

3 Discussion

The mammalian vascular barrier mainly regulates the one-way movement of blood cells and molecules across the vascular lumen. On the other hand epidermis is a largely two-way barrier; an organ with lifelong self-renewal capacity, providing a stratified epithelium that functions as a barrier to separate the organism from the environment and external pathological factors and protect it against dehydration. Studies on animal models of skin diseases and inherited skin disorders in humans generally support the notion that barrier function depends on a differentiation process that on the one hand results in coordinated protein and lipid deposition in *stratum corneum* and on the other the formation of functional tight junctions in the granular layer of the epidermis (Tsuruta *et al.*, 2002). Vascular barrier formation is dependent on the formation of adjacently positioned, adhesive barrier units, the endothelial cells that are generally sealed in their intercellular junctions by adhesive AJ and TJ complexes (Dejana, 2004).

In this thesis we addressed the role of cell autonomous insulin/IGF-1 signaling in skin barrier formation and function and in endothelial barrier function. Epidermal specific inactivation of both the insulin receptor (IR) and IGF-1 receptor ($dko^{epi-/-}$) resulted in perinatal death (Stachelscheid *et al*., 2008). Here we show that $dko^{epi-/-}$ have increased transepidermal water loss when compared to control mice, resulting in severe dehydration and early neonatal lethality. Defective barrier formation was associated with a strong delay in functional outside-in barrier formation during embryogenesis as assessed by toluidine blue assays, altered appearance of cornified envelopes as well as abnormal ceramide content of intercorneocyte lipids in the *stratum corneum*. In addition, preliminary results suggest that processing of filaggrin, an important barrier protein, might be perturbed. In contrast, our initial analysis with subcutaneously injected tracer did not reveal any obvious defects in tight junctions although this requires more detailed analysis. In line with these findings, global gene expression data (Stachelscheid and Niessen, unpublished results) revealed major changes in expression of a range of proteins involved in regulating both the structural as well as the epidermal immune barrier (Table-1).

In contrast no obvious defects in vascular integrity could be observed when insulin receptor and IGF-1R receptor were deleted in adult vascular endothelial cells using an inducible Tie2-Cre system. This could either be due to the fact that endothelial insulin/IGF-1 signaling does not regulate vascular function under steady state conditions and that they only play a role in restoring vascular function after this has been disturbed, e.g. by induction of hypoxia or wounding. On the other hand, the results showed that inactivation of especially IGF-1R gene was highly variable ranging from over 90% of deletion to less than 10% and may have therefore been insufficient to observe a functional difference. In conclusion, the work presented in this thesis shows that Insulin/IGF-1 signaling are crucial cell autonomous regulators of epidermal barrier formation and function in the skin.

3.1 Insulin/IGF-1 signaling in epidermal barrier morphogenesis

The results presented in thesis showed that absence of insulin and IGF-1 signaling resulted in prenatal death due to defective epidermal water barrier function, thereby introducing insulin/IGF-1 signaling as key regulator of mouse EPB formation. The prenatal lethality observed in dko$^{epi-/-}$ mice is similar to several other mouse models with epidermis-specific inactivation of enzymes involved in protein and lipid modification such as CAP-1/Prss8, Alox-12b, β-glucocerebrosidase, glucosyltransferase (Ugcg) and stearoyl-Coenzyme A desaturase 1 (SCD-1) (Leyvraz *et al*., 2005; Epp *et al*., 2007; Hanely *et al*., 1997; Jennemann *et al*., 2007; Binczek *et al*., 2007). Basically the observed delay of epidermal barrier formation during embryogenesis in dko$^{epi-/-}$ mice is a hallmark of most of the aforementioned knockout mice. The late recovery in barrier acquisition in exemplified mutant mice indicates that compensatory mechanisms are activated in the course of morphogenesis in order to fulfill establishing a proper barrier before transition from humid *in utero* environment to dry desiccating conditions after birth. We observed apparent success of such compensatory efforts in the skin of the P0 dko$^{epi-/-}$ mice by almost complete exclusion of LY and toluidine blue (Fig.34).

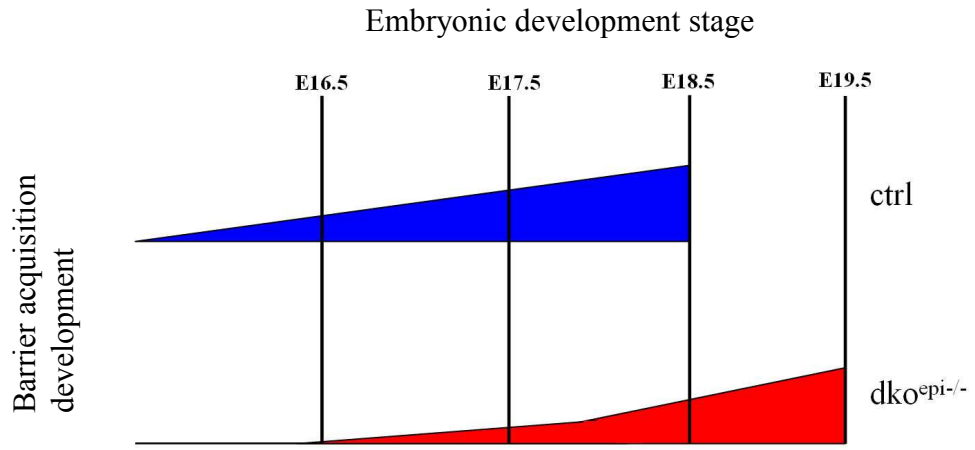

Figure 34: Delayed outside-in barrier formation in dko$^{epi-/-}$ embryos: Control mice show barrier acquisition in a constant rate between E16 and E18.5. Dko$^{epi-/-}$ embryos exhibit delayed initiation, much reduced rate of barrier acquisition and late recovery of barrier function around embryonic stage E19.

Characterization of the genes responsible for barrier recovery in our dko$^{epi-/-}$ mice requires analysis of several candidate genes which have been identified to be important in the proper establishment of the epidermal barrier. The late recovery in epidermal outside-in barrier of dko$^{epi-/-}$mice compared to control embryos, as shown by partial toluidine blue exclusion in E18.5 back skin, implicates upregulation of transcription factors between E16 until birth in these mice. These proteins are probably responsible for over production of protein or lipid components of the *stratum corneum*. The transcription factors such as Kruppel-like factor 4 (Klf4), Grainy head like-3 and AP-2 gamma

(Segre *et al*., 1999; Ting *et al*., 2005; Guttormsen *et al*., 2008) are required for proper EPB acquisition and would be interesting to analyze their expression in dko$^{epi-/-}$ epidermis.

In support of such compensatory efforts, the transcript levels for several structural proteins with late recruitment to SC belonging to Sprr, LCE and keratin protein families were found to be upregulated (Table-1).

To analyze the SC components with known essential roles in EPB formation, we analyzed the free extractable ceramides and corneocytes from dko$^{epi-/-}$. Significant deviation in the levels of long chain ceramides (Cer(C16/18 NS) and Cer(C24/26 NS)) was observed compared to control mice. This finding was invaluable as insulin/IGF-1 signaling, with known essential roles in mammalian development, was demonstrated in our work as central regulator of EPB formation *via* at least in part, regulating lipid metabolism in developing epidermis. The microarray data showed an overlap with altered lipid metabolism, as several key enzymes in ceramide synthesis and modification were affected (Table-1). One striking finding on ceramide profile of dko$^{epi-/-}$ mice was the high level of accumulated glucosylceramides (GlcCers). GlcCers are major precursors for ceramide production in the in CE (Doering *et al*., 2002), therefore are considered as probarrier lipids. The accumulated GlcCers in dko$^{epi-/-}$ mice would possibly be outlined in two ways (i) GlcCers are produced normally but could not be converted into ceramides, (ii) GlcCers are overproduced by keratinocytes as a compensatory reaction to increase ceramide production. Based on non-confirmed microarray data it appears that the second explanation is reasonable, as the levels of the GlcCer converting enzyme (Ugcg) was higher in dko$^{epi-/-}$ epidermis.

Insightful analysis of the production and conversion of various ceramide molecules in dko$^{epi-/-}$ mice demands analyzing the lipid content and mRNA transcript levels of key ceramide metabolizing enzymes (Table-1) of SC in late embryonic stage, e.g. E18. This gestational time point represents the time point during which GlcCers decline and their respective ceramides rise. This is reflected by increase in the levels of Cer(NS) and Cer(NP) by 25% and 440% respectively compared with earlier gestational time points which occurs parallel to decrease in the levels of their corresponding GlcCers indicating conversion of GlcCers to their respective ceramide types in the epidermis (Doering *et al*., 2002). Regardless of their critical role in epidermal water barrier development, we did no analyze the protein bound ceramides of the dko$^{epi-/-}$ mice. The gradual rise in the levels of ceramide types is also reported for protein bound ceramides of the epidermis (Doering *et al*., 2002) and we expect alteration in such corneocyte bound ceramids in dko$^{epi-/-}$ mice as well. The analysis of these ceramide types will be conducted and requires release of ester linked epidermal lipids by alkaline hydrolysis and TLC analysis (Doering *et al*., 2002).

Despite the delay seen in barrier acquisition for dko$^{epi-/-}$ mice, the late recovery followed a normal pattern reported in barrier development (Hardman *et al*., 1998). Normal expression of terminal differentiation markers such as involucrin, a protein marker of early differentiation normally

expressed in the upper spinous layers (Eckert *et al*., 1993), and loricrin, a marker of late differentiation (Mehrel *et al*., 1990) indicated normal development of upper spinous and granular layers of epidermis in P0 dko$^{epi-/-}$mice. Irrespective of their apparently normal epidermal differentiation, corneocytes from dko$^{epi-/-}$ mice and adult IGF-1R$^{epi-/-}$ mice, showed alteration in shape and interestingly FLG processing appeared to be impaired in dko$^{epi-/-}$ mice.

Proper CE assembly is essential in skin barrier development, as transglutaminase-1 deficient mice that lack confirmed envelopes, suffer from water loss, resulting in neonatal lethality (Matsuki *et al*., 1998). Alterations in corneocyte shape and resistance have also been described in various mouse models with defective skin barrier formation, ranging from irregularly shaped corneocytes in Prss8$^{epid-/-}$ mice to fragile corneocytes envelopes in Alox-12$^{epid-/-}$ mice (Leyvarez *et al*., 2005; Epp *et al*., 2007). Corneocyte phenotype in dko$^{epi-/-}$ mice resembled more that of Prss8$^{epid-/-}$ deficient mic. CAP1/Prss8 activates ENaC in epithelial cells and is known to be responsible for ENaC-mediated sodium current across the cells (Planès *et al*., 2010). Prss8$^{epid-/-}$ mice demonstrated impaired epidermal water barrier function, accompanied with defective FLG processing, reduced levels of protein bound ceramides and abnormality in corneocyte and outside-in barrier.

Our dko$^{epi-/-}$ mice share some skin abnormality features with Prss8$^{epi-/-}$ mice including defective outward and perhaps a defective inward barrier, morphological change of corneocytes and FLG processing. However, the epidermis in Prss8$^{epi-/-}$ mice was much thicker than the dko$^{epi-/-}$ mice; presenting thin epidermis with low stratification as a factor which could account for less efficient barrier function in dko$^{epi-/-}$ mice.

In light of the fact that filaggrin monomers are capable of binding and collapsing keratin filaments in the corneocyte (Lynley and Dale, 1983); therefore, defective monomeric FLG production could serve as one potential explanation for the abnormal corneocyte phenotype of dko$^{epi-/-}$ mice. An informative assay to demonstrate the integrity of the corneocytes in dko$^{epi-/-}$ mice is ultrasound treatment and assessment of their resistance by microscopic analysis. Nevertheless it appears that proper deposition of the lipid matrix in CE and FLG processing are coupled and mutually depend on each other. For example, mice with a targeted disruption of Alox-12b, an enzyme involved in fatty acid modification, showed a disturbed fatty acid composition of epidermal ceramides leading to neonatal death caused by water loss which was accompanied by absence of FLG (Epp *et al*., 2007). On the other hand, epidermal inactivation of the transmembrane serine protease, Matriptase/MT-SP1, which is known to process profilaggrin and produce FLG; lead to FLG loss together with the perturbation of lipid matrix formation. Therefore the judgment on whether impaired lipid production in dko$^{epi-/-}$ is merely due to loss of insulin/IGF-1 signaling and not FGL production is impossible at this point.

An interesting finding with relevance to the small reduction in FLG production in dko$^{epi-/-}$ mice which needs further validation, was almost 3 fold upregulation of a serine protease inhibitor,

Serpinb2 and downregulation of Tmprss4 (a family member of CAP-1/Prss8 protein). The family of serine protease inhibitors (SERPINs) genes comprises approximately 40 members. Serpins inhibit their target proteases by covalent binding leading to conformational change of the protease and thus abrogation of the function. Some previous studies on host-pathogen interactions have demonstrated that serpins are most likely responsible for protecting the host from bacterial proteases (Kaiserman *et al*., 2006). However new insights have revealed serpins to contribute in the reinforcement of the poorly developed epidermal cornified layer (Geng *et al*., 2006; Sevilla *et al*., 2007). Serpinb2 might potentially contribute to vitalizing the epidermal barrier of our dko$^{epi-/-}$ mice by reducing desquamation rate which is facilitated by the degradation of corneodesmosome proteins (Guerrin *et al*.,1998; Simon *et al*., 2001). On the other hand proteases involved in profilaggrin processing might be inhibited by Serpin activation in the dko$^{epi-/-}$ mice. Tmprss4 was recently shown to induce invasion and epithelial–mesenchymal transition (Kim *et al*., 2010). Low Tmprss4 transcript levels in dko$^{epi-/-}$ mice as shown by microarray data requires further validation by more quantitative techniques and would possibly shed new insights on the identification of new protease engaging profilaggrin processing.

The abnormal corneocyte phenotype in the IGF-1R$^{epi-/-}$ mice implies perturbation in protein components of CE. Therefore it is planned to investigate if adult IGF-1R$^{epi-/-}$ mice show reduced amounts of FLG similar to P0 mice. The results of this experiment might enable us to determine if FLG processing is regulated by IGF-1 signaling.

Caspase-14 was characterized as a protease involved in filaggrin processing; therefore its expression and cleavage to release functional isoforms in dko$^{epi-/-}$ epidermis was investigated. We looked for any regulatory effect of insulin/IGF-1R signaling on casp-14 expression and to investigate if reduced FLG in dko$^{epi-/-}$ epidermis was due to reduction in active casp-14 levels. Casp-14 deficient mice are sensitive to UV irradiation and represent abnormal degradation of FLG to smaller 15-20 kDa fragments (Denecker *et al*., 2007). The normal levels of non-active and active casp-14 in the epidermis of dko$^{epi-/-}$ mice suggests that insulin/IGF-1 signaling does not regulate the expression of casp-14 in the epidermis and probably this protease is not responsible for the observed impairment of FLG processing in dko$^{epi-/-}$ mice.

In order to investigate proper epidermal inside-out barrier, intraderaml biotin injection and cldn-1 immunolocalization were performed. There was indication for biotin diffusion in some areas of the epidermis above the granular layer to SC which was not conclusive and needs repetition of the experiment. In addition, TER assays did not show consistent differences between control and IGF-1R keratinocytes. On the other hand, normal cldn-1 signal was observed at cell-cell contacts in all suprabasal layers of the epidemris, indicating relatively normal assembly of TJs.

Cldn-1 WB also showed no difference in epidermal expression between experimental and control samples. Based on observed accelerated epidermal water loss and apparently normal epidermal

TJs, it is not possible in this point to make firm conclusions on integrity of TJs in dko$^{epi-/-}$ epidermis. However, abrogation of cldn-1 expression and inconsistently lower TER values seen in differentiating IGF-1R$^{-/-}$ keratinocytes implies regulation of TJs by IGF-1R mediated signaling in stratifying epithelia. In particular, the regulation of cldn-1 by IGF-1 signaling highlights requirement for in depth analysis of the downstream pathways.

UniGene	Gene name	Fold change	Affymetrix Probe Set ID
Cornified envelope components			
Sprr2f	small proline-rich protein 2F	203.84	1449833_at
Sprr2i	small proline-rich protein 2I	165.72	1422963_at
Sprr2d	small proline-rich protein 2D	14.09	1420771_at
Sprr1b	small proline-rich protein 1B	11.54	1422672_at
Sprr2k	small proline-rich protein 2K	10.21	1422425_at
Sprr2h	small proline-rich protein 2H	5.87	1422240_s_at
Lce3b	late cornified envelope 3B	157.42	1456001_at
Krt2-6a	keratin complex 2, basic, gene 6a	18.96	1422783_a_at
Krt6a	keratin 6A	20.49	1427700_x_at
Krt1-16	keratin complex 1, acidic, gene 16	13.71	1448932_at
Krt2-6a	keratin complex 2, basic, gene 6a	9.86	1422784_at
Krt2-6b	keratin complex 2, basic, gene 6b	8.2	1422588_at
Krt36	keratin 36	2.48	1427751_a_at
Krt17	keratin 17	1.6	1423227_at
Ceramide metabolism			
Ugcg	UDP-glucose ceramide glucosyltransferase	2.42, 2.31, 1.98	1421269_at, 1421268_at, 1435133_at
Psap	prosaposin	-1.55,-1.69	1421813_a_at, 1415687_a_at
Acer3	alkaline ceramidase 3	-1.51	1438435_at
Cerk	ceramide kinase	-1.76	1434034_at
Scd1	stearoyl-Coenzyme A desaturase 1	-7.78	1415964_at
Alox12e	arachidonate lipoxygenase, epidermal	-2.16	1426039_a_at
Alox5ap	arachidonate 5-lipoxygenase activating protein	-2.28	1452016_at
Alox12	arachidonate 12-lipoxygenase	-2.69	1422699_at
Epithelial host defense proteins			
Defb3	defensin beta 3	14070.49	1421806_at
Defb1	defensin beta 1	2.71	1419491_at
Ptgs2	prostaglandin-endoperoxide synthase 2	19.54, 8.89	1417262_at, 1417263_at
Ptges or mPGES-1	prostaglandin E synthase	3.62, 2.54	1439747_at, 1449449_at
Corneosome stability			
Serpinb2	serine (or cysteine) proteinase inhibitor, clade B	2.95	1419082_at
Ctss	cathepsin S	-3.29	1448591_at
Tmprss4	transmembrane protease, serine 4	-1.61	1426302_at

Table 1: List of genes derived from the gene expression analysis with relevance to epidermal differentiation and function

3.2 Insulin/IGF1 signaling in vascular barrier function

Largely normal retinal vascular barrier integrity in dko$^{veinduc-/-}$ mice indicated that insulin/IGF-1 signaling may not play a role in vascular barrier function under steady state vascular conditions. However variable efficiency of the Cre mediated deletion for IGF-1R gene in adult dko$^{veinduc-/-}$ mice prevented conclusive demonstration if insulin/IGF-1 signaling is dispensable for the maintenance of retinal vascular integrity. As knockout mice carrying a constitutively expressed Tie2Cre line provided a better deletion outcome for both genes (Kondo *et al*., 2003), such transgenic mouse line which is described to show deletion of the floxed genes exclusively in the endothelial cells would be the line of choice to cross with the IR/IGF1R$^{flox/flox}$ mice to obtain dko$^{veinduc-/-}$ mice (Pandelakis *et al*., 2001). If the mice obtained from these crossings are viable an interesting analysis is to evaluate the vascular barrier integrity in challenging hypoxia-induced conditions of oxygen induced retinopathy (OIR) assay. This assay is conducted exclusively on newborn mice and allows understanding the specific role of insulin/IGF1 receptors in either oxygen-induced vasoobliteration phase or vascular leakage promoting neovascularization phase (Smith *et al*., 1994).

The angiogenic stimuli driving the vascular reestablishment in the wounded skin are mediated by hypoxia induction in the wound site which is very similar to hypoxia conditions of OIR (Wattel *et al*., 1990). Thus another highly relevant model to understand the role of insulin/IGF-1 signaling in angiogenesis and vascular barrier function is analysing the skin wound healing response in the dko$^{veinduc-/-}$ mice which could provide information about the role of vascular IGF-1 signaling in non-healing diabetic wounds. This experiment is at the moment ongoing using dko$^{veinduc-/-}$ mice. A common microvascular-specific ocular disease in diabetes with late onset, directly related to globally imbalanced IR/IGF-1R signaling is diabetic retinopathy. Understanding the role of these signaling pathways would potentially contribute to the development of appropriate treatments set to adjust the activity levels of both pathways to normality.

3.3 Setbacks and prospects of the Par3^{exon4flox} mouse project

Although in this project we did not obtain mice with germline transmission of the targeted Par-3 allele, but two chimeric males successfully generated two pups with a distinct black coat color. This indicated fertilization of the female oocytes with sperms derived from injected ES cells. Southern blot and PCR analyses showed that both mice carried the wild type allele. Setting extensive crossings with high number of wild type females for the two promising chimeric males did not result in germline transmission. This indicated the low contribution of the injected ES cells in the blastocysts to spermatogenesis procedure in the chimeric fathers. Currently another transfection attempt with the targeting construct has been undertaken using ES cells with low passage and high germline transmission potential.

With respect to the crucial role described for Par-3 protein in cell polarity determination and the formation and function of TJs (Hirose *et al*., 2002), following generation of the $Par3^{exon4flox}$ mouse, crossings between $Par3^{exon4flox}$ and either K14-Cre or Tie2-Cre mice will be performed. $Par\text{-}3^{ve\text{-}/\text{-}}$ and $Par\text{-}3^{epi\text{-}/\text{-}}$ knockout mouse models will enable us to answer important questions on the role of Par-3 in epidermal morphogenesis and barrier acquisition in epidermis and the vascular system.

4 Materials and Methods

4.1 Mice

4.1.1 Insulin receptor and IGF-1 receptor floxed mice

The generation and genotyping of the insulin receptor floxed, IGF-1 receptor floxed and the K14-Cre mice and deletion screening by PCR have been described (Bruning *et al*., 1998; Hafner *et al*., 2004).

4.1.2 Generation of PAR-3$^{exon4\ flox/+}$ mouse

The Par-3 targeting construct was prepared by PCR amplification of the left 3.7 kb and right 5 kb flanking regions of PAR-3^{exon4} gene which after subcloning were inserted into their respective restriction sites in pEasyflox plasmid as final targeting construct. Briefly, exon 4 and its flanking 5′and 3′ region (637 bps PCR product) was inserted into 5′-AscI/MfeI-3′ sites, the short arm was inserted into 5′-NotI/AvrII-3′ sites before the first lox-p and Neo site and the long arm was inserted between the second lox-p site and Tymidine Kinase selection cassette in 5′-XhoI/PmeI-3′ restriction sites. The Par-3 targeting construct was linearized by NotI digestion, yielding a 16611 bps plasmid. The NotI-linearized plasmid was subsequently used for electroporation in cultured embryonic stems (ES) cells

Gene targeting was performed in 129/C57Black 6 hybrid ES line, V6.5. For transfection, 1x10^7 ES cells were transfected with 50 µg DNA. Approximately 9 days after transfection, G418-resistant, Ganciclovir-sensitive colonies were picked and expanded on 96-well tissue culture dishes. Genomic DNA was extracted from each clone and analysed by Southern blot and PCR analysis. The selected ES cell clones were subsequently expanded and transfected *in vitro* with Cre recombinase (HTNC) to check the efficiency of the lox-P sites in mediating neo-exon4 deletion by PCR using sense "for-sapar3-1" and anti-sense "3-floxedpar3 in LA"primers to distinguish between wild type (2 kb) and deleted (1470 bps) alleles. Recovery, microinjection and transfer of 3.5 day p.c. embryos were performed according to standard procedures. Chimeric animals (50-65% chimerism based on coat color) were bred with female C57Black 6 background. The list of all the primers for genotype determination as well as deletion and long-range cloning PCRs are provided in Table-2.

4.1.3 Feeding with tamoxifen diet

Adult (three weeks-old mice), the Tie2Cre$^{ERT2/+}$ IR/IGF-1R$^{fl/fl}$ mice and the Tie2Cre$^{ERT2+/+}$ IR/IGF-1R$^{fl/fl}$ littermates, were fed for 5-6 weeks with free access to a chow containing 0.4 mg tamoxifen per kg of food (Forde *et al*., 2002).

4.2 Molecular DNA techniques

4.2.1 DNA Ligation

For ligation of specific inserts into plasmids, the T4 ligase and its corresponding buffer (Fermentas) were used. The ligation was done overnight at 16°C. Insert DNA and vector DNA were ligated in a relation of 3:1.

4.2.2 DNA Digestion and de-phosphorylation of DNA fragments

All DNA modifying enzymes (i.e. restriction enzymes, T4 DNA ligase, calf intestinal phosphatase (CIP), Klenow fragment polymerase) were purchased from New England Biolabs and used according to the manufacturer's protocol.

4.2.3 Recombinant DNA techniques

The following standard recombinant DNA techniques were performed as described in Sambrook and colleagues (1989), or according to the manufacturer's instructions: restriction digestion, T4 DNA ligation, dephosphorylation of DNA fragments, agarose gel electrophoresis and elution of DNA fragments, phenol/chloroform extraction and ethanol precipitation. DNA sequencing and oligo synthesis was performed by the service of the Eurofins MWG (Ebersberg-Germany) and sequences were analysed using the gENTLE sequence analysis software (Magnus Manske, Cologne).

4.2.4 Polymerase Chain Reaction (PCR)

For several cloning strategies PCR were performed to amplify DNA fragments. The Expand High Fidelity PCR System (Roche) was used at a concentration of 2.6 U/reaction in combination with 0.25 µM of both sense and antisense primers, 0.25 mM dNTP mix, 1x reaction buffer and 10 ng plasmid DNA as template in 25 µl reaction volume. The template DNA was denatured at 95°C for 2 min followed by 35 rounds of amplification each consisting of 1 min at 95°C, 1 min at the appropriate annealing temperature, and 1 min per kb length of the amplified DNA fragment at 72°C for elongation. Based on the number of specific nucleotides in the primer, the following formula was used to estimate the melting temperature of primers: Tm=2(A+T)+4(G+C).

For genotyping and deletion PCRs, REDTaq™ ReadyMix PCR kit with $MgCl_2$ (Sigma) was used with primers noted in Table-2.

4.2.5 Southern Blot

DNA samples were digested with restriction enzymes and run for 24-30 h at 25 V on 0.8% agarose. Southern blotting was carried out by standard capillary methods (Sambrook *et al*., 1989) onto Hybond-N (GE Healthcare). After DNA transfer, the membrane was incubated at 80°C for 1 h to fix the DNA permanently to the membrane. 5´, 3´and Neo probes were amplified by PCR, run in 0.8% agarose gel and extracted using the QIAquick gel extraction kit. Radioactive labelling was performed applying 50-100 ng of DNA. The probes were labeled with [α32P]-dCTP (Amersham Pharmacia Biotech) using the Ladderman™ Labelling Kit (Takara) and purified using ProbeQuant™ G-50 Micro Columns (GE Healthcare).

The membrane was pre-hybridized in QuickHyb hybridization solution (Stratagene) at 65°C for 60 min. For hybridization of the DNA fragments, the radiolabelled probe was added and incubated at 65°C overnight. After washing the blot in wash buffer (2X SSC) the DNA fragments were visualized with the x-ray film (Kodak Biomax MS).

4.2.6 Bacterial Transformation

The *E.coli* strain DH5α was cultured as described elsewhere (Sambrook *et al*., 1989). For transformation and production of chemically competent DH5α, the method of Hanahan was applied (Hanahan, 1983).

4.3 Molecular RNA techniques

4.3.1 RNA isolation from cells

Isolation of RNA from cultured keratinocytes was achieved using RNeasy mini kit (Quiagen) according to the manufacturer´s instructions.

4.3.2 cDNA synthesis

For first strand cDNA synthesis of RNA, random primers in combination with Superscript II Reverse transcriptase (Invitrogen) were used according to the manufacturer's protocol.

4.3.3 Semi-quantitative RT-PCR

Semi-quantitative RT-PCR was performed using REDTaq™ ReadyMix. 1 µl of synthesized cDNA per reaction was used as template under either 30 or 40 cycles of PCR amplification.

4.4 Barrier function assays for epidermis and keratinocytes

4.4.1 Measurement of transepidermal water loss

Transepidermal Water Loss (TEWL) of 1-day-old mice was measured using a Tewameter TM-300 (Courage and Khazaka) equipped with a small-diameter (3 mm) probe and measurements were digitally recorded via a MPA5 mulitprobe adapter. Measurements were performed on belly skin until there was no fluctuation in values and were continued for 10 seconds after reaching a constant plateue. Only values obtained from the stabilized late readouts were used for statistical quantifications.

4.4.2 Lucifer yellow assay

For penetration assays, backs of newborn mice were immersed in 1mM lucifer yellow solution for 1 h after which the mice were killed (Koch *et al*, 2000). Frozen sections were counterstained with Phalloidin/DAPI and penetration of the dye was assessed by immunofluorescence microscopy.

4.4.3 Toluidine blue assay

Toluidine blue dye staining of embryos was carried out as described (Koch *et al*, 2000). Developmental stages of mice were determined by assuming that fertilization occurred in the

middle of the dark cycle the day before plugs were identified. Embryos were incubated for 1 min in 25, 50, and 75% methanol in PBS, followed by 1-min incubation in 100% methanol, and a descending series of incubations in 75, 50, and 25% methanol in PBS for 1 min. Embryos were then washed in PBS for 1 min and stained with 0.1% toluidine blue for 10 min. After staining, embryos were embedded in agarose and photographed using Olympus E-620 digital camera. Images were processed with Adobe Photoshop.

4.4.4 Inside-out barrier assay with sulfo-NHS-Biotin

TJ permeability assay using surface biotinylation technique was performed as described before (Furuse *et al*., 2002). 50 µl of 10 mg/ml EZ-Link™ Sulfo-NHS-Biotin (MW, 443 Daltons) in PBS containing 1 mM $CaCl_2$ was injected into the dermis on the back of the Ctrl and $dko^{epi-/-}$ newborns. After 30 min incubation, the skin biopsies were taken out, embedded in tissue-tec solution and frozen on dry ice. About 5 µm-thick frozen sections were used for immunofluorescence analysis.

4.4.5 Transepithelial resistance measurement

$5x10^5$ keratinocytes were plated on collagen 1 coated polycarbonate filter inserts (pore size 0.4 µm, Millipore) in a 24 well format. One day after plating, junction and barrier formation was induced by Ca^{2+} switch and electrical resistance was measured at indicated time points by using the automated ohmmeter (cellZscope) from nanoAnalytics (Münster-Germany).

4.5 Retinal vascular barrier assay

4.5.1 Perfusion with 2000 kDa FITC-dextran

$Dko^{ve-/-}$ and control mice were perfused with 200 µl of a 50 mg/ml solution of 2000 kDa FITC-dextran (sigma) prepared in PBS *via* left cardiac ventricule. After 5 min of perfusion, the eyes were extracted, fixed overnight in PFA and cornea was cut out under a stereomicroscope with a pair of spring scissors.

4.5.2 Systemic infusion with sulfo-NHS-Biotin

The experimental mice were intravenously injected with 100 µl of biotin (Cyanagen, Italy) solution (50 mg/ml in PBS) using a G-30 needle. The tracer was allowed to circulate for 10 min, after which, the mice were sacrificed and the eyes were fixed in 4% PFA overnight.

4.5.3 Preparation of retinal wholemounts

Using fine scissors, the retinas were separated from sclera and four radial incisions were made in 3, 6, 9 and 12 o'clock positions. Retinas were flattened using fine brush tips with Internal Limiting Membrane (ILM) facing upward in Gelvatol and covered by round cover slips. The cover slips were sealed with nail polish the next day to prevent tissue drying. The imaging and photo acquisition was performed with a fluorescent camera.

4.6 Sample preparation and immunoblots analysis

4.6.1 Separation of the epidermis from dermis

Epidermis was separated from the dermis by floating skin biopsies, epidermis side up, in a 0.5 M Ammonium thiocyanate (NH_4SCN) solution prepared in phosphate buffer, (0,1M Na_2HPO_4, 0,1M KH_2PO_4, pH6.8) for 20 min on ice. Epidermis was either snap frozen in liquid nitrogen or immediately processed for protein isolation.

4.6.2 Immunoblot analysis of primary keratinocytes and epidermis

Cultured keratinocytes were lysed in NP40 buffer (1% NP40, 0.1% SDS, 0.5% sodium deoxycholate, 150 mM NaCl, 50 mM Tris-HCl pH7.4). After 10 min incubation on ice, the cells were harvested with a cell scraper and transferred to a reagent tube. Lysates were cleared by centrifugation at 13000 rpm for 10 min at 4°C. Protein concentrations were determined using Bradford assay (Biorad). Lysates were diluted in Laemmli buffer, heated for 5 min at 95°C and 50 µg of total protein was separated by SDS-PAGE on either 7% or 4-12% precast gels (NuPage system) and transferred to nitrocellulose according standard blotting procedures. Membranes were blocked with 5% non fat dry milk (Haerschle) in TBS-T (0.1% Tween 20, 137 mM NaCl, 20 mM Tris-HCl pH7.5) and incubated with the primary antibody diluted in blocking solution overnight at 4°C. After wash steps in TBS-T, the membranes were incubated with the appropriate horseradish peroxidase-coupled secondary antibody. Immunoreactive proteins were detected by enhanced chemiluminescence using either the SuperSignal West Pico or SuperSignal West Femto kit (Pierce).

Frozen epidermal splits were thawed and homogenized in 2 ml Eppendorf tubes by Retsch Mixer Mill MM 400 (Düsseldorf, Germany) using little steel balls for 3 min. Epidermal samples were lysed with Urea buffer (100 mM NaH_2PO_4, , 8 M Urea, 10 mM Tris-HCl pH 8) and spun down to obtain a cleared supernatant. All other protein assays were similar to keratinocytes except the samples were not denatured by heating to avoid covalent modification of peptides in the presence of Urea. For filaggrin immunoblots, native 4-16% polyacrylamide gels (Invitrogen) were run with SDS-PAGE.

4.6.3 Quantification of immunoblot bands with ImageJ

Quantification of the bands was performed by selecting the area, mean gray value and integrated density functions of the ImageJ software on a grayscale picture. To obtain the relative signal intensity for each test sample band, the intensity values were divided to their respective β-actin band values.

4.7 Immunofluorescence techniques

4.7.1 Paraffin embedding of experimental tissues

Freshly isolated tissue samples, were washed quickly in ice cold PBS and fixed in 4% PFA overnight at 4°C. After dehydration, tissues were paraffin embedded and stored at room temperature until use. Paraffin embedded samples were cut into 5-6µm thick sections and dried overnight on glass slides at 37°C.

Eyes were fixed overnight in Methacarn fixative solution composed of 60% methanol, 30% 1,1,1-trichlorethane (TCE), 10% acetic acid, followed by dehydration procedure. Fixed samples were first incubated with RAS-paraffin No.3 (1 x 2 h 60°C), then RAS-paraffin No.6 (overnight 60°C) and were finally embedded in RAS-paraffin No.9.

4.7.2 Immunofluorescence analysis of keratinocytes and tissue sections

Keratinocytes were plated in 24 well plates on collagen coated glass cover slips. Differentiation was induced by switching from low Ca^{2+} medium (50 μM) to medium containing 1.8 mM Ca^{2+} for the indicated time points. Cells were washed with PBS and fixed for 10 min either with ice cold methanol, 4% PFA/PBS or acetone, respectively depending on the antibody used in the experiment. 4% PFA/PBS fixed cells were permeabilized by 5 min incubation with 0.5% Triton X-100/PBS. After 3 rinses in PBS, unspecific binding sites were blocked with 1% BSA/PBS for 30 min. All antibodies (see Table-3) were diluted in blocking solution and incubated overnight at 4°C, followed by 3 washes in blocking solution for each 5 min. After washing, cover slips were incubated with appropriate secondary antibodies coupled to either Alexa 488 or Alexa 594 (see Table-4). Nuclei were counterstained with either DAPI or propidium iodide. Cover slips were mounted with gelvatol on microscope slides (VWR).

Frozen sections were analysed similar to keratinocytes but paraffin sections were deparaffinized, rehydrated in ethanol series and washed twice in PBS. Afterwards the samples were unmasked using the antigen retrieval buffer A (EMS) in Retriever (PickCell Laboratories, Netherlands).

Photos were taken with a NIKON Eclipse E800 microscope equipped with a NIKON DMZ1200 camera or an Olympus IX81 microscope with the digital camera cool snapTM HQ2 (photometrics). Photos were stored with the software Softworx 3.6.1 (Applied Precision) and pictures were processed with Adobe Photoshop and ImageJ.

4.7.3 Immunofluorescent labelling of biotin in retinal wholemounts

The retinas were removed and fixed for 10 min in ice-cold acetone followed by two washes in PBS for 20 min. The samples were blocked for 2 h in blocking buffer (20% normal goat serum with 0.05% TWEEN 20). After 2 washes with PBS, samples were incubated for 1 h with Alexa fluor 488-conjugated Streptavidin, supplemented with 0.2% fish skin gelatine and 0.1% TWEEN 20 in PBS. After two washes with PBS and 10 min post fixation step in PFA, the retinas were flatmounted on glass slides as mentioned above.

4.8 Primary keratinocyte and endothelial cell culture

4.8.1 Isolation and culture of primary keratinocytes

The experiments described were performed with primary keratinocytes isolated from K14Cre/+; IGF-1R$^{fl/fl}$ (IGF-1R$^{-/-}$) and IGF-1Rfl/fl (ctrl) mice. All experiments were done under sterile conditions.

Epidermis of newborn pups was separated from dermis by overnight trypsin digestion and subsequent mechanical stripping. Epidermis was chopped into peaces and agitated in low Ca^{2+} (50 µM) keratinocyte medium at 37°C for 1 h. Cell suspension was plated on collagen type 1 coated dishes (0.03 mg/ml) in co-culture with a J2 3T3 fibroblast feeder layer.

Keratinocyte cell culture medium

- DMEM (FAD)-medium (Growth medium for keratinocytes)
- Insulin5 µg/ml
- Chelated FCS 10%
- L-glutamine2 mM
- Cholera toxin 10^{-10} M
- Hydrocortisone 0.4 µg/ml
- Epidermal growth factor 10 ng/ml
- Penicillin (100 units/ml) and streptomycin (100 µg/ml)

PBS: Dulbecco´s phosphate buffered saline without calcium and magnesium

Trypsin: 1x trypsin/ EDTA, 0.05 % (w/v)

4.8.2 Splitting

In order to split the cells, growth medium was removed and the cells were washed twice with PBS and trypsinized for approximately 10 min at 37 °C. Trypsin was inactivated by adding 3 fold amount of complete medium. The suspension was transferred into a 15 ml falcon and centrifuged at 800 rpm for 5 min. The supernatant was discarded and cells were resuspended in required volume of growth medium and plated on newly coated 6 cm dishes.

4.8.3 Differentiation and induction by Ca^{2+} switch

Confluent keratinocytes were differentiated by raising calcium level from 50 µM to 1.8 mM and subsequent incubation for indicated time points.

4.8.4 Mouse Lung Endothelial Cells (MLECs) isolation

For endothelial cell isolation, lungs from either Tie2Cre$^{ERT2/+}$ IR/IGF-1R$^{fl/fl}$ or Tie2Cre$^{ERT2+/+}$ IR/IGF-1R$^{fl/fl}$ were aseptically removed and homogenized by a combination of mechanical and enzymatic digestion with sharp blades and type 1 collagenase. Collagenase treatment of the minced tissue was conducted with gentle agitation at 37°C for 30 min. The single cells were subject to two rounds of positive selection using PECAM-1 conjugated dynabeads before plating and later in passage-0 after reaching confluency. Endothelial cells in all steps were grown on plastic dishes coated with gelatine (0.1% v/v) /fibronectin (10 µg/ml) /collagen (10 µg/ml). Wash and splitting steps were similar to keratinocytes.

Endothelial cell culture medium

The growth medium was purchased from Promocell (Heidelberg-Germany) with following composition:

- DMEM medium
- Heparin 90 µg/ml
- Fetal Calf Serum 0.02 ml/ml
- Hydrocortisone 1 µg/ml
- 10 ng/ml epidermal growth factor (EGF)
- Endothelial Cell Growth Supplement 0.004 ml/ml
- Penicillin (100 units/ml) and streptomycin (100 µg/ml)
- Epidermal Growth Factor (recombinant human) 0.1 ng/ml
- Basic Fibroblast Growth Factor (recombinant human) 1 ng/ml

4.8.5 HTNC treatment of primary endothelial cells

$4x10^5$ primary endothelial cells were grown in a 10 cm dish and allowed to attach to the plate. HTNC protein at 5 µM in a 1:1 mixture of DMEM/PBS (without FCS and other additives) was sterilized with syringe-attached filters and diluted serially to obtain two fold dilution series. After overnight incubation, the cells were washed twice with PBS and fresh medium was added.

4.8.6 Tamoxifen treatment of primary endothelial cells

48 mM stock solution of 4-Hydroxy-Tamoxifen (OHT) was prepared by dissolving and vortexing 5 mg of OHT in 296 µl of 100% EtOH. This stock was further diluted to make a working stock of 4 mM solution in 100% EtOH. Finally, the cells were treated with 2 µM OHT in growth medium overnight.

4.9 Corneocyte and lipid analysis

4.9.1 Cornified envelope preparations

The ears from mice were excised and heated for 10 min in cornified envelope extraction buffer: 0.1 mM Tris (pH 8) and 20 mM DTT, 5 mM EDTA, 2% SDS (Hohl *et al*., 1991) at 96°C, cornified envelopes were collected by centrifugation and were resuspended in TE buffer (10 mM Tris, 1 mM EDTA) and analyzed by phase-contrast microscopy (Olympus CKX41 microscope).

4.9.2 Analysis of corneocytes by ImageJ

The area and circularity indices of the photographed corneocytes were measured using area and circularity functions of the ImageJ software after defining a scale bar with equal size for ctrl and $dko^{epi-/-}$ mice. In total, 100 corneocytes were analyzed for each mouse and the data were analyzed by statistical software GraphPad Prism 5.

4.9.3 Lipid extraction and analysis

Epidermal free lipids were extracted from 3 mg of dry *stratum corneum* of different newborn skins. The lipid were analysed by thin layer chromatography using a solution containing chloroform/methanol/glacial acetic acid 190:9:1 (v/v/v) in the Lipidomics facility of the University of Cologne.

4.9.4 Ceramide nomenclature legend

Sphingoid bases:

S = Sphingosine

P = Phytosphingosine

H = 6-Hydroxysphingosine

Fatty acids:

N = not hydroxylated

A = α-hydroxylated

O = ω-hydroxylated

E = esterified with linoleic acid

Table-2: List of primers and their respective PCR products

Primer ID	Sense primer	Antisense primer	Product
Cldn1sense antisense	TCTACGAGGGACTGTGGATG	TCAGATTCAGCAAGGAGTCG	Cldn-1 RT-PCR
600bp5'/1kb3	TCCCTCAGGCTTCATCCGCAA	CTTCAGCTTTGCAGGTGCACG	IGF-1R wt/flox typing
IR5´/IR3´	CTGAATAGCTGAGACCACAG	GATGTGCACCCCATGTCG	IR wt/flox typing
IGF-1R Del 5' 1kb3	TTATGCCTCCTCTCTTCATC	CTTCAGCTTTGCAGGTGCACG	IGF-1R deletion PCR
forinsulInt-5 revInsulInt-3	ACGCCTACACATCACATGCATATG	CCTCCTGAATAGCTGAGACCACAG	IR deletion PCR
5 floxedpar3 in int/ 3-floxedpar3 in la	GCCCTGTGTGAGCATTACTG	TCCCTGGAACTGAGGAAGAC	Par-3 wt/flox typing
K14-2202snew CreSL2as	GATGAAAGCCAAGGGGAATG	CATCACTCGTTGCATCGACC	K-14 Cre transgene typing
SC1_for SC3_rev	GTCCAATTTACTGACCGTACAC	CTGTCACTTGGTCGTGGCAGC	Tie2creERT2 transgene typing
3probe5-par3 3probe3-par3	TAGCAGCATGGGAAGTAAATG	GACAATCTGAGCTCATGTTAC	Par-3 exon4, 3´probe
Scai-5-5-1-560 Scai-5-3-1-560	TCAGGAGATTCTGATCCCAC	AAAGGGGAGAACAGGACAC	Par-3 exon4, 5´probe
Par-3, Primer 1 Par-3, Primer 2	CCTGCGTACAGTCTCCCGGC	AGCTGTCGTGGACCAGCGGGT	Par-3, 1st ATG site in exon 1
Par-3, Primer 3 Par-3, Primer 2	CGCGACAGGTAGAAGCATCCATC	AGCTGTCGTGGACCAGCGGGT	Par-3, 2nd ATG site in exon 4
Par-3, Primer 4	CACCGCCCTCGGCCACGAATC	TTGCCGTAGACGCTGTATCCG	Stop site for Par-3 variant 3

Par-3, Primer 5			
Par-3, Primer 4 Par-3, Primer 6	CACCGCCCTCGGCCACGAATC	GGCTTTGTGCACACAAGGCAG	Stop site for Par-3 variant 1
Par-3, Primer 7 Par-3, Primer 8	GGGAGCCCTGCTGCACCTGAG	GTCCATAAGTCCCAGGACATG	Stop site for Par-3 variant 2
GAPDH for GAPDH rev	TGCCCCCATGTTTGTGATG	TGTGGTCATGAGCCCTTCC	GAPDH RT-PCR
for-sapar3-1 3-floxedpar3 in la	GCCCTGGCTATCCTGAAACT	TCCCTGGAACTGAGGAAGAC	Par-3 deletion PCR
5-kpn-f6-431 R2.3 neo63	AATAGTAACCACCCTGGACC	TCCAGACTGCCTTGGGAAAA	Par-3 ES cell screening of Short arm-Neo- 4.3 kb
Forloxp-la 3probe3-par3	GCTATACGAAGTTATAAGCTTAAGC	GACAATCTGAGCTCATGTTAC	Par-3 ES cell screening of Long arm-3´Loxp- 5.63 kb
5saparnoti-2 3sapardavr	GCGGCCGCTGTATGGCTCTGACTTGAAGACAACAAC	CCTAGGATCCGATTGAATTCAGATCTTTAGAC	Par-3 short arm 3.7 kb PCR
5flpardAsc 3flpardmfe	GGCGCGCCTTCAATCCCACATGATAGGA	CAATTGGATCCATCAGAAGATCATACT	Par-3 floxed exon4 PCR, 622 pbs
5lapardXhoi 3lapardpme	CTCGAGGATATCGTGTTTTGAAATGATAATATATCAG	GTTTAAACCTAGGGAAGAGTGCAATTCTC	Par-3 long arm 5 kb PCR
ForNeoprobe553 RevNeoprobe553	TGAATGAACTGCAGGACGAGGCA	ATTGCTGAAGAGCTTGGCGGC	Neo probe for southern blot

Table-3: Primary antibodies

Antigene	Source	Working dilution	Catalog number	company
Filaggrin	Rabbit	WB:1/1000 IF: 1/500	PRB-417P	Convance
Loricrin	Rabbit	WB:1/1000 IF: 1/500	PRB-145P	Convance
Involucrin	Rabbit	WB:1/1000 IF: 1/500	PRB-140C	Convance
Casp-14	Rabbit	WB:1/2000 IF: 1/1000		From P.Vandenabeele Ghent-Belgium
Cldn-1	Rabbit	WB:1/1000 IF: 1/500	51-9000	Zymed
ZO-1	Rabbit	WB:1/1000 IF: 1/500	61-7300	Zymed
β-catenin	Rabbit	WB:1/1000	RMA-12741.	Epitomics

		IF: 1/500	Lot:Yf060402r	
PECAM-1	Rat	Coating Dynabeads:1/1000	553708	BD Pharmingen
Actin	Mouse	WB 1/10000		C4, Sigma Aldrich

Table-4: Secondary antibodies

Antigene	Source	Working dilution	Catalog number	company
Alexafluor 488 anti-rabbit	Goat	IF 1/500	A21206	Molecular Probes
Alexafluor 488 Streptavidin		IF 1/500	S32354	Molecular Probes
Phalloidin TRITC	*Amanita Phalloides*	IF 1/500	P-1951	Sigma
Anti-Rat IgG Dynabeads	Sheep		11035	Invitrogen
IgG-HRP anti-rabbit	Goat	WB 1/5000		BioRad
IgG-HRP anti-mouse	Goat	WB 1/5000		BioRad
Alexafluor 594 anti-rabbit	Donkey	IF 1/500	A21207	Invitrogen

5 Abbreviations

BSA bovine serum albumin

Bp base pairs

BRB blood retinal barrier

C carbon atom

°C degree Celsius

CAP channel-activating serine protease

cDNA complementary DNA

CE cornified envelope

Cer Ceramide

Cre site specific recombinase from phage P1(causes recombination)

DAPI 4`6-Diamidino-2-phenylindol

DKO double knockout

DNA deoxyribonucleic acid

DMSO dimethylsulfoxide

DR diabetic retinopathy

E embryonic day

ECL enhanced chemiluminescence

EDTA ethylene diamine tetra acetic acid

EGF epidermal growth factor

ENaC epithelial sodium channel

ERT estrogen receptor

EtOH ethanol

FCS fetal calf serum

Fig figure

FLG filaggrin

floxed/lox lox P flanked

Foxo1 forkhead-O transcription factor 1

GAPDH Glycerinaldehyd-3-phosphat-Dehydrogenase

GlcCer Glucosylated ceramide

GTP Guanosintriphosphat

HTNC His-Tat-NLS-Cre

g gram

h hours

H&E hematoxylin/eosin

HRP horse radish peroxidase

Hz hertz

IF immunofluorescent

IGF-1 insulin-like growth factor 1

IGF-1R insulin-like growth factor 1receptor

IR insulin receptor

K keratin

Kb Kilo base

kDa kilo Dalton

KO knockout

LCE late cornified envelope

LY lucifer yellow

mg milligram

min minute

µl micro liter

ml Milliliter:

µm micro molar

mM millimolar

mRNA messenger RNA

n nano

Neo^R Neomycin resistance

NGS normal goat serum

NVU neurovascular unit

OIR oxygen-induced retinopathy

P postnatal day

PAGE polyacrylamide gel electrophoresis

PBS phosphate buffered saline

PCR polymerase chain reaction

PI3K phosphatidylinositol 3 kinase

PIP2 phosphatidylinositol (4,5) biphosphate

PIP3 phosphatidylinositol (3,4,5) triphosphate

PFA paraformaldehyde

PMSF phenylmethylsulphonylfluorid

Prss8 protease serine S1 family member 8

RAS-paraffin Richard-Allan Scientific paraffin

Rac1 Ras-related C3 botulinum toxin substrate 1

RNA ribonucleic acid

RNase ribonuclease

ROP retinopathy of prematurity

RT real time

rpm rounds per minute

SC *stratum corneum*

SDS sodium dodecyl sulphate

Sprr Small prolie rich protein

TBS tris buffered saline

TE Tris-EDTA buffered

TEWL transepidermal water loss

Tie2 Tyrosine kinase with immunoglobulin and epidermal growth factor homology

domains-2

Tween polyoxethylene-sorbitan-monolaureate

U unit

vs. versus

v/v volume/volume

w/v weight per volume

WB western blot

6 References:

Abbas A, Grant PJ, Kearney MT. Role of IGF-1 in glucose regulation and cardiovascular disease. Expert Rev Cardiovasc Ther. 2008 Sep; 6(8):1135-49.

Accili D, Drago J, Lee EJ, Johnson MD, Cool MH, Salvatore P, Asico LD, José PA, Taylor SI, Westphal H. Early neonatal death in mice homozygous for a null allele of the insulin receptor gene. Nat Genet. 1996 Jan; 12(1):106-9.

Anderson JM, Van Itallie CM, Fanning AS. Setting up a selective barrier at the apical junction complex. Curr Opin Cell Biol. 2004 Apr; 16(2):140-5.

Arnqvist HJ. The role of IGF-system in vascular insulin resistance. Horm Metab Res. 2008 Sep; 40(9):588-92

Aurrand-Lions M, Johnson-Leger C, Wong C, Du Pasquier L, Imhof BA. Heterogeneity of endothelial junctions is reflected by differential expression and specific subcellular localization of the three JAM family members. Blood. 2001 Dec 15; 98(13):3699-707.

Backendorf C, Hohl D. A common origin for cornified envelope proteins? Nat Genet. 1992 Oct; 2(2):91.

Barber AJ, Antonetti DA.Mapping the blood vessels with paracellular permeability in the retinas of diabetic rats. Invest Ophthalmol Vis Sci. 2003 Dec; 44(12):5410-6.

Barreca A, De Luca M, Del Monte P, Bondanza S, Damonte G, Cariola G, Di Marco E, Giordano G, Cancedda R, Minuto F. In vitro paracrine regulation of human keratinocyte growth by fibroblast-derived insulin-like growth factors. J Cell Physiol. 1992 May; 151(2):262-8.

Baserga R, Hongo A, Rubini M, Prisco M, Valentinis B.The IGF-I receptor in cell growth, transformation and apoptosis. Biochim Biophys Acta. 1997 Jun 7; 1332(3):F105-26.

Bennett WR, Crew TE, Slack JM, Ward A. Structural-proliferative units and organ growth: effects of insulin-like growth factor 2 on the growth of colon and skin. Development. 2003 Mar; 130(6):1079-88.

Benton R, St Johnston DA conserved oligomerization domain in drosophila Bazooka/PAR-3 is important for apical localization and epithelial polarity. Curr Biol. 2003 Aug 5; 13(15):1330-4.

Benyoucef S, Surinya KH, Hadaschik D, Siddle K. Characterization of insulin/IGF hybrid receptors: contributions of the insulin receptor L2 and Fn1 domains and the alternatively spliced exon 11 sequence to ligand binding and receptor activation. Biochem J. 2007 May 1; 403(3):603-13.

Bernstein MH, Hollenberg MJ. Fine structure of the choriocappillaris and retinal capillaries. Invest Ophthalmol. 1965 Dec; 4(6):1016-25.

Binczek E, Jenke B, Holz B, Günter RH, Thevis M, Stoffel W. Obesity resistance of the stearoyl-CoA desaturase-deficient (scd1-/-) mouse results from disruption of the epidermal lipid barrier and adaptive thermoregulation. Biol Chem. 2007 Apr; 388(4):405-18.

Bol DK, Kiguchi K, Gimenez-Conti I, Rupp T, DiGiovanni J. Overexpression of insulin-like growth factor-1 induces hyperplasia, dermal abnormalities, and spontaneous tumor formation in transgenic mice. Oncogene. 1997 Apr 10; 14(14):1725-34.

Brüning JC, Michael MD, Winnay JN, Hayashi T, Hörsch D, Accili D, Goodyear LJ, Kahn CR. A muscle-specific insulin receptor knockout exhibits features of the metabolic syndrome of NIDDM without altering glucose tolerance. Mol Cell. 1998 Nov; 2(5):559-69.

Candi E, Schmidt R, Melino G. The cornified envelope: a model of cell death in the skin. Nat Rev Mol Cell Biol. 2005 Apr; 6(4):328-40.

Cardoso FL, Brites D, Brito MA. Looking at the blood-brain barrier: molecular anatomy and possible investigation approaches. Brain Res Rev. 2010 Sep 24; 64(2):328-63.

Chao W, D'Amore PA. IGF2: epigenetic regulation and role in development and disease. Cytokine Growth Factor Rev. 2008 Apr; 19(2):111-20.

Chen X, Macara IG. Par-3 controls tight junction assembly through the Rac exchange factor Tiam1. Nat Cell Biol. 2005 Mar; 7(3):262-9.

Chen J, Smith LE. Retinopathy of prematurity. Angiogenesis. 2007; 10(2):133-40. 27.

Clauser E. (1994) Insulin receptor and diabetes Rev Prat. May 1; 44(9):1154-62.

Dale BA, Resing KA, Presland RB. Keratohyalin granule proteins. In: Leigh I, Lane B, Watt F (eds). The Keratinocyte Handbook. Cambridge: Cambridge University Press, 1994, pp 323-350

Davidson MK, Russ PK, Glick GG, Hoffman LH, Chang MS, Haselton FR. Reduced expression of the adherens junction protein cadherin-5 in a diabetic retina. Am J Ophthalmol. 2000 Feb; 129(2):267-9.

Daughaday WH, Rotwein P. Insulin-like growth factors I and II. Peptide, messenger ribonucleic acid and gene structures, serum, and tissue concentrations. Endocr Rev. 1989 Feb; 10(1):68-91.

De Meyts P, Whittaker J. Structural biology of insulin and IGF1 receptors: implications for drug design. Nat Rev Drug Discov. 2002 Oct; 1(10):769-83.

Denecker G, Hoste E, Gilbert B, Hochepied T, Ovaere P, Lippens S, Van den Broecke C, Van Damme P, D'Herde K, Hachem JP, Borgonie G, Presland RB, Schoonjans L, Libert C, Vandekerckhove J, Gevaert K, Vandenabeele P, Declercq W. Caspase-14 protects against epidermal UVB photodamage and water loss. Nat Cell Biol. 2007 Jun; 9(6):666-74.

Dejana E. Endothelial cell-cell junctions: happy together. Nat Rev Mol Cell Biol. 2004 Apr; 5(4):261-70.

Denley A, Bonython ER, Booker GW, Cosgrove LJ, Forbes BE, Ward CW, Wallace JC. Structural determinants for high-affinity binding of insulin-like growth factor II to insulin receptor (IR)-A, the exon 11 minus isoform of the IR. Mol Endocrinol. 2004 Oct; 18(10):2502-12.

Denley A, Cosgrove LJ, Booker GW, Wallace JC, Forbes BE. Molecular interactions of the IGF system. Cytokine Growth Factor Rev. 2005 Aug-Oct; 16(4-5):421-39.

DiGiovanni J, Bol DK, Wilker E, Beltrán L, Carbajal S, Moats S, Ramirez A, Jorcano J, Kiguchi K. Constitutive expression of insulin-like growth factor-1 in epidermal basal cells of transgenic mice leads to spontaneous tumor promotion. Cancer Res. 2000 Mar 15; 60(6):1561-70.

Doering T, Holleran WM, Potratz A, Vielhaber G, Elias PM, Suzuki K, Sandhoff K. Sphingolipid activator proteins are required for epidermal permeability barrier formation. J Biol Chem. 1999a Apr 16; 274(16):11038-45.

Doering T, Proia RL, Sandhoff K. Accumulation of protein-bound epidermal glucosylceramides in beta-glucocerebrosidase deficient type 2 Gaucher mice. FEBS Lett. 1999b Mar 26; 447(2-3):167-70.

Doering T, Brade H, Sandhoff K. Sphingolipid metabolism during epidermal barrier development in mice. J Lipid Res. 2002 Oct; 43(10):1727-33.

Duncan FE, Moss SB, Schultz RM, Williams CJ. PAR-3 defines a central subdomain of the cortical actin cap in mouse eggs. Dev Biol. 2005 Apr 1; 280(1):38-47.

Ebnet K, Suzuki A, Horikoshi Y, Hirose T, Meyer Zu Brickwedde MK, Ohno S, Vestweber D. The cell polarity protein ASIP/PAR-3 directly associates with junctional adhesion molecule (JAM). EMBO J. 2001 Jul 16; 20(14):3738-48.

Ebnet K, Aurrand-Lions M, Kuhn A, Kiefer F, Butz S, Zander K, Meyer zu Brickwedde MK, Suzuki A, Imhof BA, Vestweber D. The junctional adhesion molecule (JAM) family members JAM-2 and JAM-3 associate with the cell polarity protein PAR-3: a possible role for JAMs in endothelial cell polarity. J Cell Sci. 2003 Oct 1; 116(Pt 19):3879-91.

Ebnet K, Suzuki A, Ohno S, Vestweber D. Junctional adhesion molecules (JAMs): more molecules with dual functions?J Cell Sci. 2004 Jan 1; 117(Pt 1):19-29.

Eckert RL, Green H.Structure and evolution of the human involucrin gene. Cell. 1986 Aug 15; 46(4):583-9.

Eckert RL, Yaffe MB, Crish JF, Murthy S, Rorke EA, Welter JF. Involucrin--structure and role in envelope assembly. J Invest Dermatol. 1993 May; 100(5):613-7.

Ellis MJ, Leav BA, Yang Z, Rasmussen A, Pearce A, Zweibel JA, Lippman ME, Cullen KJ. Affinity for the insulin-like growth factor-II (IGF-II) receptor inhibits autocrine IGF-II activity in MCF-7 breast cancer cells. Mol Endocrinol. 1996 Mar; 10(3):286-97.

Epp N, Fürstenberger G, Müller K, de Juanes S, Leitges M, Hausser I, Thieme F, Liebisch G, Schmitz G, Krieg P. 12R-lipoxygenase deficiency disrupts epidermal barrier function. J Cell Biol. 2007 Apr 9; 177(1):173-82.

Erickson KK, Sundstrom JM, Antonetti DA. Vascular permeability in ocular disease and the role of tight junctions. Angiogenesis. 2007; 10(2):103-17.

Feil R, Brocard J, Mascrez B, LeMeur M, Metzger D, Chambon P. Ligand-activated site-specific recombination in mice. Proc Natl Acad Sci U S A. 1996 Oct 1; 93(20):10887-90.

Feng W, Wu H, Chan LN, Zhang M. Par-3-mediated junctional localization of the lipid phosphatase PTEN is required for cell polarity establishment. J Biol Chem. 2008 Aug 22; 283(34):23440-9.

Feng Z, Levine AJ. The regulation of energy metabolism and the IGF-1/mTOR pathways by the p53 protein. Trends Cell Biol. 2010 Jul; 20(7):427-34.

Forde A, Constien R, Gröne HJ, Hämmerling G, Arnold B. Temporal Cre-mediated recombination exclusively in endothelial cells using Tie2 regulatory elements. Genesis. 2002 Aug; 33(4):191-7.

Frasca F, Pandini G, Sciacca L, Pezzino V, Squatrito S, Belfiore A, Vigneri R. The role of insulin receptors and IGF-I receptors in cancer and other diseases. Arch Physiol Biochem. 2008 Feb; 114(1):23-37.

Frystyk J. Free insulin-like growth factors -- measurements and relationships to growth hormone secretion and glucose homeostasis. Growth Horm IGF Res. 2004 Oct; 14(5):337-75.

Fernández AM, Kim JK, Yakar S, Dupont J, Hernandez-Sanchez C, Castle AL, Filmore J, Shulman GI, Le Roith D. Functional inactivation of the IGF-I and insulin receptors in skeletal muscle causes type 2 diabetes. Genes Dev. 2001 Aug 1; 15(15):1926-34.

Furuse M, Hirase T, Itoh M, Nagafuchi A, Yonemura S, Tsukita S, Tsukita S. Occludin: a novel integral membrane protein localizing at tight junctions. J Cell Biol. 1993 Dec; 123(6 Pt 2):1777 88.

Furuse M, Fujita K, Hiiragi T, Fujimoto K, Tsukita S. Claudin-1 and -2: novel integral membrane proteins localizing at tight junctions with no sequence similarity to occludin. J Cell Biol. 1998a Jun 29; 141(7):1539-50.

Furuse M, Sasaki H, Fujimoto K, Tsukita S. A single gene product, claudin-1 or -2, reconstitutes tight junction strands and recruits occludin in fibroblasts. J Cell Biol. 1998b Oct 19; 143(2):391-401.

Furuse M, Hata M, Furuse K, Yoshida Y, Haratake A, Sugitani Y, Noda T, Kubo A, Tsukita S. Claudin-based tight junctions are crucial for the mammalian epidermal barrier: a lesson from claudin-1-deficient mice. J Cell Biol. 2002 Mar 18; 156(6):1099-111.

Gan SQ, McBride OW, Idler WW, Markova N, Steinert PM. Organization, structure, and polymorphisms of the human profilaggrin gene. Biochemistry. 1990 Oct 9; 29(40):9432-40.

Gao L, Macara IG, Joberty G. Multiple splice variants of Par3 and of a novel related gene, Par3L, produce proteins with different binding properties. Gene. 2002 Jul 10; 294(1-2):99-107.

Gavard J, Gutkind JS. VEGF controls endothelial-cell permeability by promoting the beta-arrestin-dependent endocytosis of VE-cadherin. Nat Cell Biol. 2006 Nov; 8(11):1223-34.

Geng S, Mezentsev A, Kalachikov S, Raith K, Roop DR, Panteleyev AA. Targeted ablation of Arnt in mouse epidermis results in profound defects in desquamation and epidermal barrier function. J Cell Sci. 2006 Dec 1; 119(Pt 23):4901-12.

Getsios S, Huen AC, Green KJ. Working out the strength and flexibility of desmosomes. Nat Rev Mol Cell Biol. 2004 Apr; 5(4):271-81.

Gibbs S, Fijneman R, Wiegant J, van Kessel AG, van De Putte P, Backendorf C. Molecular characterization and evolution of the SPRR family of keratinocyte differentiation markers encoding small proline-rich proteins. Genomics. 1993 Jun; 16(3):630-7.

González-Mariscal L, Betanzos A, Nava P, Jaramillo BE. Tight junction proteins. Prog Biophys Mol Biol. 2003 Jan; 81(1):1-44.

Guerrin M, Simon M, Montézin M, Haftek M, Vincent C, Serre G. Expression cloning of human corneodesmosin proves its identity with the product of the S gene and allows improved characterization of its processing during keratinocyte differentiation. J Biol Chem. 1998 Aug 28; 273(35):22640-7.

Guttormsen J, Koster MI, Stevens JR, Roop DR, Williams T, Winger QA. Disruption of epidermal specific gene expression and delayed skin development in AP-2 gamma mutant mice. Dev Biol. 2008 May 1; 317(1):187-95.

Hafner M, Wenk J, Nenci A, Pasparakis M, Scharffetter-Kochanek K, Smyth N, Peters T, Kess D, Holtkötter O, Keratin 14 Cre transgenic mice authenticate keratin 14 as an oocyte-expressed protein. Genesis. 2004 Apr; 38(4):176-81

Hanahan D. Studies on transformation of Escherichia coli with plasmids. J Mol Biol. 1983 Jun 5; 166(4):557-80.

Hanley K, Jiang Y, Holleran WM, Elias PM, Williams ML, Feingold KR. Glucosylceramide metabolism is regulated during normal and hormonally stimulated epidermal barrier development in the rat. J Lipid Res. 1997 Mar; 38(3):576-84.

Hardman MJ, Sisi P, Banbury DN, Byrne C. Patterned acquisition of skin barrier function during development. Development. 1998 Apr; 125(8):1541-52.

Harhaj NS, Felinski EA, Wolpert EB, Sundstrom JM, Gardner TW, Antonetti DA. VEGF activation of protein kinase C stimulates occludin phosphorylation and contributes to endothelial permeability. Invest Ophthalmol Vis Sci. 2006 Nov; 47(11):5106-15.

Haurigot V, Villacampa P, Ribera A, Llombart C, Bosch A, Nacher V, Ramos D, Ayuso E, Segovia JC, Bueren JA, Ruberte J, Bosch F. Increased intraocular insulin-like growth factor-I triggers blood-retinal barrier breakdown. J Biol Chem. 2009 Aug 21;284(34):22961-9.

Hawkins BT, Davis TP. The blood-brain barrier/neurovascular unit in health and disease. Pharmacol Rev. 2005 Jun; 57(2):173-85.

Heidary G, Vanderveen D, Smith LE. Retinopathy of prematurity: current concepts in molecular pathogenesis. Semin Ophthalmol. 2009 Mar-Apr;24(2):77-81.

Hirose T, Izumi Y, Nagashima Y, Tamai-Nagai Y, Kurihara H, Sakai T, Suzuki Y, Yamanaka T, Suzuki A, Mizuno K, Ohno S. Involvement of ASIP/PAR-3 in the promotion of epithelial tight junction formation. J Cell Sci. 2002 Jun 15; 115(Pt 12):2485-95.

Hirose T, Karasawa M, Sugitani Y, Fujisawa M, Akimoto K, Ohno S, Noda T. PAR3 is essential for cyst-mediated epicardial development by establishing apical cortical domains. Development. 2006 Apr; 133(7):1389-98.

Hofman P, Blaauwgeers HG, Tolentino MJ, Adamis AP, Nunes Cardozo BJ, Vrensen GF, Schlingemann RO. VEGF-A induced hyperpermeability of blood-retinal barrier endothelium in vivo is predominantly associated with pinocytotic vesicular transport and not with formation of fenestrations. Vascular endothelial growth factor-A. Curr Eye Res. 2000 Aug; 21(2):637-45.

Hohl D, Mehrel T, Lichti U, Turner ML, Roop DR, Steinert PM. Characterization of human loricrin. Structure and function of a new class of epidermal cell envelope proteins. J Biol Chem. 1991 Apr 5; 266(10):6626-36.

Iden S, Rehder D, August B, Suzuki A, Wolburg-Buchholz K, Wolburg H, Ohno S, Behrens J, Vestweber D, Ebnet K.A distinct PAR complex associates physically with VE-cadherin in vertebrate endothelial cells. EMBO Rep. 2006 Dec; 7(12):1239-46.

Ikenouchi J, Furuse M, Furuse K, Sasaki H, Tsukita S, Tsukita S. Tricellulin constitutes a novel barrier at tricellular contacts of epithelial cells. J Cell Biol. 2005 Dec 19; 171(6):939-45.

Ishibashi T, Tanaka K, Taniguchi Y. Disruption of blood-retinal barrier in experimental diabetic rats: an electron microscopic study. Exp Eye Res. 1980 Apr; 30(4):401-10.

Izumi Y, Hirose T, Tamai Y, Hirai S, Nagashima Y, Fujimoto T, Tabuse Y, Kemphues KJ, Ohno S.An atypical PKC directly associates and colocalizes at the epithelial tight junction with ASIP, a mammalian homologue of Caenorhabditis elegans polarity protein PAR-3. J Cell Biol. 1998 Oct 5; 143(1):95-106.

Jennemann R, Sandhoff R, Langbein L, Kaden S, Rothermel U, Gallala H, Sandhoff K, Wiegandt H, Gröne HJ. Integrity and barrier function of the epidermis critically depend on glucosylceramide synthesis. J Biol Chem. 2007 Feb 2; 282(5):3083-94.

Johansson A, Driessens M, Aspenström P. The mammalian homologue of the Caenorhabditis elegans polarity protein PAR-6 is a binding partner for the Rho GTPases Cdc42 and Rac1. J Cell Sci. 2000 Sep; 113 (Pt 18):3267-75.

Joussen AM, Murata T, Tsujikawa A, Kirchhof B, Bursell SE, Adamis AP. Leukocyte-mediated endothelial cell injury and death in the diabetic retina. Am J Pathol. 2001 Jan; 158(1):147-52.

Joussen AM, Poulaki V, Mitsiades N, Cai WY, Suzuma I, Pak J, Ju ST, Rook SL, Esser P, Mitsiades CS, Kirchhof B, Adamis AP, Aiello LP. Suppression of Fas-FasL-induced endothelial

cell apoptosis prevents diabetic blood-retinal barrier breakdown in a model of streptozotocin-induced diabetes. FASEB J. 2003 Jan; 17(1):76-8.

Kalinin AE, Kajava AV, Steinert PM. Epithelial barrier function: assembly and structural features of the cornified cell envelope. Bioessays. 2002 Sep; 24(9):789-800

Kim S, Kang HY, Nam EH, Choi MS, Zhao XF, Hong CS, Lee JW, Lee JH, Park YK. TMPRSS4 induces invasion and epithelial-mesenchymal transition through upregulation of integrin alpha5 and its signaling pathways. Carcinogenesis. 2010 Apr; 31(4):597-606.

Kitamura T, Kahn CR, Accili D. Insulin receptor knockout mice. Annu Rev Physiol. 2003; 65:313-32.

Koch PJ, de Viragh PA, Scharer E, Bundman D, Longley MA, Bickenbach J, Kawachi Y, Suga Y, Zhou Z, Huber M, Hohl D, Kartasova T, Jarnik M, Steven AC, Roop DR. Lessons from loricrin-deficient mice: compensatory mechanisms maintaining skin barrier function in the absence of a major cornified envelope protein. J Cell Biol. 2000 Oct 16; 151(2):389-400.

Kondo T, Vicent D, Suzuma K, Yanagisawa M, King GL, Holzenberger M, Kahn CR. Knockout of insulin and IGF-1 receptors on vascular endothelial cells protects against retinal neovascularization. J Clin Invest. 2003 Jun; 111(12):1835-42.

Koni PA, Joshi SK, Temann UA, Olson D, Burkly L, Flavell RA. Conditional vascular cell adhesion molecule 1 deletion in mice: impaired lymphocyte migration to bone marrow. J Exp Med. 2001 Mar 19; 193(6):741-54.

Leyvraz C, Charles RP, Rubera I, Guitard M, Rotman S, Breiden B, Sandhoff K, Hummler E. The epidermal barrier function is dependent on the serine protease CAP1/Prss8. J Cell Biol. 2005 Aug 1; 170(3):487-96.

Lin D, Edwards AS, Fawcett JP, Mbamalu G, Scott JD, Pawson T. A mammalian PAR-3-PAR-6 complex implicated in Cdc42/Rac1 and aPKC signaling and cell polarity. Nat Cell Biol. 2000 Aug; 2(8):540-7.

Liu JP, Baker J, Perkins AS, Robertson EJ, Efstratiadis A. Mice carrying null mutations of the genes encoding insulin-like growth factor I (Igf-1) and type 1 IGF receptor (Igf1r). Cell. 1993 Oct 8; 75(1):59-72.

Lofqvist C, Willett KL, Aspegren O, et al. Quantification and localization of the IGF/insulin system expression in retinal blood vessels and neurons during oxygen-induced retinopathy in mice. Invest Ophthalmol Vis Sci. 2009; 50:1831–1837.

Lynley AM, Dale BA. The characterization of human epidermal filaggrin. A histidine-rich, keratin filament-aggregating protein. Biochim Biophys Acta. 1983 Apr 14; 744(1):28-35.

Määttä A, DiColandrea T, Groot K, Watt FM. Gene targeting of envoplakin, a cytoskeletal linker protein and precursor of the epidermal cornified envelope. Mol Cell Biol. 2001 Oct; 21(20):7047-53.

Maeng YS, Choi HJ, Kwon JY, Park YW, Choi KS, Min JK, Kim YH, Suh PG, Kang KS, Won MH, Kim YM, Kwon YG. Endothelial progenitor cell homing: prominent role of the IGF2-IGF2R-PLCbeta2 axis. Blood. 2009 Jan 1; 113(1):233-43.

Marenholz I, Zirra M, Fischer DF, Backendorf C, Ziegler A, Mischke D. Identification of human epidermal differentiation complex (EDC)-encoded genes by subtractive hybridization of entire YACs to a gridded keratinocyte cDNA library. Genome Res. 2001 Mar; 11(3):341-55.

Markova NG, Marekov LN, Chipev CC, Gan SQ, Idler WW, Steinert PM. Profilaggrin is a major epidermal calcium-binding protein. Mol Cell Biol. 1993 Jan; 13(1):613-25.

Marshall D, Hardman MJ, Nield KM, Byrne C. Differentially expressed late constituents of the epidermal cornified envelope. Proc Natl Acad Sci U S A. 2001 Nov 6; 98(23):13031-6.

Matsuki M, Yamashita F, Ishida-Yamamoto A, Yamada K, Kinoshita C, Fushiki S, Ueda E, Morishima Y, Tabata K, Yasuno H, Hashida M, Iizuka H, Ikawa M, Okabe M, Kondoh G, Kinoshita T, Takeda J, Yamanishi K. Defective *stratum corneum* and early neonatal death in mice lacking the gene for transglutaminase 1 (keratinocyte transglutaminase). Proc Natl Acad Sci U S A. 1998 Feb 3; 95(3):1044-9.

Maxwell DS, Pease DC. The electron microscopy of the choroid plexus. J Biophys Biochem Cytol. 1956 Jul 25; 2(4):467-74.

McKinley-Grant LJ, Idler WW, Bernstein IA, Parry DA, Cannizzaro L, Croce CM, Huebner K, Lessin SR, Steinert PM. Characterization of a cDNA clone encoding human filaggrin and localization of the gene to chromosome region 1q21. Proc Natl Acad Sci U S A. 1989 Jul; 86(13):4848-52.

Mehrel T, Hohl D, Rothnagel JA, Longley MA, Bundman D, Cheng C, Lichti U, Bisher ME, Steven AC, Steinert PM, et al. Identification of a major keratinocyte cell envelope protein, loricrin. Cell. 1990 Jun 15; 61(6):1103-12.

Michels C, Aghdam SY, Niessen CM. Cadherin-mediated regulation of tight junctions in stratifying epithelia. Ann N Y Acad Sci. 2009 May; 1165:163-8.

Michels C, Buchta T, Bloch W, Krieg T, Niessen CM. Classical cadherins regulate desmosome formation. J Invest Dermatol. 2009 Aug; 129(8):2072-5.

Mizutani M, Kern TS, Lorenzi M. Accelerated death of retinal microvascular cells in human and experimental diabetic retinopathy. J Clin Invest. 1996 Jun 15; 97(12):2883-90.

Moseley WS, Seldin MF. Definition of mouse chromosome 1 and 3 gene linkage groups that are conserved on human chromosome 1: evidence that a conserved linkage group spans the centromere of human chromosome 1. Genomics. 1989 Nov; 5(4):899-905.

Moxham CP, Duronio V, Jacobs S. Insulin-like growth factor I receptor beta-subunit heterogeneity. Evidence for hybrid tetramers composed of insulin-like growth factor I and insulin receptor heterodimers. J Biol Chem. 1989 Aug 5; 264(22):13238-44.

Müller-Decker K, Scholz K, Neufang G, Marks F, Fürstenberger G. Localization of prostaglandin-H synthase-1 and -2 in mouse skin: implications for cutaneous function. Exp Cell Res. 1998 Jul 10; 242(1):84-91.

Nagai-Tamai Y, Mizuno K, Hirose T, Suzuki A, Ohno S. Regulated protein-protein interaction between aPKC and PAR-3 plays an essential role in the polarization of epithelial cells. Genes Cells. 2002 Nov; 7(11):1161-71.

Näthke IS, Hinck L, Swedlow JR, Papkoff J, Nelson WJ. Defining interactions and distributions of cadherin and catenin complexes in polarized epithelial cells. J Cell Biol. 1994 Jun; 125(6):1341-52.

Navaratna D, McGuire PG, Menicucci G, Das A. Proteolytic degradation of VE-cadherin alters the blood-retinal barrier in diabetes. Diabetes. 2007 Sep; 56(9):2380-7.

Nemes Z, Marekov LN, Fésüs L, Steinert PM. A novel function for transglutaminase 1: attachment of long-chain omega-hydroxyceramides to involucrin by ester bond formation. Proc Natl Acad Sci U S A. 1999 Jul 20; 96(15):8402-7.

Niessen CM. Tight junctions/adherens junctions: basic structure and function. J Invest Dermatol. 2007 Nov; 127(11):2525-32.

Niessen CM, Gottardi CJ. Molecular components of the adherens junction. Biochim Biophys Acta. 2008 Mar; 1778(3):562-71.

Nitta T, Hata M, Gotoh S, Seo Y, Sasaki H, Hashimoto N, Furuse M, Tsukita S. Size-selective loosening of the blood-brain barrier in claudin-5-deficient mice. J Cell Biol. 2003 May 12; 161(3):653-60.

Ong PY, Ohtake T, Brandt C, Strickland I, Boguniewicz M, Ganz T, Gallo RL, Leung DY. Endogenous antimicrobial peptides and skin infections in atopic dermatitis. N Engl J Med. 2002 Oct 10; 347(15):1151-60.

Pandini G, Vigneri R, Costantino A, Frasca F, Ippolito A, Fujita-Yamaguchi Y, Siddle K, Goldfine ID, Belfiore A. Insulin and insulin-like growth factor-I (IGF-I) receptor overexpression in breast cancers leads to insulin/IGF-I hybrid receptor overexpression: evidence for a second mechanism of IGF-I signaling. Clin Cancer Res. 1999 Jul; 5(7):1935-44.

Peitz M, Pfannkuche K, Rajewsky K, Edenhofer F. Ability of the hydrophobic FGF and basic TAT peptides to promote cellular uptake of recombinant Cre recombinase: a tool for efficient genetic engineering of mammalian genomes. Proc Natl Acad Sci U S A. 2002 Apr 2; 99(7):4489-94.

Peng X, Haldar S, Deshpande S, Irani K, Kass DA. Wall stiffness suppresses Akt/eNOS and cytoprotection in pulse-perfused endothelium. Hypertension. 2003 Feb; 41(2):378-81.

Planès C, Randrianarison NH, Charles RP, Frateschi S, Cluzeaud F, Vuagniaux G, Soler P, Clerici C, Rossier BC, Hummler E. ENaC-mediated alveolar fluid clearance and lung fluid balance depend on the channel-activating protease 1. EMBO Mol Med. 2010 Jan; 2(1):26-37.

Pollak M. Insulin and insulin-like growth factor signaling in neoplasia. Nat Rev Cancer. 2008 Dec; 8(12):915-28.

Presland RB, Haydock PV, Fleckman P, Nirunsuksiri W, Dale BA. Characterization of the human epidermal profilaggrin gene. Genomic organization and identification of an S-100-like calcium binding domain at the amino terminus. J Biol Chem. 1992 Nov 25; 267(33):23772-81.

Presland RB, Function of filaggrin and caspase-14 in formation and maintenance of the epithelial barrier. Dermatol Sinica 2009; 27: 1-14

Rajpathak SN, Gunter MJ, Wylie-Rosett J, Ho GY, Kaplan RC, Muzumdar R, Rohan TE, Strickler HD. The role of insulin-like growth factor-I and its binding proteins in glucose homeostasis and type 2 diabetes. Diabetes Metab Res Rev. 2009 Jan; 25(1):3-12.

Rice RH, Crumrine D, Hohl D, Munro CS, Elias PM. Coss-linked envelopes in nail plate in lamellar ichthyosis. Br J Dermatol. 2003 Nov; 149(5):1050-4.

Rothnagel JA, Steinert PM. The structure of the gene for mouse filaggrin and a comparison of the repeating units. J Biol Chem. 1990 Feb 5; 265(4):1862-5.

Rothnagel JA, Longley MA, Bundman DS, Naylor SL, Lalley PA, Jenkins NA, Gilbert DJ, Copeland NG, Roop DR. Characterization of the mouse loricrin gene: linkage with profilaggrin and the flaky tail and soft coat mutant loci on chromosome 3. Genomics. 1994 Sep 15; 23(2):450-6.

Sadagurski M, Weingarten G, Rhodes CJ, White MF, Wertheimer E. Insulin receptor substrate 2 plays diverse cell-specific roles in the regulation of glucose transport. J Biol Chem. 2005 Apr 15; 280(15):14536-44.

Sadagurski M, Nofech-Mozes S, Weingarten G, White MF, Kadowaki T, Wertheimer E. Insulin receptor substrate 1 (IRS-1) plays a unique role in normal epidermal physiology. J Cell Physiol. 2007 Nov; 213(2):519-27.

Saitou M, Furuse M, Sasaki H, Schulzke JD, Fromm M, Takano H, Noda T, Tsukita S. Complex phenotype of mice lacking occludin, a component of tight junction strands. Mol Biol Cell. 2000 Dec; 11(12):4131-42.

Saltiel AR, Kahn CR. Insulin signaling and the regulation of glucose and lipid metabolism. Nature. 2001 Dec 13; 414(6865):799-806.

Sambrook J. Fritsch E.F. and T. Maniatis. Molecular Cloning A Laboratory Manual. Second edition. Cold Spring Harbor Laboratory Press.1989, p.1.74.

Sandhoff R. Very long chain sphingolipids: tissue expression, function and synthesis. FEBS Lett. 2010 May 3; 584(9):1907-13.

Schmoranzer J, Fawcett JP, Segura M, Tan S, Vallee RB, Pawson T, Gundersen GG. Par3 and dynein associate to regulate local microtubule dynamics and centrosome orientation during migration. Curr Biol. 2009 Jul 14; 19(13):1065-74.

Segre JA, Bauer C, Fuchs E. Klf4 is a transcription factor required for establishing the barrier function of the skin. Nat Genet. 1999 Aug; 22(4):356-60.

Sell C, Ptasznik A, Chang CD, Swantek J, Cristofalo VJ, Baserga R. IGF-1 receptor levels and the proliferation of young and senescent human fibroblasts. Biochem Biophys Res Commun. 1993 Jul 15; 194(1):259-65.

Sevilla LM, Nachat R, Groot KR, Klement JF, Uitto J, Djian P, Määttä A, Watt FM. Mice deficient in involucrin, envoplakin, and periplakin have a defective epidermal barrier. J Cell Biol. 2007 Dec 31; 179(7):1599-612.

Shin K, Fogg VC, Margolis B. Tight junctions and cell polarity. Annu Rev Cell Dev Biol. 2006; 22:207-35.

Shakib M, Cunha-Vaz JG. Studies on the permeability of the blood-retinal barrier. IV. Junctional complexes of the retinal vessels and their role in the permeability of the blood-retinal barrier. Exp Eye Res. 1966 Jul; 5(3):229-34

Shapiro L, Weis WI. Structure and biochemistry of cadherins and catenins. Cold Spring Harb Perspect Biol. 2009 Sep; 1(3):a003053.

Simon M, Bernard D, Minondo AM, Camus C, Fiat F, Corcuff P, Schmidt R, Serre G. Persistence of both peripheral and non-peripheral corneodesmosomes in the upper *stratum corneum* of winter xerosis skin versus only peripheral in normal skin. J Invest Dermatol. 2001 Jan; 116(1):23-30.

Smith LE, Wesolowski E, McLellan A, Kostyk SK, D'Amato R, Sullivan R, D'Amore PA. Oxygen-induced retinopathy in the mouse. Invest Ophthalmol Vis Sci. 1994 Jan; 35(1):101-11.

Soos MA, Siddle K.Immunological relationships between receptors for insulin and insulin-like growth factor I. Evidence for structural heterogeneity of insulin-like growth factor I receptors involving hybrids with insulin receptors. Biochem J. 1989 Oct 15; 263(2):553-63.

Soos MA, Field CE, Siddle K. Purified hybrid insulin/insulin-like growth factor-I receptors bind insulin-like growth factor-I, but not insulin, with high affinity. Biochem J. 1993 Mar 1;290 (Pt 2):419-26.

Stachelscheid H, Ibrahim H, Koch L, Schmitz A, Tscharntke M, Wunderlich FT, Scott J, Michels C, Wickenhauser C, Haase I, Brüning JC, Niessen CM. Epidermal insulin/IGF-1 signaling control interfollicular morphogenesis and proliferative potential through Rac activation. EMBO J. 2008 Aug 6; 27(15):2091-101.

Steinert PM, Cantieri JS, Teller DC, Lonsdale-Eccles JD, Dale BA. Characterization of a class of cationic proteins that specifically interact with intermediate filaments. Proc Natl Acad Sci U S A. 1981 Jul; 78(7):4097-101.

Steinert PM, Marekov LN. Initiation of assembly of the cell envelope barrier structure of stratified squamous epithelia. Mol Biol Cell. 1999 Dec; 10(12):4247-61.

Takada M, Hattori S.Presence of fenestrated capillaries in the skin. Anat Rec. 1972 Jun; 173(2):213-9.

Takekuni K, Ikeda W, Fujito T, Morimoto K, Takeuchi M, Monden M, Takai Y. Direct binding of cell polarity protein PAR-3 to cell-cell adhesion molecule nectin at neuroepithelial cells of developing mouse. J Biol Chem. 2003 Feb 21; 278(8):5497-500.

Tanentzapf G, Tepass U. Interactions between the crumbs, lethal giant larvae and bazooka pathways in epithelial polarization. Nat Cell Biol. 2003 Jan; 5(1):46-52.

Taniguchi CM, Emanuelli B, Kahn CR. Critical nodes in signaling pathways: insights into insulin action. Nat Rev Mol Cell Biol. 2006 Feb; 7(2):85-96.

Tavakkol A, Elder JT, Griffiths CE, Cooper KD, Talwar H, Fisher GJ, Keane KM, Foltin SK, Voorhees JJ. Expression of growth hormone receptor, insulin-like growth factor 1 (IGF-1) and IGF-1 receptor mRNA and proteins in human skin. J Invest Dermatol. 1992 Sep; 99(3):343-9.

Tserentsoodol N, Shin BC, Suzuki T, Takata K.Colocalization of tight junction proteins, occludin and ZO-1, and glucose transporter GLUT1 in cells of the blood-ocular barrier in the mouse eye. Histochem Cell Biol. 1998 Dec; 110(6):543-51.

Ting SB, Caddy J, Hislop N, Wilanowski T, Auden A, Zhao LL, Ellis S, Kaur P, Uchida Y, Holleran WM, Elias PM, Cunningham JM, Jane SM. A homolog of Drosophila grainy head is essential for epidermal integrity in mice. Science. 2005 Apr 15; 308(5720):411-3.

Tsuruta D, Green KJ, Getsios S, Jones JC. The barrier function of skin: how to keep a tight lid on water loss. Trends Cell Biol. 2002 Aug; 12(8):355-7.

Tunggal JA, Helfrich I, Schmitz A, Schwarz H, Günzel D, Fromm M, Kemler R, Krieg T, Niessen CM. E-cadherin is essential for *in vivo* epidermal barrier function by regulating tight junctions. EMBO J. 2005 Mar 23; 24(6):1146-56.

Turksen K, Troy TC.Barriers built on claudins. J Cell Sci. 2004 May 15; 117(Pt 12):2435-47.

Ullrich A, Gray A, Tam AW, Yang-Feng T, Tsubokawa M, Collins C, Henzel W, Le Bon T, Kathuria S, Chen E, et al. Insulin-like growth factor I receptor primary structure: comparison with insulin receptor suggests structural determinants that define functional specificity. EMBO J. 1986 Oct; 5(10):2503-12.

Vasioukhin V, Bauer C, Yin M, Fuchs E. Directed actin polymerization is the driving force for epithelial cell-cell adhesion. Cell. 2000 Jan 21; 100(2):209-19.

Vicent D, Ilany J, Kondo T, Naruse K, Fisher SJ, Kisanuki YY, Bursell S, Yanagisawa M, King GL, Kahn CR. The role of endothelial insulin signaling in the regulation of vascular tone and insulin resistance. J Clin Invest. 2003 May; 111(9):1373-80.

Vorbrodt AW, Dobrogowska DH. Molecular anatomy of intercellular junctions in brain endothelial and epithelial barriers: electron microscopist's view. Brain Res Brain Res Rev. 2003 Jun; 42(3):221-42.

Wallow IH, Engerman RL. Permeability and patency of retinal blood vessels in experimental diabetes. Invest Ophthalmol Vis Sci. 1977 May; 16(5):447-61.

Wattel F, Mathieu D, Coget JM, Billard V. Hyperbaric oxygen therapy in chronic vascular wound management. Angiology 1990; 41:59–65.

Williams CD, Rizzolo LJ.Remodeling of junctional complexes during the development of the outer blood-retinal barrier. Anat Rec. 1997 Nov; 249(3):380-8

Wu H, Feng W, Chen J, Chan LN, Huang S, Zhang M. PDZ domains of Par-3 as potential phosphoinositide signaling integrators. Mol Cell. 2007 Dec 14; 28(5):886-98.**7**

Acknowledgements

Next to will of the God, this thesis is the outcome of the tremendous support and stimulation from my family, scientist colleagues and all other supportive fellows in the University of Cologne. I am exceedingly grateful to my adviser, Prof. Carien Niessen. She was the central organizer for the progress and troubleshooting in the course of my thesis work. Besides providing me a science project, Carien taught me big important lessons in science profesion as well as in personal life. I am also highly indebted to organizers of the international graduate school for genetics and functional genomics (IGS-GFG) for providing the funding and supportive environment in Germany. Thereby my deepest thanks go to Dr. Brigitte von Wilcken-Bergmann, Dr. Isabell Witt, Mrs. Kathy Joergens and Prof. Maria Leptin in IGS-GFG.

I would also thank members of my thesis committee, Prof. Dr. Jens C. Breuning, Mats Paulsson for their patience with my committee meeting, critical reading of my manuscript and their comments.

My kind colleagues in the Niessen lab provided a very friendly and sociable atmosphere which facilitated my graduate career much easier outside my home land. Specially I wish to thank Mehmet Akyuez, Dr. Christian Michels and Christian Guenschmann who never hesitated to offer help in hard times. I would like to sincerely thank all present and former members of the lab, specially Dr. Karla Seifert, Dr. Jeanie Scott, Annika Schmitz and Dr.Barbara Boggetti for excellent support and resolving scientific problems. Nadine Niehoff always helped me thoroughly in handling cell culture experiments and TER evaluations. Drs. Thomas Wunderlich, Andre Kleinridders and Mr. Martin Pal in the institute for genetics (University of Cologne) helped in the designing and generation of the Par-3 construct. I appreciate the help and discussions that all other laboratory and campus colleagues provided to me during my graduate career. I wish to express my cordial thanks to the secretarial, cleaning and disposal personal of the CMMC and the animal facility of the pharmacology department.

The countless guiltless embryos and mice that were generated during my work were key for our understanding of scientific questions and I regret their scarification for scientific purposes and ask for forgiveness from God.

My best friends, Mr. Amir Tahmasebipour, Prof. Steven W. Barger and Prof. Sue Griffin (University of Arkansas for medical sciences) provided me invaluable success formulas in life and science and contributed chiefly to my science accomplishments.

Finally my parents who brought me to this world of wonders and educated me in the direction of highly admired merits, as well as my brother Mesut and my sister Ilaha contributed morally and emotionally to my achievement in life and academics and I wish to thank them from the bottom of my heart.

8 Erklärung

Ich versichere, dass ich die von mir vorgelegte Dissertation selbständig angefertigt, die benutzten Quellen und Hilfsmittel vollständig angegeben und die Stellen der Arbeit – einschließlich Tabellen, Karten und Abbildungen -, die anderen Werken im Wortlaut oder dass diese Dissertation noch keiner anderen Fakultät oder Universität zur Prüfung vorgelegen worden ist sowie, dass ich eine solche Veröffentlichung vor Abschluss des Promotionsverfahren nicht vornehmen werde. Die Bestimmungen dieser Promotionsordnung sind mir bekannt. Die von mir vorgelegte Dissertation ist von Prof. Dr. Jens C. Brüning betreut worden.

Köln, November Saeed Yadranji Aghdam

Curriculum Vitae

Name Saeed Yadranji Aghdam
Nationality Iranian
Date of birth June 23, 1981
Place of Birth Tabriz, Iran.

Education

Sept 2006- Jan 2011 PhD fellowship, Institute for genetics, University of Cologne, Germany
PI Prof. Carien Niessen

Oct 2002- Feb 2006 M.Sc. degree in Developmental Biology, Tehran University, Iran
The role of Lithium Chloride on rat microglial cell survival *in vitro*
PI Dr. Bahman Zeinali

Sept 1998- Feb 2002 B.Sc. degree in Animal Biology, Tabriz university, Iran

Sep 1993- May 1998 Diploma in Natural sciences, Valfadjr high school Tabriz-Iran

Publications:

Michels C. **Aghdam S. Y.** Niessen C. M. Cadherin-Mediated Regulation of Tight Junctions in Stratifying Epithelia. **Ann. N.Y. Acad. Sci.** 1165: 163–168 (2009)

Aghdam S. Y. Barger S. W. Glycogen Synthase Kinase-3 in Neurodegeneration and Neuroprotection: Lessons from Lithium. **Curr. Alzh. Res**. 4: 21-31 (2007)

Pashmi M. Ghorashi S. A. Salehi A. R. Moini M. Javanmard A. Qanbari S. **Aghdam S. Y.** Polymorphism of Bovine Lymphocyte Antigen DRB3.2 Alleles in Iranian Native Sarabi Cows. **Asian-Aust. J. Anim. Sci.** 19 : 775-778 (2006)